THE USE OF BURNABLE NEUTRON ABSORBERS TO MITIGATE THE EFFECTS OF COOLANT VOIDING ON CANDU 37-ELEMENT FUEL

UTILISATION D'ABSORBEURS CONSOMMABLES DE NEUTRONS DANS LA GRAPPE DE COMBUSTIBLE CANDU À 37 CRAYONS POUR ATTÉNUER LES EFFETS DE LA FORMATION DE VIDE DANS LE CALOPORTEUR

A Thesis Submitted to the Division of Graduate Studies
of the Royal Military College of Canada
by

Mark Couture

In Partial Fulfillment of the Requirements for the Degree of
Master of Applied Science in Nuclear Engineering

December 2019

Abstract

A study of the mitigating effects that burnable neutron absorbers have on coolant voiding in CANDU 37-element fuel was conducted. The purpose of this study was to determine if safety margins can be improved from the addition of small amounts of burnable neutron absorbers in the fuel through the simulation and analysis of a large loss of coolant accident. Burnable neutron absorbers Gd_2O_3, Eu_2O_3, and B_2O_3 have been shown to dampen the refuelling and plutonium transients with negligible impact on the fuel burnup. The lattice code WIMS-AECL was used to compute macroscopic cross sections which were passed to the diffusion code RFSP-IST to model a CANDU reactor undergoing a primary heat transport system reactor inlet header break. Combinations of burnable neutron absorbers Gd_2O_3, Eu_2O_3, and B_2O_3 were added to the CANLUB layer of specific fuel pins and core power distributions were computed for comparison against a natural uranium fuel case. Results show a reduction in the core enthalpy change when burnable neutron absorbers are added, along with a reduction in the side-to-side power oscillation during the transient. The reduction in the enthalpy change implies that the positive void reactivity experienced in CANDU reactors during the early phase of the loss of coolant accidents could be mitigated through the addition of burnable neutron absorbers in the fuel.

Keywords: CANDU, burnable neutron absorbers, BNAF, 37-element fuel, LOCA, loss-of-coolant accident, CVR, coolant void reactivity, WIMS-AECL, RFSP-IST.

Résumé

On a mené une étude sur les effets qu'ont les absorbeurs consommables de neutrons dans les grappes de combustible CANDU à 37 crayons sur l'atténuation de la formation de vide dans le caloporteur. Le but de ce travail était de déterminer si l'on peut améliorer les marges de sûreté par l'ajout de petites quantités d'absorbeurs consommables de neutrons dans le combustible au moyen de la simulation et de l'analyse d'un accident par perte importante de caloporteur. On a montré que les absorbeurs consommables de neutrons Gd_2O_3, Eu_2O_3 et B_2O_3 peuvent atténuer les phénomènes transitoires résultants du rechargement de combustible et du pic du plutonium tout en ayant un impact négligeable sur le burn-up du combustible. Le code de réseau WIMS-AECL a été utilisé pour calculer les sections efficaces macroscopiques dont les valeurs étaient transmises au code de diffusion RFSP-IST afin de modéliser un réacteur CANDU subissant une rupture importante à l'entrée du système primaire de caloporteur. Des combinaisons des absorbeurs consommables de neutrons Gd_2O_3, Eu_2O_3 et B_2O_3 ont été ajoutées à la couche de CANLUB pour des crayons de combustible spécifiques et les distributions de densités de puissance dans le cœur du réacteur ont été calculées et comparées à celle pour un réacteur n'utilisant que du combustible à uranium naturel. Les résultats montrent une réduction de la variation de l'enthalpie du cœur lorsque l'on ajoute des absorbeurs consommables de neutrons. On constate aussi une réduction de l'oscillation latérale de la puissance durant la période transitoire. La réduction observée de la variation de l'enthalpie implique que la réactivité positive due à la fraction de vide qui se produit dans les réacteurs CANDU durant la phase initiale des accidents de perte de caloporteur peut être atténuée par l'ajout dans le combustible d'absorbeurs consommables de neutrons.

Mots-clefs : CANDU, absorbeurs consommables de neutrons, CANC (combustible avec absorbeurs consommables de neutrons), grappe de combustible à 37 crayons, APC, accident par perte de caloporteur, RFVC, réactivité associée à la fraction de vide du caloporteur, WINS-AECL, RFSP-IST.

Contents

List of Tables

List of Figures

List of Abbreviations and Acronyms

AECL: Atomic Energy of Canada Limited
BNA: Burnable Neutron Absorber
BNAF: Burnable Neutron Absorber Fuel
CANDU: Canada Deuterium Uranium
CCP: Critical Channel Power
CHF: Critical Heat Flux
CPPF: Channel Power Peaking Factor
CNSC: Canadian Nuclear Safety Commission
DBA: Design Basis Accident
ECI: Emergency coolant injection
FPD: Full power day
FPR: Fission product release
IST: Industry Standard Toolset
LOCA: Loss of coolant accident
LWR: Light water reactor
NOP: Neutron overpower
NPP: Nuclear power plant
OP&P: Operating Policies and Principles
PHTS: Primary Heat Transport System
PHWR: Pressurized heavy water reactor
RFSP: Reactor Fuelling Simulation Program
RIH: Reactor inlet header
ROH: Reactor outlet header
RRS: Reactor Regulating System
SDS1: Shutdown System 1
SDS2: Shutdown System 2
SFP: Saturating Fission Product
WIMS: Winfrith Improved Multigroup Scheme

Acknowledgements

I would like to extend my sincere thanks to Dr. Paul Chan and Dr. Hugues Bonin of the Royal Military College of Canada. Their exceptional support throughout the writing of this thesis, as well as providing me with the opportunity to work part-time on this degree program is truly appreciated. Without their understanding and accommodation this academic venture would certainly not have been possible.

I also acknowledge Natural Sciences and Engineering Research Council of Canada, as well as the CANDU Owner's Group for their past and ongoing support of the Nuclear Fuel Research Group at the Royal Military College of Canada.

Finally, I would like to thank my family, my fiancée, Madalyn, and dog, River, for their endless support throughout this journey.

1 Introduction and Research Objective

Canada Deuterium Uranium (CANDU) reactors have been used to generate electricity commercially in Canada since the Nuclear Power Demonstration Generating Station began operation as part of Ontario Hydro in 1962 [1]. Nuclear power plants (NPP) in Canada are subject to regulation by the Canadian Nuclear Safety Commission (CNSC) and are accountable for maintaining plant operating parameters within safe limits as defined in the NPP Safety Report and Operating Policies and Principles (OP&P) [2] [3].

The Large Loss of Coolant Accident (LOCA) in CANDU reactors involves a break in the primary heat transport system of a magnitude significant enough that the Reactor Regulating System (RRS) can no longer maintain reactivity control [4]. For the purpose of conducting safety analyses, the limiting cases for fuel channel integrity and fission product release (FPR) are the thirty-five percent reactor inlet header (RIH) break and the one hundred percent reactor outlet header (ROH) break [5]. The large LOCA accident is linked to an inherent CANDU characteristic, the positive void reactivity coefficient, which results in a significant reactivity increase immediately following such an accident [6].

Unlike the light water reactor (LWR) the CANDU pressurized heavy water reactor (PHWR) has separate heat transport and moderator systems, using different isotopic percentages of heavy water D_2O, rather than light water H_2O. The positive void reactivity coefficient in CANDU reactors is caused by this difference. This means that a loss of system coolant does not result in a loss of system moderator causing a decrease in neutron resonance absorption and an increase in the rate of fission triggered by fast neutrons [7]. The power transient following a large LOCA is terminated by actuation of one of the two shutdown systems, shutdown system 1 (SDS1) and shutdown system 2 (SDS2), in response to a credited neutronic trip following the accident [4] [8]. SDS1 consists of vertical rods made of neutron absorbing stainless steel and cadmium and are normally poised and located outside of the core [9]. SDS2 consists of horizontally assembled liquid injection nozzles in line with a pressurized nitrogen tank and a neutron absorbing gadolinium nitrate solution for fast injection in case of an SDS2 trip [10].

The concept of using burnable neutron absorbers to improve refuelling and plutonium transients in CANDU 37-element fuel has been investigated. Results indicate that a combination of gadolinium oxide, Gd_2O_3, and europium oxide, Eu_2O_3, can successfully mitigate the refuelling and plutonium transients [11]. Related research has shown that combinations of the burnable neutron absorbers Gd_2O_3 and Eu_2O_3 can be implemented in CANDU fuel with negligible impact on the fuel discharge burnup [12] and to mitigate end flux peaking [13]. An effective burnable neutron absorber has a high neutron absorption cross-section and undergoes radiative capture to become an isotope that has a lower absorption cross-section [14]. In these studies Gd_2O_3 was selected to address the initial refuelling transient due to a lack of xenon-135 concentration in the fresh fuel and Eu_2O_3 was selected to lessen the plutonium-239 peak that occurs approximately thirty to fifty full power days following refuelling [11] [12] [13].

The current study explores the impact of burnable neutron absorbers on large LOCA safety margin. In line with the studies conducted by *Chan et al*., burnable neutron absorbers were added to the CANLUB layer in a CANDU 37-element fuel bundle. The industry standard toolset (IST) physics codes Winfrith Improved Multigroup Scheme (WIMS-AECL) [15] was used in conjunction with the Reactor Fuelling Simulation Program (RFSP-IST) [16] CERBERUS improved quasi-static model to simulate a large reactor inlet header break large loss of coolant accident. This study aims to demonstrate that introducing a small amount of burnable neutron absorbers to the fuel mitigates the power pulse following such an accident, particularly for reactor startup after a refurbishment or long shutdown. The primary research objective of this study is to demonstrate that the addition of burnable neutron absorbers mitigates the effect of coolant voiding on CANDU 37-element fuel.

2 Background

2.1 CANDU Reactor Physics

Physics plays an important role in nuclear safety analysis and is a necessity when it comes to understanding the means by which nuclear reactors are operated and controlled. Some of the key concepts relevant to the current study are introduced in this section.

2.1.1 Radioactive Decay

The basic atomic structure used throughout is in line with the notation ${}^{A}_{Z}X$ where A is the atomic mass corresponding to the total number of protons and neutrons, Z is the atomic number corresponding to the number of protons in the nuclide, and X is the chemical symbol of the element.

The release of energy from nuclear fission is a result of heavy nuclei becoming unstable, or radioactive, as the number of neutrons in the nucleus increases relative to the number of protons [17]. The actual mass of nuclides is always inferior to the sum of the masses of the components (protons, neutrons, and electrons). The difference between the actual mass and the sum of the components' masses is called the mass defect. The mass defect is given by Equation 1 [18].

$$\Delta = \left[Zm_p + (A - Z)m_n\right] - {}^{A}m_z \tag{1}$$

The mass defect can be converted to the energy stored in the nucleus by means of Equation 2, implying that the same energy would be required to disassemble the nucleus, referred to as the binding energy [19]. Unstable nuclei with more neutrons than protons tend to decay to nuclei with a smaller neutron-to-proton ratio. In some cases, this decay may be the fission process [20]. A process in which a nuclide is converted to a new nuclide with a higher binding energy per nucleon, results in conversion of mass to energy as shown in Equation 2 [19].

$$E = mc^2 \tag{2}$$

The chart in Figure 1 demonstrates the instability nuclei encounter as the number of neutrons in the nucleus begins to deviate from the number of protons.

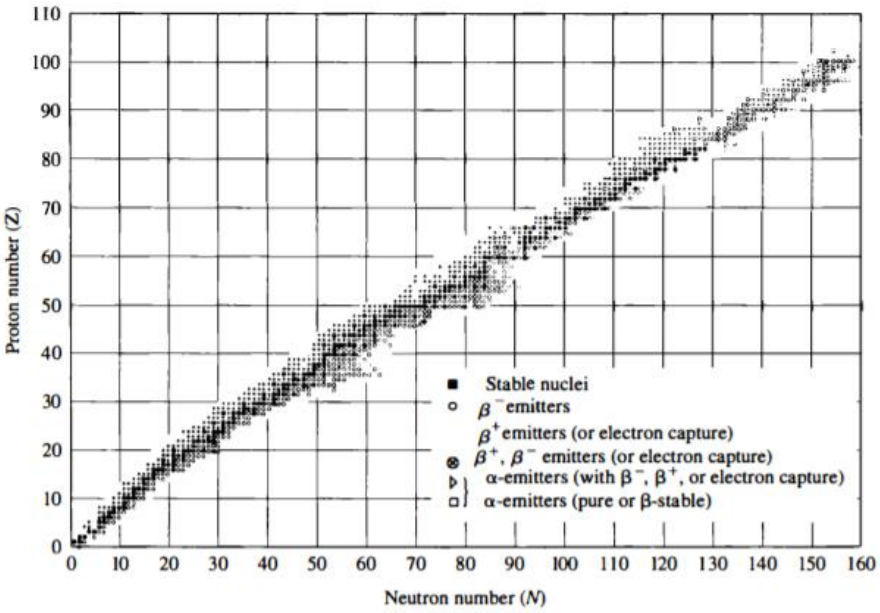

Figure 1: Nuclei stability based on number of neutrons and protons [20].

Various types of decay are possible for unstable nuclei, the three most significant being beta, alpha, and gamma emission [17]. Beta-minus decay arises when an unstable nucleus undergoes a process in which one of its neutrons had converted to a proton, typically releasing an electron and an antineutrino in the process [21]. Alpha decay occurs when a nucleus emits a helium-4 nucleus [22]. Gamma decay occurs as a result of a transition from an excited state to a lesser excited state, with the emission of a photon in the process [17].

2.1.2 Neutron Interactions

CANDU reactors operate and are controlled by utilizing neutrons to trigger nuclear reactions in the core of the reactor. When a neutron interacts with a nuclide, it can undergo either an elastic or an inelastic scattering interaction or be absorbed by the nuclide. Three of the neutron reactions involving absorption are activation, radiative capture, and fission [23].

Neutron activation arises when a neutron is absorbed in a nuclide, yielding a heavier product that is most often radioactive. This means that the new nuclide has a high probability of decaying by means of gamma ray, beta particle, or alpha particle emission [24]. An example of neutron activation is the production of cobalt-60, which is used typically for radiation therapy and sterilization of one-time-use medical equipment due to the high-energy gamma rays emitted by the resulting nuclide as shown in Equation 3 [25].

$$^{59}_{27}Co + n \rightarrow {}^{60}_{27}Co \rightarrow {}^{60}_{28}Ni + e^{-} + v_e \quad (3)$$

Radiative capture occurs when a neutron is absorbed in a nuclide and the product then decays by gamma ray emission [26]. An important example of radiative capture in the CANDU reactor is in uranium-238, which makes up much of the natural uranium fuel. Uranium-238 captures a neutron to become uranium-239 and can undergo two successive beta decays to become plutonium-239 as shown in Equation 4.

$$^{238}_{92}U + n \rightarrow {}^{239}_{92}U \rightarrow {}^{239}_{93}Np \rightarrow {}^{239}_{94}Pu \quad (4)$$

Fission following neutron absorption occurs in heavy nuclei due to the lower excitation energy required to induce fission in nuclides with a low binding energy per nucleon [17]. Neutron induced fission is the basis for operation of the CANDU reactor. It stems essentially from fission in naturally occurring uranium-235, making up only a small percentage of the natural uranium fuel in the reactor core at approximately 0.72% [27]. Following fission, two intermediate mass fission products are released along with an average of two to three neutrons, gamma rays, and an excess energy as shown in one of many examples in Equation 5 [19].

$$^{235}_{92}U + n \rightarrow {}^{236}_{92}U \rightarrow {}^{144}_{56}Ba + {}^{89}_{36}Kr + 3n + 177MeV \quad (5)$$

One fission fragment of interest is radioactive iodine-131 due to its biological accumulation and concentration in the thyroid when ingested, posing a significant health risk to the public if exposed [28]. Spontaneous fission is also possible in heavy unstable nuclei but has a much lower probability of occurrence. The fission fragments are also radioactive, undergoing a series of alpha, beta, and gamma decays. Of interest in CANDU reactors is the production of xenon-135 from iodine-135 as shown in Equation 6 where tellerium-135 is one fission fragment of uranium-235.

$$^{135}_{52}Te \rightarrow {}^{135}_{53}I \rightarrow {}^{135}_{54}Xe \rightarrow {}^{135}_{55}Ce \rightarrow {}^{135}_{56}Ba \quad (6)$$

where fission products tellurium-135, iodine-135, and xenon-135 are all beta emitters, as well as cesium-135, with barium-135 being a stable nuclide. Xenon-135 is of interest because it is a neutron poison, having a high probability of absorbing a neutron and therefore acting as a neutron sink in the reactor [23]. The probability of a specific nucleus having an interaction when encountering a neutron is given by its nuclear cross section [17].

2.1.3 Nuclear Cross Sections

Each nucleus has a probability associated with a specific interaction with a given neutron. Determining these probabilities is conducted experimentally and the results are used in calculations related to neutron transport; the nuclear cross section represents these probabilities [19]. There are two types of cross sections which are considered, the microscopic cross section and the macroscopic cross section. The microscopic cross section, σ, is represented in units of barns, where one barn is equal to 10^{-24} cm^2, whereas the macroscopic cross section, Σ, is represented in units of

cm^{-1} [29]. Cross sections are collected by global nuclear data organizations to create libraries which are used by physics codes for reactor modeling and simulation [17].

Microscopic cross sections represent the probability of an interaction for a single nucleus occurring without shielding considerations for other nuclei or the incident beam of neutrons [30]. This is based on consideration for a uniform beam of neutrons incident toward a thin target material as show in Figure 2.

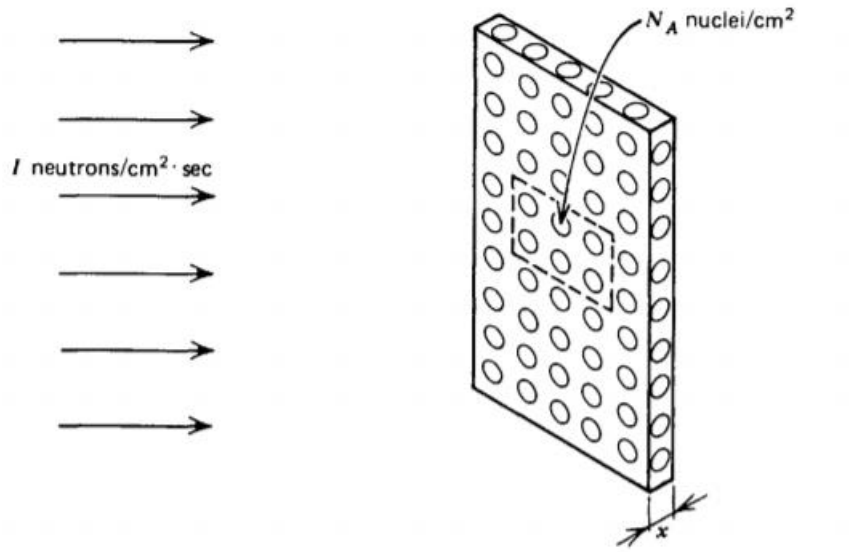

Figure 2: Incident uniform beam of neutrons on target material [19].

The microscopic cross section is represented in terms of the reaction rate, neutron beam intensity, and number of atoms per unit area as shown in Equation 7 [31].

$$R = \sigma I N \tag{7}$$

where R is given in units of reactions cm^{-3} s^{-1} , I in units of incident particles cm^{-2} s^{-1}, and N in units of target nuclei(cm^{-3}) yielding a result for σ in cm^2 [19]. This result implies that a larger cross-sectional area leads to a greater probability of said interaction occurring in the material. There are three main microscopic cross sections used in nuclear reactor physics calculations including fission, σ_f, radiative capture or absorption, σ_a, and scattering, σ_s, which may be summed to obtain a total cross-sectional area for the nuclei [30].

Macroscopic cross sections represent the volumetric probability of interaction for all the nuclei contained in a certain target region [32]. The macroscopic cross section is represented in terms of the microscopic cross section and the number of atoms per unit volume, or atomic number density, as shown in Equation 8 [19].

$$\Sigma = \sigma N \tag{8}$$

where σ is the microscopic cross section in units of cm^2 and N is the atomic number density in units of nuclei(cm^{-3}) yielding a macroscopic cross section in units of cm^{-1}. The macroscopic cross section considers both the combined probabilities of

interaction for single nuclei in each volume along with the atomic number density for said volume. Thus, the probability of interaction for a mixed material is said to be a sum of each computed macroscopic cross section, which may be used to compute a combined probability of specific interaction in materials [17].

2.1.4 Neutron Chain Reaction

The operation of a nuclear reactor is based on a sustained neutron chain reaction. In order to provide appropriate control of a nuclear reactor, the control system must be adjusted such that each generation of neutrons is, on average, equal to the subsequent generation such that a constant quantity of neutrons is maintained in the system. The term used to describe this behaviour is called criticality and is defined by the multiplication factor in Equation 9 [31].

$$k = \frac{N_x}{N_{x-1}} \tag{9}$$

where N_x is the number of neutrons produced in the current generation and N_{x-1} is the number of neutrons produced in the previous generation. A k value equal to one corresponds to critical, a k value less than one corresponds to subcritical, and a k value greater than one corresponds to supercritical. These values imply that for each successive generation of neutrons, the neutron population is either remaining constant, decreasing, or increasing with time, respectively. The reactor core is controlled such that a k value close to one is maintained.

To relate the multiplication factor to a deviance from critical, the term reactivity is defined as per Equation 10 [31].

$$\rho = \frac{k_{eff} - 1}{k_{eff}} \tag{10}$$

where ρ gives an indication of magnitude of a reactivity change relative to zero and k_{eff} is the quantity related to k_∞ that accounts for neutron leakage in finite reactor. Whereas k_∞ is defined for a reactor with infinite dimensions for which there is no neutron leakage. For any k_{eff} value greater than one, ρ has a value greater than zero implying a reactivity insertion has occurred and the opposite being true for any k_{eff} value less than one, giving a negative value for ρ.

To grasp how the core chain reaction is maintained it is important to understand the neutron lifecycle between generations. This lifecycle is best described using what is known as the six-factor formula in nuclear engineering, shown in Equation 11 [19].

$$k_{eff} = \epsilon p f \eta \Lambda_f \Lambda_t \tag{11}$$

where ϵ is the fast fission factor, p is the resonance escape probability, f is the thermal utilization factor, η is the thermal regeneration factor, and Λ_f and Λ_t are the fast and thermal non-leakage probabilities.

The thermal regeneration factor is the average number of neutrons created for each radiative capture occurring in the nuclear fuel as shown in Equation 12. Note that this given equation is only true when there is only one fissile isotope in the fuel.

$$\eta = \frac{\nu \sigma_f^F}{\sigma_a^F} \tag{12}$$

where ν is the average number of neutrons produced for each fission reaction, σ_f is the microscopic fission cross section for the fuel, and σ_a is the microscopic absorption cross section for the fuel. The typical thermal regeneration factor value in thermal reactors such as the CANDU is approximately 1.2 [33].

The thermal utilization factor is the probability that a neutron undergoing the radiative capture interaction is absorbed in the fuel rather than in some other material as shown in Equation 13 [33].

$$f = \frac{\Sigma_a^F}{\Sigma_a} \tag{13}$$

where Σ_a^F is the macroscopic cross section for the fuel and Σ_a is the macroscopic absorption cross section representing absorptions in the entire region. The typical thermal utilization factor in thermal reactors is approximately 0.95 [33].

The resonance escape probability is the percentage of neutrons that are thermalized in the moderator without being absorbed in the slowing down process as shown in Equation 14 [31].

$$p = e^{-\frac{1}{\xi}\int_E^{E_0} \frac{\Sigma_a}{\Sigma_a + \Sigma_s} \frac{dE'}{E'}} \tag{14}$$

where ξ is the scattering lethargy or the average logarithmic energy lost by a neutron during a collision, Σ_s is the macroscopic scattering cross section, Σ_a is the macroscopic absorption cross section, and the integral is the accumulation of various energies with which the neutrons are slowed to. The typical resonance escape probability value in a thermal reactor is approximately 0.9 [33].

The fast fission factor represents the ratio of total fission neutrons to fission neutrons resulting just from the thermal fission process as shown in Equation 15.

$$\epsilon = \frac{neutrons\ from\ thermal\ fission + neutrons\ from\ fast\ fission}{neutrons\ from\ thermal\ fission} \tag{15}$$

The fast fission factor accounts for the possibility that a fast neutron causes fission in the fissile isotope uranium-235 but also in the more abundant fissionable isotope uranium-238 and has a typical value in thermal reactors of approximately 1.03 [33].

The fast-non-leakage probability and thermal non-leakage probabilities are the system leakage probabilities for fast and thermal neutrons respectively. The typical value for the fast-non-leakage probability in CANDU reactors is approximately 0.995 and thermal-non-leakage probability is approximately 0.98 [33], such high values obtained from the large dimensions of CANDU reactor cores.

Given the six factors and typical values for thermal reactors the neutron lifecycle between generations is described as follows: Assume 100 fast neutrons are initially produced from fission, then 102 fast neutrons (a two percent increase) are seen due to the fast fission effect, and 99 fast neutrons (ninety-seven percent of the new

neutron total) are not lost due to the fast-non-leakage probability. Then 86 neutrons (eighty-seven percent of the remaining neutrons) are slowed to thermal energies without being lost due to resonance absorption. 85 of these neutrons (ninety-nine percent of the remaining neutrons) are not lost due to the thermal non-leakage probability. Ninety-five percent of the remaining thermal neutrons (in other words 4 thermal neutrons) are absorbed in materials other than the fuel due to the thermal utilization factor. Of the remaining 81 thermal neutrons which trigger fission after being absorbed in the fuel, creating approximately two to three neutrons per fission, the total number of neutrons in the system obtained by multiplying the 81 thermal neutrons that are causing fissions by the thermal regeneration factor (1.2) is close to 100, equal to the original quantity at one hundred percent for the cycle to start anew. The small discrepancy is caused by the rounding of the intermediate values.

2.1.5 Reactor Kinetics

Reactivity changes in CANDU reactors are relatively common. On-power refuelling, reactivity device movement for control, and unanticipated operational occurrences impacting the reactivity of the core are all examples [34]. Reactor kinetics involves the study of how the core neutron flux changes based on variations in reactivity, and forms the basis for reactor control in terms of prompt and delayed neutron response, both of which are introduced briefly in this section.

Prompt neutrons are created directly from fission as shown in Equation 18. This equation is based on a simplified point kinetics model where the entire reactor is treated as a single point in space [17] [31].

$$\frac{dN(t)}{dt} = \frac{k-1}{l}N(t) + S(t) \tag{18}$$

where *k* is the neutron multiplication factor, *l* is the average time it takes for a neutron to slow from fast to thermal energy, *N(t)* is the number of neutrons at time *t*, and *S(t)* is the source term at time *t*. Solving this differential equation and knowing the number of neutrons, *N*, is directly related to the power, *P*, one obtains the solution shown in Equation 19 [17] [31].

$$P(t) = P_0 e^{\frac{\Delta k t}{l}} \tag{19}$$

where P_0 is the initial reactor power. From this equation, one can derive a formula for what is known as the reactor period. The reactor period is the time it takes for power to increase by e, or approximately 2.718 times, as shown in Equation 20 [17] [31].

$$\tau = \frac{l}{\Delta k} \tag{20}$$

For a reactor operating only on prompt neutrons, a small reactivity change will result in a change in power by a factor of e in a very short period based on an average neutron lifetime of approximately 1 ms [35]. Control, safe operation, and design for shutdown capability of a reactor with this characteristic would be extremely difficult.

Delayed neutrons dampen the amplitude of this type of response by extending the actual reactor period, making control much more manageable [17].

Delayed neutrons are emitted by what are known as precursors. Precursors are fission products that remain unstable with a measurable half-life and beta decay to radioisotopes that decay with a neutron emission [36]. Considering delayed neutrons, Equation 18 becomes Equation 21 [17] [37].

$$\frac{dN(t)}{dt} = \frac{kN}{l}(1 - \beta) + \lambda C + \frac{N}{l} = \frac{kN}{l}(\Delta k - \beta) + \lambda C \tag{21}$$

where β is the delayed neutron fraction, λ is the half-life of the delayed neutron precursors, and C is the concentration of the precursors. Solving this differential equation in a similar manner one obtains a solution with two terms, the second of which quickly decays leaving Equation 22.

$$P(t) = P_0 \frac{\beta}{\beta - \Delta k} e^{\frac{\lambda \Delta k}{\beta - \Delta k} t} \tag{22}$$

where the ratio of the delayed neutron fraction to the difference between the delayed neutron fraction and the change in reactivity leads to what is known as a prompt jump, or fast increase or decrease immediately following the change in reactivity. The prompt jump is followed by a stabilization period in the exponential term, as the delayed neutron precursor bank is built in.

Following a similar reactivity addition as described above, but with a delayed neutron fraction for fissile uranium-235, it may be noted that the prompt jump term causes an immediate increase in power. This is followed by a short stabilization period followed by an increase of the reactor power according to the exponential term, but with a much longer reactor period. This larger reactor period makes it possible to design regulating control systems better capable of responding to the required changes in core reactivity under both normal and accident operation.

2.1.6 Reactivity Coefficients

During unit operation, changes to the reactor power occur for several reasons. Some of these reasons include unit startup and shutdown as well as intentional and spurious changes during normal operation. Throughout power changes, the temperatures in the fuel, coolant, and moderator change. These changes impact the core reactivity and have a feedback effect on the power change. The combined effect of the temperature coefficients, along with the coefficient resulting from void formation or collapse along fuel channels, yield what is known as the power coefficient. The power coefficient can also be described as the total reactivity feedback resulting from a change in reactor power. The reactivity coefficients arise from the change in reactivity due to temperature and density changes, yielding the fuel temperature coefficient, the coolant temperature coefficient, the moderator temperature coefficient, and the coolant void reactivity coefficient. There are three primary reasons behind the reactivity changes that are represented by the coefficients: the Doppler Broadening effect, the spectrum hardening, and the density change which accompanies the change in temperature [38].

Doppler broadening occurs due to broadening of the resonance peaks described by the absorption cross section in uranium-238 shown in Figure 3. As seen in Figure 3 the resonance region consists of peaks where the probability of a certain interaction increases over a specific energy range. Doppler broadening occurs when the fuel temperature is increased. This causes the absorption peaks in the resonance region to broaden and causing the resonance escape probability to decrease as a result of this phenomenon [17].

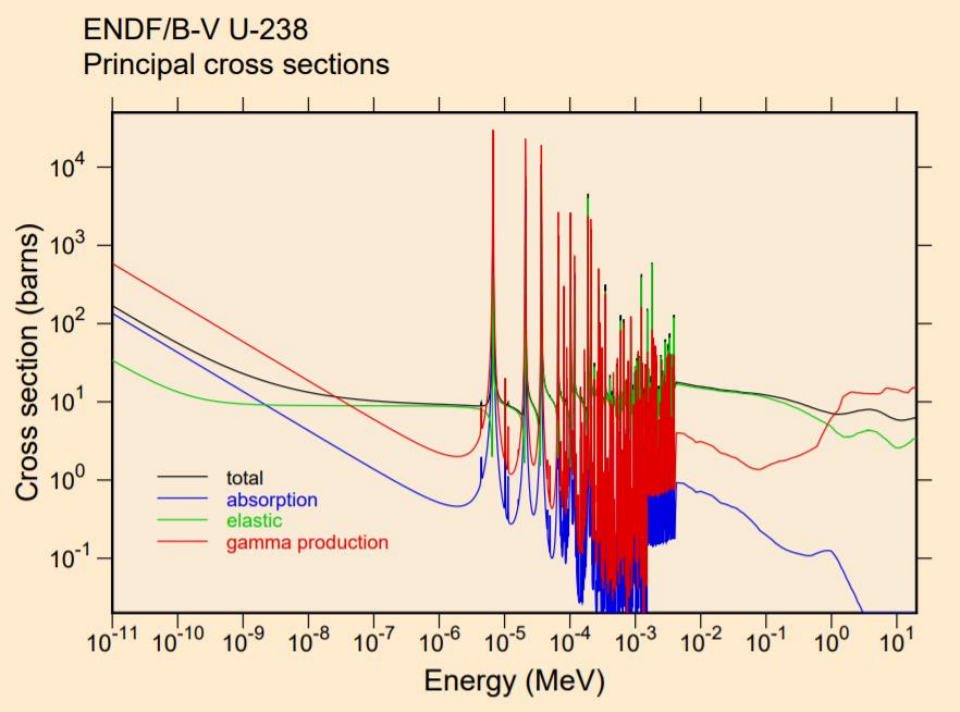

Figure 3: Uranium-238 principal cross sections [39].

CANDU reactors operate primarily on thermal neutrons inducing fission in uranium-235. Thermalization of neutrons requires a decrease in energy of the fast neutrons that are emitted by fission due to numerous elastic collisions within the moderator. The average neutron energy in a thermal reactor at equilibrium is approximately 0.025 eV (at 20 ^{o}C). Any change to the temperature in the moderator or surrounding systems will impact this equilibrium value causing shifts in the cross-section to energy spectrums for various isotopes [40]. The reactivity effect of this change is known as spectrum hardening and primarily impacts the thermal regeneration factor, or average number of neutrons created for each radiative capture occurring in the fuel [41].

Changes in temperature to a closed system have a proportional impact on density of the materials such as the fuel, the coolant, and the moderator. Namely, temperature increases results in a decrease in density. This applies to both the moderator and coolant systems in a CANDU reactor. A decrease in density of the heavy water

moderator impacts the macroscopic neutron absorption cross section, increasing the thermal utilization factor [41]. A decrease in the density of these fluids also results in decreases of the non-leakage probabilities for both fast and thermal neutrons This results in a decrease of the reactivity in a reactor as more neutrons can leak from the core [41].

The reactivity coefficient due to the fuel temperature in CANDU reactors is largely negative, approximately -15 μk $°C^{-1}$. For equilibrium fuel, corresponding to the fuel composition at refuelling equilibrium, it is less negative at approximately -4 μk $°C^{-1}$ [38]. The reactivity coefficient due to the moderator temperature in CANDU reactors is negative for fresh fuel, approximately -15 μk $°C^{-1}$, positive for fresh fuel with poison added to the moderator, approximately 70 μk $°C^{-1}$, and more positive for equilibrium fuel, approximately 90 μk $°C^{-1}$ [38]. The reactivity coefficient due to the coolant temperature in CANDU reactors starts negative for fresh fuel but becomes positive as full power steady state operating conditions are reached [38]. However, the overall reactivity coefficient due to the temperature remains negative in CANDU reactors. This implies that for a positive change in the reactor power, there will be an inherent negative reactivity feedback limiting the extent of the increase in reactor power.

The reactivity coefficient due to the void in CANDU reactors is positive, making it a topic of interest when conducting safety analysis and determining both depth and rate of reactivity insertion requirements for the shutdown systems in case of such an accident [38]. The reasoning behind the positive void reactivity coefficient in CANDU reactors and its relevance to this study is discussed further in Section 2.3.

2.2 CANDU Reactors

Understanding the reactor systems relevant to the current study and expected response to accident and operational conditions is of benefit to the reader. As such, a high-level overview of the operational and control systems of the CANDU reactor is provided in this section.

2.2.1 Operational Overview

Unique features of the CANDU pressurized heavy water reactor include horizontal fuel channel assemblies allowing for on-power refuelling, a high pressure D_2O coolant system and a low pressure D_2O moderator system, reactivity devices distributed throughout the low pressure moderator system, natural uranium fuel, and two independent and diverse shutdown systems [42]. A schematic diagram of the electricity generation at a nuclear station is shown in Figure 4.

At a high level, heat is created in the nuclear fuel and is removed by the pressurized heavy water coolant in the primary heat transport system. The heat removed from the nuclear reactor core is transferred to a conventional side system by means of a tube in shell heat exchanger, known as the steam generator, allowing steam to be created. The steam is passed to sets of turbines which rotate and are coupled to a

generator, producing electricity that is stepped up through a transformer and is passed to the grid.

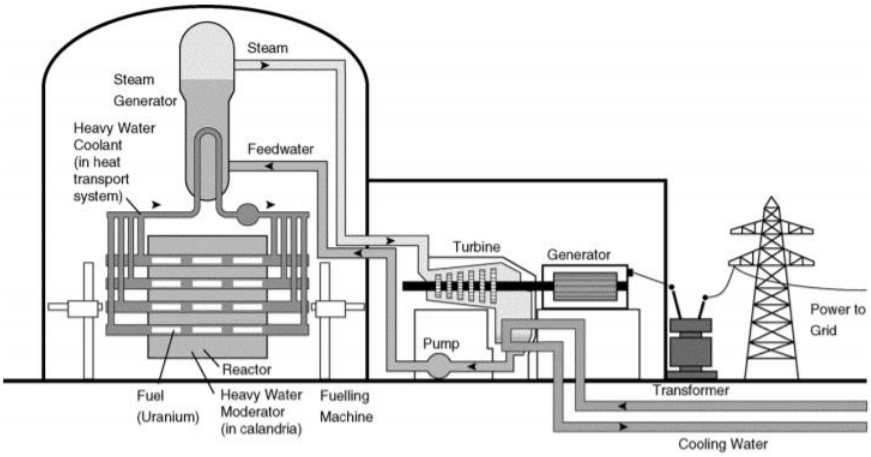

Figure 4: CANDU nuclear power plant schematic [23].

2.2.2 Steam Supply

The steam supply system, also known as the nuclear side of the station, is responsible for production of steam. The conventional side of the station is responsible for steam utilization. The nuclear side consists of horizontal fuel channel assemblies, primary heat transport, moderator, and steam generators [9].

The CANDU-6 fuelling system consists of three hundred eighty horizontal fuel channel assemblies, each filled with twelve fuel bundles [42]. The fuel bundle has thirty-seven fuel elements or fuel rods, each containing uranium dioxide pellets [43]. A CANDU thirty-seven element fuel bundle is shown in Figure 5.

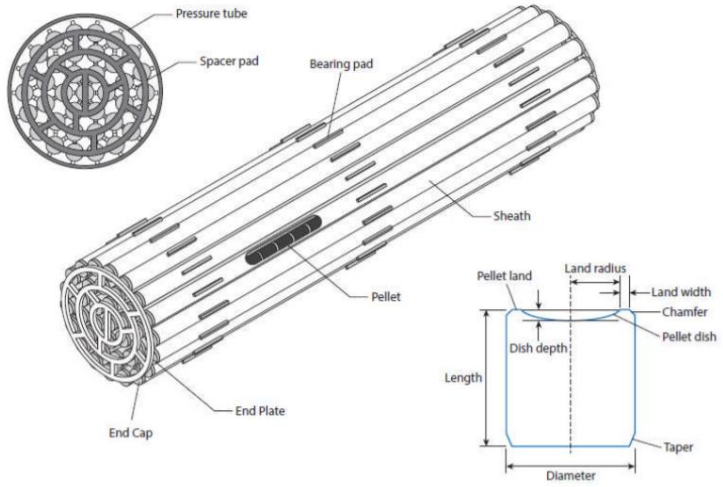

Figure 5: CANDU 37-element fuel bundle [44].

As seen in Figure 5, each fuel rod is made leak-tight by welded end caps which are themselves welded to end plates, thus holding the fuel elements in place. Bearing pads are spaced along the outside of the fuel bundle such that direct contact with the surrounding pressure tube in the fuel channel is minimized. The fuel elements in the bundle are made of zircalloy with a thin wall sheath, allowing the sheath to collapse around the fuel pellets for optimal heat transfer under normal operating conditions [45]. The fuel pellets in a typical thermal fuel element operate normally at a maximum centerline temperature slightly below 1500 ºC, while the sheath operates at 400 ºC (inside diameter) and 300 ºC (outside diameter). The temperature of the heat transport system water through each channel is between two hundred eighty and three hundred twenty degrees Celsius [46]. The fission products are contained within the fuel and sheath, acting as the first and second barriers within the defense in depth model for barriers to fission product release [43].

The primary heat transport system transfers heat created in the reactor core to the steam generators, providing the critical functions of removing heat and cooling the fuel. The primary heat transport system acts as the third barrier within the defense in depth model, keeping the fission products contained in the case where a fuel element may be damaged [43]. The system operates in two main loops through the reactor core, each with a set of pumps on either end [47]. Heavy water is pumped through the channels in the reactor core, removing heat, and through a set of boilers in the corresponding quadrant [47]. After the heavy water's heat is removed through the boilers, the heavy water coolant is passed back through the pumps on the opposite end of the core and through the fuel channels in the alternate direction to repeat the same cooling cycle.

The moderator system consists of high isotopic heavy water at approximately 99.9% D_2O, optimal for the slowing down, or moderating, of neutrons through elastic scattering [48] [49]. It is separate and distinct from the primary heat transport system, a design characteristic different from pressurized light water reactors [50]. The moderator system provides its own cooling function, as it removes a small portion of the reactor heat. It is credited as an ultimate heat sink in case of an accident where core cooling is lost and no makeup water is available [51]. The moderator system operates at low pressure and allows for reactivity devices to be inserted between the fuel channel assemblies for reactivity control as described in Section 2.2.3

There are three steam generators for each quadrant of the primary heat transport system as described above [42]. The purpose of the steam generators is to remove heat from the primary heat transport system and generate steam that is passed to the turbines. A light water system is used to feed the secondary side of the boilers, maintaining a certain level in each steam generator based on reactor operating conditions [51]. Loss of feedwater to the steam generators is an example of a loss of coolant accident as the primary heat transport system would have no heat sink, and temperatures in the reactor core would continually rise until an alternative method of heat removal is implemented or the unit is shut down.

2.2.3 Reactor Control

The reactor is controlled by the reactor regulating system (RRS). The RRS utilizes neutron flux measurement instruments to generate control signals. These control signals manipulate the reactivity control devices to change both the bulk and spatial core power distribution [42]. Long term reactivity control is attained through on-power refuelling while fast acting bulk and spatial control is through the liquid zone control system [45]. Flux flattening, xenon override, and the ability to provide additional positive or negative reactivity is attained through adjuster rods. These adjuster rods are located vertically in the low-pressure moderator between the fuel channels. Control absorbers are located above the core and are used for fast addition of negative reactivity [9]. A gadolinium nitrate injection system into the moderator is also available for addition of negative reactivity [52].

The fuelling system is the primary means by which long term reactivity control is maintained [45]. On average, eight to sixteen fuel bundles are replaced daily in two fuelling runs where fresh fuel bundles are pushed into a fuel channel of the core and an equal amount of spent bundles are removed at the opposite end of the same channel, ensuring that the core reactivity is maintained [45]. Bidirectional fuelling based on primary heat transport system flow direction enables axial flux flattening as shown in Figure 6.

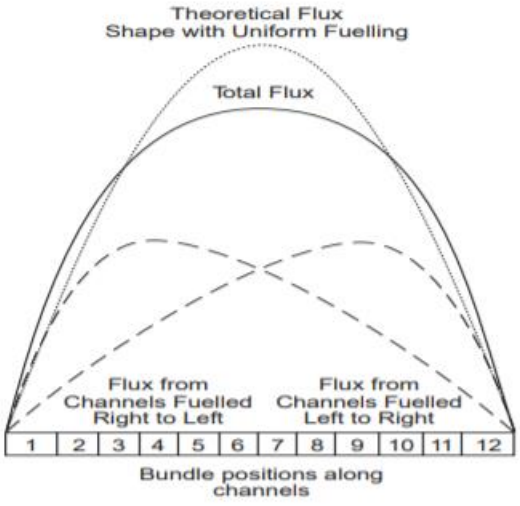

Figure 6: Axial flux flattening via bidirectional refuelling [53].

Many parameters are taken into consideration when selecting channels to refuel in the reactor. One of these considerations is called differential fuelling. Differential fuelling is determined by a calculation that takes different core regions into consideration, forcing high power channels close to the center of the core to be refueled more frequently [53]. This process inherently flattens the radial flux distribution. Refuelling causes localized flux increases and results in deviations from what is known as the reference or time-average flux shape [45]. The ratio of the difference between the actual channel power and its reference channel power is

called the channel power peaking factor (CPPF). The CPPF is used in the calibration of the neutron overpower protective system to ensure that adequate trip coverage is maintained [54].

The liquid zone control system consists of fourteen light water compartments distributed throughout the reactor core in seven axial zone pairs [52]. Light water has a relatively high neutron absorption cross section, meaning it has a high probability of absorbing a neutron upon interaction. The liquid zone levels are adjusted by the reactor regulating system to maintain a normalized flux distribution corresponding to the desired reactor power setpoint on a bulk level, and are also capable of adjusting spatially based on reactivity changes such as refuelling [45] [9]. Namely, when one of the axial zone pairs is fuelled into, a localized flux increase occurs. The regulating system then signals the liquid zone level for that axial pair to increase such that more neutrons are absorbed in that region. Based on normalization, this increase in liquid zone level on one side of the reactor results in a decrease to the axial zone pair on the opposite side. Channel selection for refuelling takes this behaviour into consideration to maintain radial balance across the reactor core.

The adjuster absorbers and control absorbers are made of similar material, typically stainless steel and cadmium, yielding a high macroscopic absorption cross section which makes them useful for neutron control such as the liquid zone control system [9]. Adjuster absorbers normally in core are inserted through guide tubes between the fuel channels in the low-pressure moderator system [52]. Adjuster absorbers are used for three primary purposes including the addition of positive reactivity in the core if required through removal, xenon override capability in case of a reactor trip, and flux flattening [42]. Flux flattening via the adjuster absorbers is shown in Figure 7.

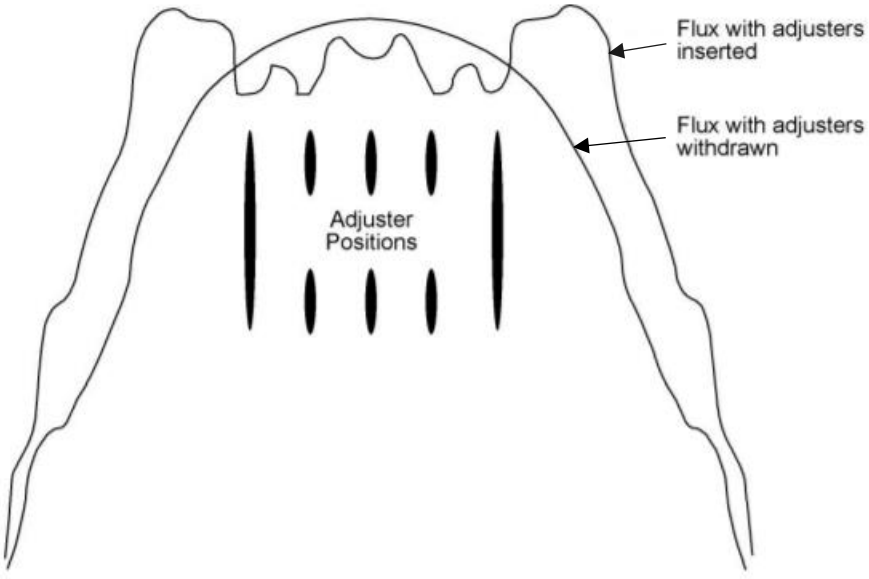

Figure 7: Radial flux flattening via adjuster rods [53].

In addition, control absorbers are located outside of the core and are capable of being rapidly inserted to reduce flux, and subsequently reactor power, in case of an abnormal unit condition requiring a fast power reduction [9].

Lastly, gadolinium or boron poison addition to the moderator is possible as a means of reducing core reactivity if required for power reduction or fuelling ahead. This is a process in which the reactor is fuelled above the normal liquid zone control range with moderator poison added to suppress the true liquid zone level. This process is used to compensate for extended periods of no fuelling [55].

The reactor regulating system controls all reactivity devices based on power error [9]. Power error is defined as the difference between the reactor power setpoint input by the unit operator and the true reactor power determined by power measurement instrumentation in-core [56]. The liquid zone control system is the primary means by which this power error is minimized. Any reactivity change required to minimize power error outside of the control of the liquid zones is handled by the adjuster and control absorbers [52].

2.2.4 Special Safety Systems

The special safety systems in the CANDU reactor are intended to ensure the control, cooling, and containment functions are maintained in any unit operating or accident state [10]. The four special safety systems include the shutdown systems, SDS1 and SDS2, along with emergency coolant injection (ECI), and the reactor containment [57].

SDS1 consists of vertical rods, similar to the control absorbers in that the material used is typically stainless steel and cadmium. The SDS1 rods are normally poised outside of the core [9]. The typical reactivity of the SDS1 rods is approximately -80 mk [9]. In case of a trip SDS1 will drop the rods into the core, shutting the reactor down [10].

SDS2 consists of horizontally assembled liquid injection nozzles in line with a pressurized nitrogen tank and a gadolinium nitrate solution for fast injection in case of an SDS2 trip [9]. The typical reactivity of the SDS2 liquid poison is approximately -300 mk [9]. In case of a trip, SDS2 will inject poison into the core, shutting the reactor down [10].

ECI consists of emergency water stored outside of the core [42]. In case of a loss of coolant accident ECI injects light water in high, medium, and low-pressure phases into the primary heat transport system quadrant headers to ensure core cooling is maintained [10].

The reactor containment consists of an epoxy lined concrete structure located around the reactor core [53]. The containment structure is maintained at a negative pressure, such that if fission products were to escape the first barriers including the fuel pellet, fuel sheath, and the primary heat transport system, they would still be constrained within the containment structure with controlled leakage [10].

2.3 Loss of Coolant Accidents

The loss of coolant accident is important in CANDU reactors as it defines the requirements for both reactivity rate and depth for the shutdown systems to effectively stop the transient resulting from the large positive void coefficient [57]. A small in-core break LOCA is limiting for reactivity depth, while a large break LOCA is limiting for rate of power increase [57]. The present study focuses on the large LOCA accident.

2.3.1 Accident Overview

The large loss of coolant accident involves a break in the primary heat transport system greater than twice the area of the largest feeder pipe [57]. As such, to be assessed as a large break LOCA the pipe failure must occur in large piping such as a reactor inlet or outlet header, rather than small piping such as the primary heat transport system pressure tubes in core. A schematic of the CANDU steam supply system outlining possible large break LOCA pipe failure locations is shown in Figure 8.

The large break LOCA results in a significant loss of system coolant into the containment and a rapid depressurization in the primary heat transport system. Voiding of the coolant results in an increase in reactivity, and subsequent power increase due to the positive void reactivity coefficient described in Section 2.3.2 until one or both shutdown systems actuate and shut down the reactor via a neutronic or process trip. High pressure emergency coolant injection is initiated following the accident, injecting light water into the primary heat transport system to maintain core cooling and fuel geometry. This is followed by medium pressure injection, and finally low-pressure recirculation of the water from the containment sumps back through the primary heat transport system.

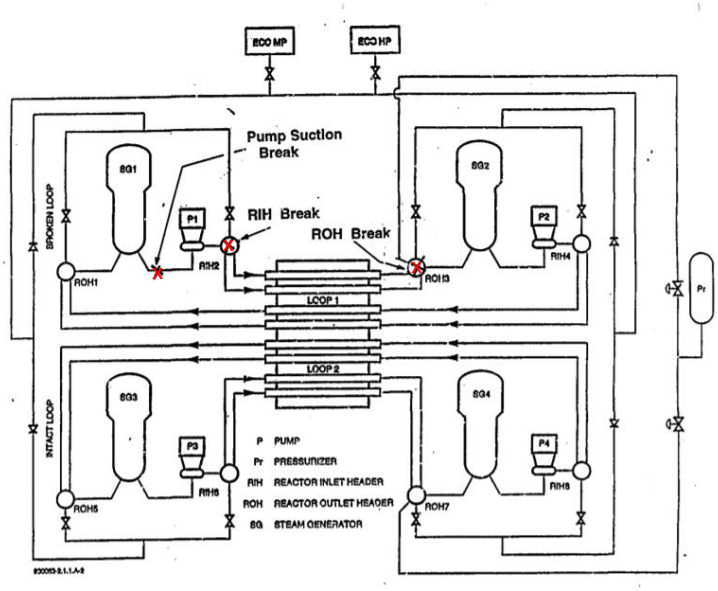

*Figure 8: CANDU large LOCA break location schematic as indicated by (**X**) [7].*

2.3.2 Physics Implications

Coolant voiding in CANDU reactors impacts the fast fission factor, the resonance escape probability, the thermal regeneration factor, and the thermal utilization factor [7]. The primary heat transport system coolant operates at a lower heavy water isotopic percentage than the moderator at approximately 99.0% and approximately 99.9% respectively [58], but still leads to some neutron moderation. Removing the coolant due to voiding means the ratio of fast to thermal neutrons that are present in the fuel is higher than under normal operating conditions, leading to more fast fission in uranium-238 and increasing the fast fission factor. In a similar manner, less neutrons are reaching thermal energies by passing through the resonance energy region. This means less neutrons are absorbed in that region, leading to an increase in the resonance escape probability because of the high purity moderator. These two factors are the primary reason for the positive void reactivity coefficient.

In addition, the spectrum hardening has a helpful effect in that it reduces the magnitude of the positive void coefficient by contributing negative reactivity, albeit significantly less than the positive effect just described. As the neutrons reenter the fuel through the voided coolant from the moderator, the temperature causes a decrease in the thermal regeneration factor η. As such, a high isotopic coolant minimizes the positive reactivity contribution due to voiding. One way to understand this phenomenon is that having an increase in coolant isotopic means more neutrons are thermalized in the coolant and not the moderator, reducing the dependency on thermalization in the moderator to maintain a critical core state. In this case, if coolant is suddenly lost, the number of neutrons available in the moderator is low when compared to a low isotopic coolant, which would require a higher neutron economy in the moderator to maintain a critical core.

The overall reactivity insertion resulting from full core coolant voiding is approximately 13-15 mk [7]. Safety analysis determines acceptable operating states based on defining the safe operating envelope. All normal operating conditions fall within requirements such that the shutdown systems can actuate in time and with enough reactivity to maintain control of the reactor [57].

2.3.3 Safety Analysis

The primary concern during a large loss of coolant accident is the shutdown system actuation time. Under the worst-case unit conditions, the shutdown systems must act in time to suppress the positive reactivity transient such that the accident is terminated within the reactivity limits and has enough reactivity depth to maintain the reactor in a subcritical state [7] [9]. Physics analyses are required, coupling both core diffusion models with thermalhydraulic codes to determine how the core power distribution changes during the accident in order to determine the upper bound of the safe operating envelope based on shutdown system requirements. Shutdown system actuation is expected within the first second of the accident, and as such this is typically the time period that is focused on within these analyses [7] [9] [57]. Following shutdown system actuation, the emergency coolant injection system is expected to maintain core cooling and the analysis transitions to cooling

requirements to maintain the fuel geometry and, in the case of an emergency coolant injection failure, severe accident management [9] [57].

2.4 Burnable Neutron Absorbers

The use of burnable neutron absorbers in CANDU fuel is a novel concept that involves changing the specifications of the fuel bundle. Research conducted to date has demonstrated some of the ways in which burnable neutron absorbers may improve fuel performance. This section provides an overview of current research status and outlines the implications of burnable neutron absorber addition in the current study.

2.4.1 Concept Overview

A burnable neutron absorber is a nuclide that has a high probability of absorbing a neutron, meaning it has a high neutron absorption cross section. After radiative capture the product becomes a nuclide which often has little interaction with neutrons and therefore little impact on the core reactivity. When assessing burnable neutron absorbers for selection, numerous parameters must be considered. Some of these parameters include cross sections, nuclear reaction products, half-life, distribution within the bundle, and concentration or amount of the burnable neutron absorber to be implemented. Topics of interest in the CANDU industry which have been studied to date include mitigation of the refuelling and plutonium transients in fuel, impact on core reactivity and burnup during refuelling for an extended period, and impact on end-flux peaking.

Two well-known refuelling transients are related to reactivity increases immediately following refuelling and after thirty to fifty full power days in core. The first transient is known as the xenon-free effect, due to the absence of the neutron absorbing fission product xenon-135 in the fresh fuel. The second transient is a result of plutonium-239 build-up from neutron absorption in uranium-238. These refuelling transients cause localized flux peaks in the core, impacting the design or time reference flux shape and subsequently reducing margins to SDS1 and SDS2 trip on the neutron overpower system. In a study conducted by *Chan et al*. it was concluded that ~180 mg Gd_2O_3 and ~1000 mg Eu_2O_3, distributed uniformly in the CANLUB layer of each fuel bundle, are enough to suppress the refuelling transient and lower the axial plutonium peak, with a negligible discharge burnup penalty [11]. The selection of Gd_2O_3 was based on gadolinium-155 and gadolinium-157 burn-out rate closely mirroring that of xenon-135, matching closely to the time range required to mitigate the refuelling transient. Eu_2O_3 selection was based on its extended chain of stable isotopes with high thermal absorption cross sections [59].

In additional studies, the use of burnable neutron absorbers was investigated to determine the impact on end flux peaking and extended refuelling simulations respectively [13] [12]. End flux peaking occurs between fuel bundles positioned end to end within the fuel channel, resulting in elevated power and subsequently elevated temperatures in this region [13]. This study concluded that Eu_2O_3 was the best burnable neutron absorber to mitigate the effect of end flux peaking due to its high thermal absorption cross section along with its extended duration in core from its

chain of stable isotopes with high thermal absorption cross sections [13] [59]. Additionally, the extended refuelling study concluded that channel powers decreased when burnable neutron absorbers Gd_2O_3 and Eu_2O_3 were added to the fuel relative to simulations based on natural uranium fuel that does not contain burnable neutron absorbers [12]. The radial form factor (RFF) and channel power peaking factors were also shown to decrease in the refuelling study when burnable neutron absorbers were added [12].

2.4.2 Implication in Current Study

The primary research objective of this study is to demonstrate that the addition of burnable neutron absorbers mitigates the effect of coolant voiding on CANDU 37-element fuel. The novelty of this thesis relies on the demonstration that the use of a small amount of burnable neutron absorbers could mitigate LOCA consequences. As discussed in Section 2.3 a large positive reactivity insertion is expected following a large loss of coolant accident. This study aims to demonstrate that the magnitude of this reactivity change, and corresponding power pulse, is less significant when burnable neutron absorbers are added to the fuel.

3 Methodology

3.1 Physics Codes

Industry standard physics codes are used to calculate the flux and power distribution in the reactor core. These codes are used for both safety and operational analyses. The two codes focused on in this study are WIMS-AECL [15] and RFSP-IST [16], with computations for reactivity device incremental cross sections carried out using DRAGON-IST [60]. The nuclear data library used in each of these codes is ENDF/B [61].

3.1.1 WIMS-AECL

WIMS-AECL is a two-dimensional deterministic lattice code that primarily uses the collision probability theory and a multigroup solution to the integral form of the neutron transport equation. It is used to calculate cell homogenized macroscopic cross section fuel tables which can be used in diffusion codes. The form of the neutron transport equation solved using WIMS-AECL is shown below in Equation 23:

$$[\Omega \cdot \Delta + \Sigma_t(r,E)]\Psi(\mathrm{r},\mathrm{E},\Omega) - \int_0^\infty dE' \int_{4\pi} d\Omega' \Sigma_s(r,E' \to E, \Omega' \to \Omega)\Psi(\mathrm{r},\mathrm{E}',\Omega')$$

$$= \chi(\mathrm{E}) \int_0^\infty dE' \int_{4\pi} d\Omega' \nu(r,E')\Sigma_f(r,E')\Psi(r,E',\Omega') \qquad (23)$$

where $\Psi(r,E,\Omega)$ is the neutron flux distribution, r = (x,y,z) is the position vector specified by cartesian coordinates, $\Omega(\Omega_x, \Omega_y, \Omega_z)$ is the direction vector specified by azimuth and polar angles ϕ and θ, E is the neutron energy, $\Sigma_t(r,E)$ is the total macroscopic cross section at energy E, $\Sigma_f(r,E')$ is the macroscopic fission cross section at energy E', $\chi(E)$ is the fission spectrum, $\nu(r,E)$ is the number of secondary neutrons per fission at energy E', $\Sigma_s(r,E'\rightarrow E,\Omega'\rightarrow\Omega)$ is the scattering cross section from and to the specified energy and direction, $\nabla = i\partial/\partial x + j\partial/\partial y + k\partial/\partial z$ is the spatial

gradient and the double integral represents angular integration over a unit sphere [62].

Overall, Equation 23 is governed by the balance of neutron production and neutron loss terms. Neutron production results from the second and third terms due to fission at a specific energy and position in the third term and scattering resulting in a neutron at the required energy and position in the second term. Neutron loss results from absorption or leakage in the first term.

WIMS-AECL can also provide fuel burnup and leakage calculations. The WIMS-AECL input file takes user-defined geometric and material parameters for four main regions including the fuel, the clad, the coolant, and the moderator as shown in Figure 9.

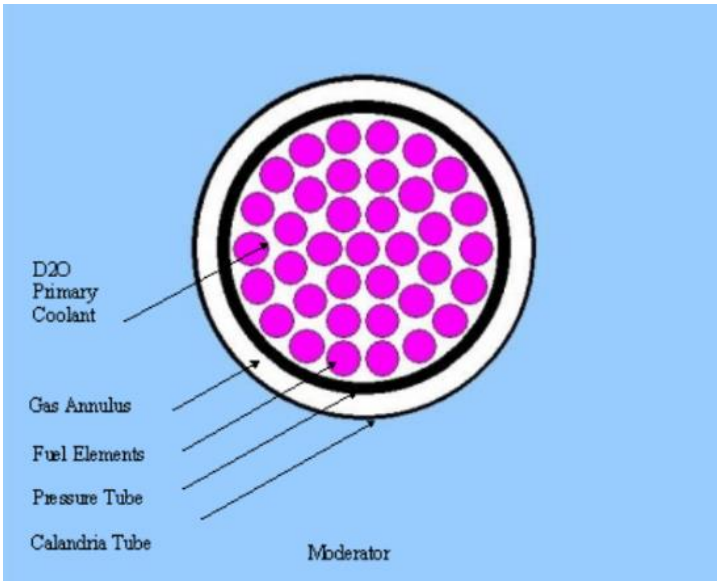

Figure 9: CANDU lattice cell as defined in WIMS-AECL input files [63].

From user input, WIMS-AECL relies on evaluated nuclear reaction data libraries such as ENDF/B to extract microscopic cross sections based on the materials defined to accumulate macroscopic cross sections. Two types of fuel tables are required in this study including uniform parameter and simple cell model (SCM) fuel tables.

Uniform parameter fuel tables generated using WIMS-AECL account only for changes in lattice irradiation, not changes to local parameters such as coolant density and temperature, moderator temperature, and fuel temperature. This makes the uniform parameter models useful for simple computations, such as analyses related to k_∞ where all local parameters are held constant. For the purposes of this study, uniform parameter fuel tables are used to establish initial steady-state core conditions in RFSP-IST as significant changes to any of the local parameters are not required during normal unit operation.

Simple cell model fuel tables account for changes to local parameters such as coolant density and temperature, moderator temperature, and fuel temperature, along with

irradiation. This type of a fuel table is useful for models requiring changes in these parameters, such as transient analyses with varying thermalhydraulic conditions, as is the case in the RFSP-IST CERBERUS module in this study. Effectively what the simple cell model allows the user to do is define a range of conditions, calculating cross sections for each combination of varied parameters for use in diffusion code simulations.

3.1.2 RFSP-IST

RFSP-IST is a full core diffusion code that utilizes the fuel tables created by WIMS-AECL, extrapolating the results of the cell homogenized cross sections to create a three-dimensional core model. The goal of RFSP-IST is to calculate parameters related to full core neutronics, most importantly core power distribution using the two-group approximation to the steady-state neutron diffusion equation shown in Equation 24:

$$-\nabla \cdot D_1(r)\nabla\phi_1(r) + \big(\Sigma_{a1}(r) + \Sigma_{12}(r)\big)\phi_1(r) - \Sigma_{21}(r)\phi_2(r) - \frac{1}{k_{eff}}\Big(\nu\Sigma_{f1}(r)\phi_1(r) + \nu\Sigma_{f2}(r)\phi_2(r)\Big) = 0$$

$$-\nabla \cdot D_2(r)\nabla\phi_2(r) + \big(\Sigma_{a2}(r) + \Sigma_{21}(r)\big)\phi_2(r) - \Sigma_{12}(r)\phi_1(r) = 0 \qquad (24)$$

where $\phi_1(r)$ is the group-1 neutron flux, $\phi_2(r)$ is the group-2 neutron flux, $\Sigma_a(r)$ is the group-1 fast neutron absorption cross section, $\Sigma_{a2}(r)$ is the group-2 fast neutron absorption cross section, $\nu\Sigma_{f1}(r)$ is the fast group production cross section, $\nu\Sigma_{f2}(r)$ is the thermal group production cross section, $\Sigma_{12}(r)$ is the down-scatter cross section for neutrons passing from the fast to thermal group, $\Sigma_{21}(r)$ is the up-scatter cross section for neutrons passing from the thermal to fast group, $D_1(r)$ is the group-1 fast diffusion coefficient, $D_2(r)$ is the group-2 thermal diffusion coefficient, and k_{eff} is the multiplication constant [64].

RFSP-IST uses macroscopic cross section fuel tables derived from lattice codes such as WIMS-AECL, and incremental cross sections for modelling reactivity devices from supercell codes such as DRAGON-IST to create its reactor model. The RFSP-IST input file defines the entire geometry of the reactor core, including channel assembly and reactivity device location. RFSP-IST has the capability to model fast transients, such as a large loss of coolant accident, using the improved quasi-static method in the CERBERUS module to perform spatial neutron kinetics, as utilized in the current study.

The CERBERUS module in RFSP-IST solves the time-dependent neutron diffusion equation in two energy groups and three dimensions as shown in Equation 25:

$$\big(-M + F_p\big)\phi(r,t) + \sum_{g=1}^{G} \lambda_g \, C_g(r,t)\Big|_0^1 = \frac{1}{v}\frac{\partial\phi(r,t)}{\partial t} \qquad (25)$$

where M is the leakage, absorption, and scattering matrix, F_p is the prompt production matrix, $C_g(r,t)$ is the space-time concentration of group g delayed neutron precursor with decay constant λ_g, and $1/v$ is the inverse speed matrix [64].

The improved quasistatic method involves the factorization of the flux into a space-independent time-varying amplitude and shape function which is dependent of both time and space. This creates a coupled system of equations for the shape, amplitude, and precursor concentrations which allows the time dependent solution to be obtained for each time step in the transient simulation [64].

3.2 User Codes

A series of user codes were developed to automate the process of generating input files, running the physics code executable files, and post-processing and visualization of the output file data. A flow diagram of the relationships between each of the codes is shown in Figure 10 and is described in this section. Select samples of the Octave and BATCH scripts are included in Appendix item A.

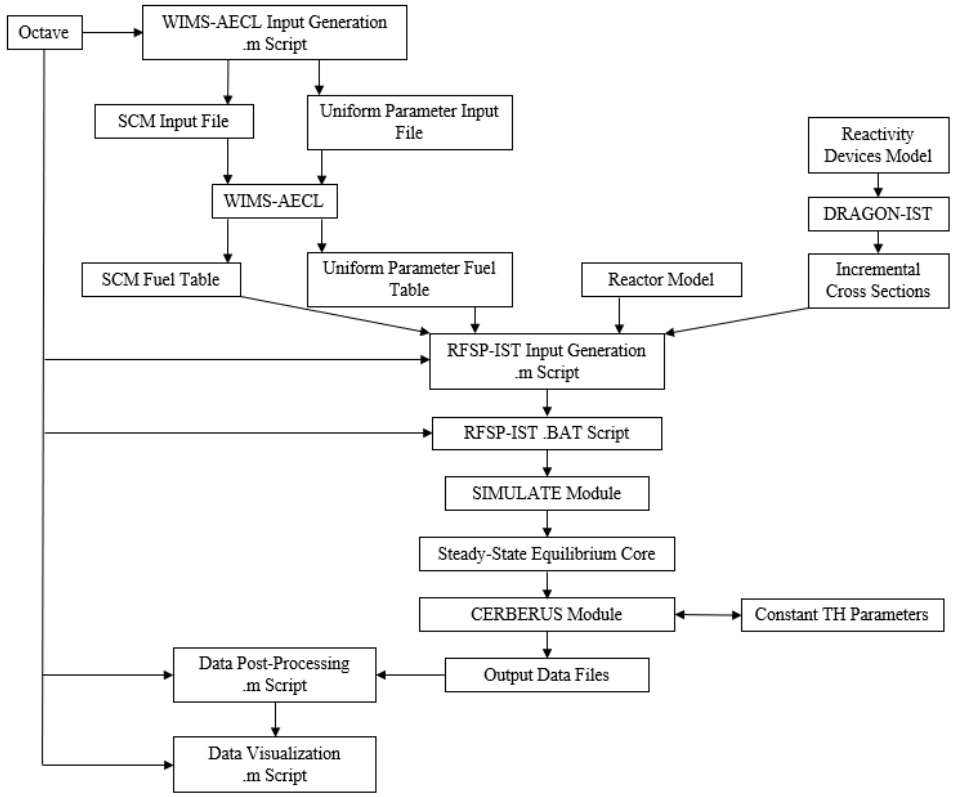

Figure 10: User and IST codes flow diagram.

3.2.1 Input File Generation

The input file generation codes are executed for creation of WIMS-AECL uniform parameter and simple cell model input files. The script reads in a template input file in each form and writes a new file based on material specifications as well as local parameters including fuel temperature, coolant temperature and density, and

moderator temperature. The input file generation scripts reduce error probability and add consistency to troubleshooting in case of errors.

3.2.2 Physics Code Execution

The physics code execution files write .BAT script files for the Windows system to execute. This allows each of the IST physics codes to be executed from the Octave script rather than individually through the command line.

3.2.3 Output File Post-Processing

The output file post-processing scripts parse each output file. This code is used to extract useful parameters including total core power, channel powers, maximum channel power and location, and maximum bundle power and location.

3.2.4 Output File Visualization

The output file visualization script allows the parameters extracted from the output file post-processing scripts to be plotted in both two and three dimensions for ease of visualization. This script also creates summary tables for each case including maximum core, channel, and bundle powers for comparison.

3.3 Model

This section provides an overview of the model used during each of the Phase One and Phase Two studies outlined in Section 4. The fuel and reactor model are described in this section along with simulation uncertainty. Further details regarding the specifics of the two phases are provided respectively in Section 4.1 and Section 4.2.

3.3.1 Overview

The RFSP-IST SIMULATE module is used to establish the initial steady-state core power distribution. The RFSP-IST CERBERUS module then simulates an inlet header pipe break based on changing thermalhydraulic core conditions and performs calculations for the transient power response in 0.1s intervals up to 0.3s. This short time range allows one to analyze the fast power pulse resulting from the accident prior to shutdown system actuation. This methodology also allows one to analyze the impact that the addition of burnable neutron absorbers has on the initial power shift at 0.1s due to the negative CANDU fuel temperature coefficient, and the subsequent transient progression due to the large CANDU void reactivity coefficient.

Based on the WIMS-AECL and RFSP-IST models developed, a generic CANDU-6 core is modeled, utilizing thirty-seven element fuel with twelve fuel bundles per channel, and three hundred eighty channels making up the reactor core. The thermalhydraulic parameters input to the CERBERUS module for each channel in the core are shown in Figure 11, where the west side corresponds to the left side of the reactor when looking at the cross sectional view provided.

	1	2	3	4	5	6	7	8	9	10	11	12	13	14	15	16	17	18	19	20	21	22	
A									8	3	8	1	2	1									A
B						8	3	8	1	2	1	8	3	8	1	2	1						B
C					8	3	8	3	8	3	8	1	2	1	2	1	2	1					C
D				8	3	8	3	8	3	4	3	2	1	2	1	2	1	2	1				D
E			8	3	8	3	8	3	4	3	5	1	2	1	2	1	2	1	2	1			E
F			3	8	3	4	3	4	3	4	3	2	1	2	1	2	1	2	1	2			F
G		3	9	3	9	3	4	3	4	3	4	1	2	1	2	1	2	1	2	1	2		G
H		9	3	9	3	4	3	4	3	4	3	2	1	2	1	2	1	2	1	2	1		H
J	9	3	9	3	5	3	5	3	5	3	4	1	2	1	2	1	2	1	2	1	2	1	J
K	3	9	3	4	3	5	3	5	3	5	3	2	1	2	1	2	1	2	1	2	1	2	K
L	9	3	9	3	4	3	4	3	5	3	4	1	2	1	2	1	2	1	2	1	2	1	L
M	3	9	3	6	3	6	3	6	3	7	3	2	1	2	1	2	1	2	1	2	1	2	M
N	9	3	9	3	6	3	6	3	7	3	7	1	2	1	2	1	2	1	2	1	2	1	N
O	3	9	3	9	3	6	3	6	3	7	3	2	1	2	1	2	1	2	1	2	1	2	O
P		3	9	3	9	3	6	3	6	3	7	1	2	1	2	1	2	1	2	1	2		P
Q		10	3	10	3	6	3	6	3	7	3	2	1	2	1	2	1	2	1	2	1		Q
R			10	3	10	3	6	3	6	3	7	1	2	1	2	1	2	1	2	1			R
S			3	10	3	10	3	6	3	7	3	2	1	2	1	2	1	2	1	2			S
T				3	10	3	10	3	6	3	7	1	2	1	2	1	2	1	2				T
U					3	10	3	10	3	10	3	2	1	2	1	2	1	2					U
V						3	10	3	10	3	10	1	2	1	2	1	2						V
W									3	10	3	2	1	2									W
	1	2	3	4	5	6	7	8	9	10	11	12	13	14	15	16	17	18	19	20	21	22	

Figure 11: Thermalhydraulic nodal inputs based on break location (west side corresponds to the left side). Each node value contains a set of thermalhydraulic data including coolant temperature and density, and fuel temperature for each bundle within the fuel channel at each time step in the transient simulation. A value of 10 represents the most significant changes in the thermalhydraulic parameters, namely the greatest loss of coolant through the channel as a result of the break.

As seen in Figure 11, a value of ten indicates a significant loss of flow at this particular node, whereas a value of one indicates minimal loss of flow, implying that the inlet header break has occurred in the southwest primary heat transport system quadrant. Each node defined corresponds with a set of data for each fuel bundle including fuel temperature, coolant density, and coolant temperature.

To break down each simulation performed using this model with respect to Section 4, Table 1 below was created for reference:

Table 1: Summary of simulations performed in Section 4.

Model Simulation Summary		
Phase	Section	Simulation
One	4.1.1	CERBERUS Base Test Case
	4.1.2	Generic CANDU 6 Natural Uranium (NU)
	4.1.3	Generic CANDU-6 with 1 mg Gd_2O_3 added
Two	4.2.1	Fresh NU Fuel
	4.2.2	Fresh Fuel with Evenly Distributed 180 mg Gd_2O_3 and 1000 mg B_2O_3 in each element
	4.2.3	Fresh Fuel with 180 mg Gd_2O_3 and 1000 mg B_2O_3 in the center pin
	4.2.4	Equilibrium NU Fuel
	4.2.5	Equilibrium Fuel with Evenly Distributed 180 mg Gd_2O_3 and 1000 mg B_2O_3 in each element
	4.2.6	Equilibrium Fuel with 180 mg Gd_2O_3 and 1000 mg B_2O_3 in the center pin
	4.2.7	Startup Following Long Shutdown NU Fuel
	4.2.8	Startup Following Long Shutdown Fuel with Evenly Distributed 180 mg Gd_2O_3 and 1000 mg B_2O_3 in each element
	4.2.9	Startup Following Long Shutdown Fuel with 180 mg Gd_2O_3 and 1000 mg B_2O_3 in the center pin

3.3.2 Simulation Uncertainty

As is the case in studies of this nature, it is important to account for simulation uncertainty when considering results. In order to come up with a reasonable approximation for simulation uncertainty, results from several core simulations for the various modules available in the deterministic RFSP-IST are benchmarked against station data as well as stochastic codes such as MCNP [65].

For the purpose of the improved quasistatic CERBERUS module, specifically the delayed and prompt neutron kinetics involved in the calculations, results from the simulation output were compared against a planned trip test and subsequent flux rundown at the Point Lepreau Nuclear Generating Station [64]. The results indicated that the calculations from CERBERUS were within measurement uncertainty for this case. In addition, for void reactivity calculations, it was determined that WIMS-AECL and RFSP-IST overestimate in calculation by 1.6-2.0 mk, with an

uncertainty of +/- 1.1 mk [64]. This result was attributed to the fundamental nuclear data used in the ENDF libraries, the resonance treatment in WIMS-AECL, and the approximations made in the fuel bundle input model.

For computations related to full CANDU core simulations for channel powers and bundle powers, benchmarking was performed against the stochastic code MCNP Monte Carlo simulations. This study determined that the average percent difference for calculated channel powers was within 2.6% and for calculated bundle powers it was within 3.5% [64].

The simulation uncertainties documented in this section are indicative of inherent bias associated with the physics computations performed. This bias is distinct from the uncertainty which propagates from the modeling and experimental error in the microscopic cross sections used by WIMS-AECL. The propagation of said uncertainties was deemed outside the scope of this study. The results presented throughout this study are to upwards of five significant digits, with the expectation that any propagated uncertainty falls within the inherent computational bias in WIMS-AECL and RFSP-IST.

4 Results

4.1 Phase One Results

For the purpose of the preliminary analysis outlined in this section, three separate simulations were performed. The first consists of the RFSP-IST test case which was used in the development of the input and output file processing scripts to establish a consistent format for the subsequent simulation analyses. This simulation was performed for an equilibrium core. The second is the same RFSP-IST core simulation with all-natural uranium fuel modeled in WIMS-AECL to serve as a base case for the simulation with burnable neutron absorbers to be compared against. The third uses 1 mg Gd_2O_3 distributed throughout the bundle to establish that the uniform parameter and simple cell fuel tables are being generated and implemented in a working model and serves as a preliminary comparison. From this model, the expected change to the flux shape based on the addition of Gd_2O_3 may be analyzed. The second and third simulations were conducted for a fresh core with no burnup.

4.1.1 RFSP-IST CERBERUS Test case

Absolute core channel powers were computed, in kW, for each time step in the hypothetical large loss of coolant accident simulation. Case 1 corresponds to the initial steady-state power distribution at 0s, Case 2 at 0.1s following the hypothetical large loss of coolant accident, Case 3 at 0.2s, and Case 4 at 0.3s as seen in Figure 12.

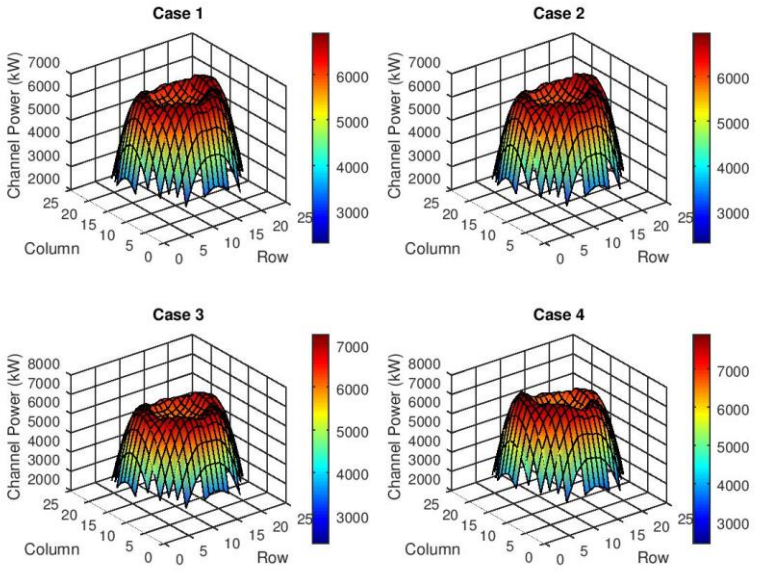

Figure 12: LLOCA transient test case absolute results from RFSP-IST. Case 1 corresponds to the time at 0s, Case 2 at 0.1s, Case 3 at 0.2s, and Case 4 at 0.3s. Channel powers shown are in units of kW and channel location in the core is depicted by the row and column along the x and y axis respectively. A summary of key parameters for each of the time steps as the transient progresses is provided in Table 2.

From Case 1 to Case 2, it may be noted that a shift in power away from the break region of the core is experienced. It is expected that this is a result of the negative fuel temperature coefficient coming in faster than the void coefficient and causing a decrease in power in the portion of the core experiencing the loss of coolant. From Case 2 to Case 3 the power distribution begins to shift back toward the break side of the core, and from Case 3 to Case 4 the power has fully shifted to the break region. It may also be noted that the magnitude of the power change increases as the time steps progress, the most significant being from Case 3 to Case 4 where the highest channel powers are in the range of 7000-8000 kW. Significant unit parameters were extracted from these simulations and are summarized in Table 2.

Table 2: Test case absolute results summary. Core Power (sum of all channel powers) in MW, Maximum Channel Power in kW, and Maximum Bundle Power in kW are provided from RFSP-IST for each time step in the LLOCA simulation.

Test Case				
Parameter	Initial Steady-State	Transient t=0.1s	Transient t=0.2s	Transient t=0.3s
Core Power (MW)	2061.4	2070.8	2129.2	2270.8
MCP (kW)	6915.9	6967.3	7235.1	7906.9
MBP (kW)	781.2	788.3	813.0	912.8

It may be noted that the total reactor power increases at every time step in the transient, as does the maximum in core channel and bundle power. As expected, the maximum channel and bundle powers shift away from, and then toward the break side of the core throughout the simulation.

For the purpose of comparing between different runs, a channel power difference calculation was performed for each case in the simulation relative to the initial steady state power distribution. The nomenclature implies Case 11 represents the difference between Case 1 relative to Case 1, and as such returns a flat delta power distribution. Case 21 represents Case 2 less Case 1, Case 31 is Case 3 less Case 1, and Case 41 is Case 4 less Case 1 as shown in Figure 13.

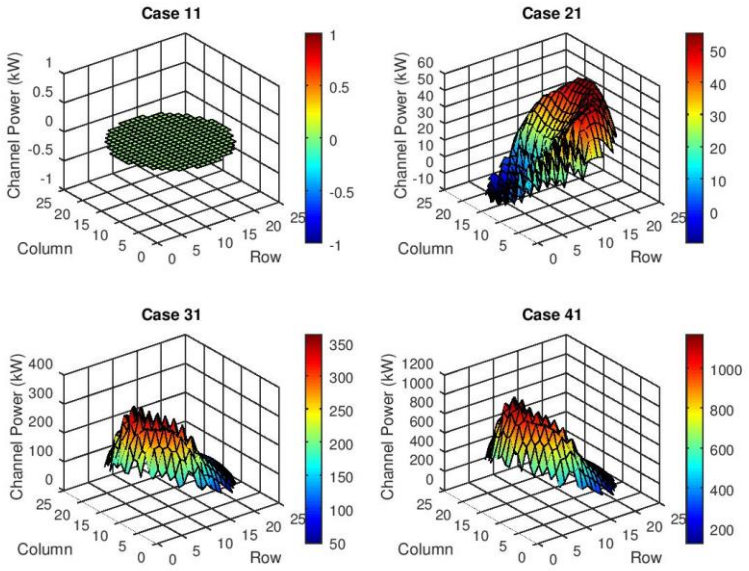

Figure 13: LLOCA transient test case difference results from RFSP-IST. Case 11 corresponds to the time at 0s, Case 21 at 0.1s, Case 31 at 0.2s, and Case 41 at 0.3s. Changes in channel power are shown are in units of kW and channel location in the core is depicted by the row and column along the x and y axis respectively. A summary of key parameters for each of the time steps as the transient progresses is provided in Table 3.

Rather than looking at absolute channel powers to gauge core power distribution, the difference in channel power relative to the initial steady-state distribution allows one to visualize how the transient is progressing during the simulation. Results in this case are in line with expectations, given the initial reduction in the neutron flux in the break quadrant of the core and subsequent increase throughout the following steps.

The information gathered through the difference calculation is summarized in a similar manner in Table 3.

Table 3: Test case difference results summary. Change in Core Power (sum of all channel powers) in MW, Change in Maximum Channel Power in kW, and Change in Maximum Bundle Power in kW, relative to the initial steady-state power distribution, are provided from RFSP-IST for each time step in the LLOCA transient simulation.

Test Case			
Parameter	Transient t=0.1s	Transient t=0.2s	Transient t=0.3s
Δ Core Power (MW)	9.4	67.8	209.4
Δ MCP (kW)	51.4	319.2	991.0
Δ MBP (kW)	7.1	31.8	131.6

4.1.2 CANDU-6 Natural Uranium

In the first simulation, an original thirty-seven element CANDU fuel bundle was modelled and used in the RFSP-IST simulations to act as a base case for the burnable neutron absorber cases to be compared against. The resulting core power distribution is shown in Figure 14.

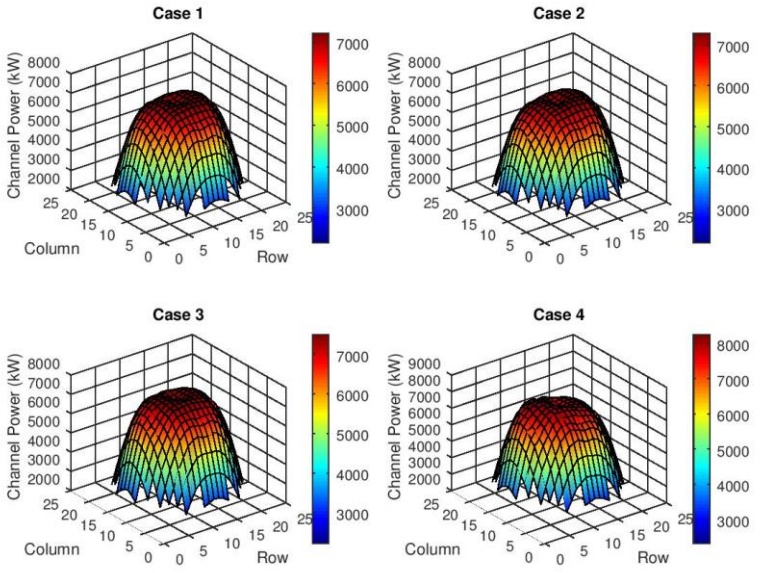

Figure 14: LLOCA transient natural uranium absolute results from RFSP-IST. Case 1 corresponds to the time at 0s, Case 2 at 0.1s, Case 3 at 0.2s, and Case 4 at 0.3s. Channel powers shown are in units of kW and channel location in the core is depicted by the row and column along the x and y axis respectively. A summary of key parameters for each of the time steps as the transient progresses is provided in Table 4.

It may be noted that the original thirty-seven element fuel flux distribution is less peaked than the RFSP-IST test case. It is expected that this is a result of no depleted

fuel being used in this core. It may also be noted that a similar change in the flux distribution is encountered, shifting away from the break region of the core and transitioning back to the break side as time progresses.

A summary of significant unit parameters is included in Table 4.

Table 4: Natural uranium absolute results summary. Core Power (sum of all channel powers) in MW, Maximum Channel Power in kW, and Maximum Bundle Power in kW are provided from RFSP-IST for each time step in the LLOCA transient simulation.

Natural Uranium				
Parameter	Initial Steady-State	Transient t=0.1s	Transient t=0.2s	Transient t=0.3s
Core Power (MW)	2061.4	2073.5	2139.3	2292.8
MCP (kW)	7220.1	7290.4	7498.2	8258.4
MBP (kW)	752.3	760.5	808.3	895.6

It may be noted that the maximum channel and bundle powers are for fuel channels closer to the center of the core, a result of the differing initial steady-state flux distribution.

The difference in channel powers for each step of the simulation relative to the original steady-state power distribution is shown in Figure 15.

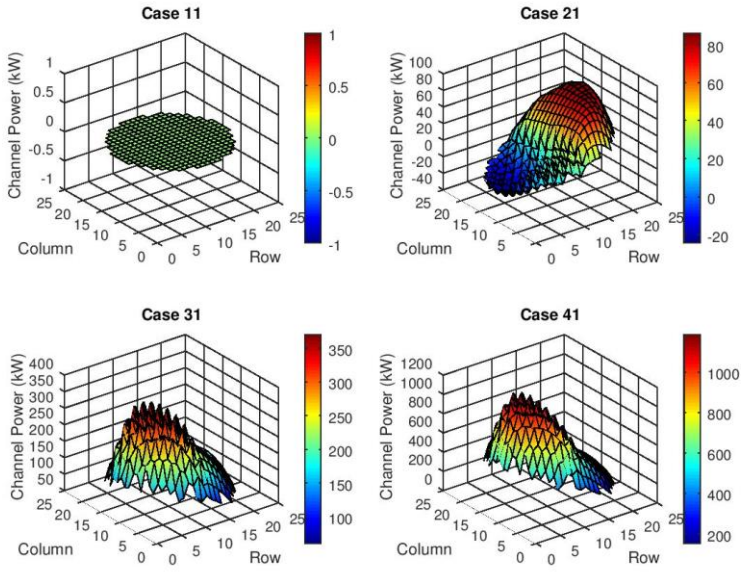

Figure 15: LLOCA transient natural uranium case difference results from RFSP-IST. Case 11 corresponds to the time at 0s, Case 21 at 0.1s, Case 31 at 0.2s, and Case 41 at 0.3s. Changes in channel power are shown are in units of kW and channel location in the core is depicted by the row and column along the x and y axes.

Comparing Figure 15 with Figure 13, it may be noted that a very similar behaviour is encountered between the two models. This is to be expected as each model is made up of primarily natural uranium fuel.

A summary of the data is shown in Table 5.

Table 5: Natural uranium difference results summary. Change in Core Power (sum of all channel powers) in MW, Change in Maximum Channel Power in kW, and Change in Maximum Bundle Power in kW, relative to the initial steady-state power distribution, are provided from RFSP-IST for each time step in the LLOCA transient simulation.

Natural Uranium			
Parameter	Transient t=0.1s	Transient t=0.2s	Transient t=0.3s
Core Power (MW)	12.1	77.9	231.4
MCP (kW)	70.3	278.1	1038.3
MBP (kW)	8.2	56.0	143.3

Comparing Table 5 with Table 3 it may be noted that the change in total core power, channel power, and bundle power are each greater for the second case than the first. This behaviour is expected as the initial steady-state power distribution varied slightly due to the absence of depleted fuel in the second case, yielding higher initial channel powers and bundle powers close to the center of the core. The comparison of these two simulations yields important information about the behaviour that is expected throughout each analysis conducted in the current study.

4.1.3 CANDU-6 Natural Uranium with Gd_2O_3

The third model included 1 mg Gd_2O_3 distributed uniformly throughout the CANLUB layer of each element in the bundle for comparison against the natural uranium model. The amount of 1 mg was selected to act as a proof of concept for the purposes of the preliminary analysis and will vary around the ~180 mg Gd_2O_3 and ~1000 mg Eu_2O_3 (~$4.9E10^3$ wt% per bundle), recommended by *Chan et al*. [11]. The core power distribution by channel power is shown in Figure 16.

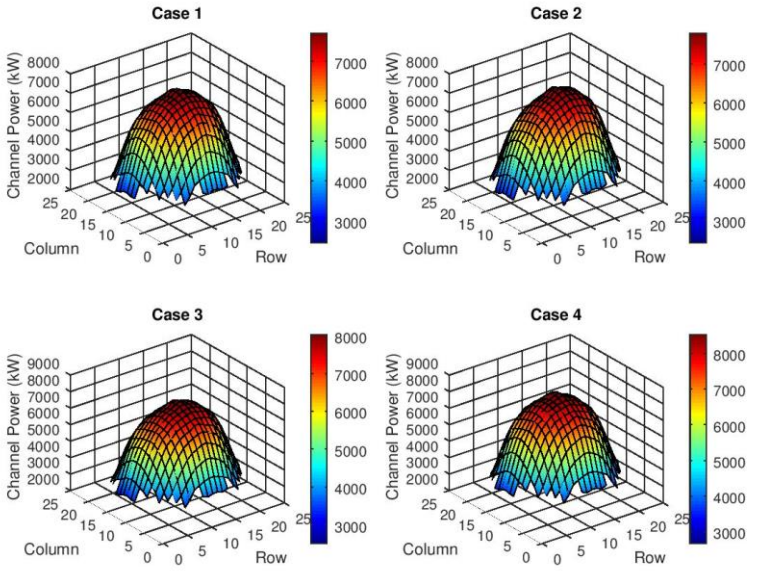

Figure 16: LLOCA transient natural uranium with Gd_2O_3 absolute results from RFSP-IST. Case 1 corresponds to the time at 0s, Case 2 at 0.1s, Case 4 at 0.2s, and Case 3 at 0.3s. Channel powers shown are in units of kW and channel location in the core is depicted by the row and column along the x and y axis respectively. A summary of key parameters for each of the time steps as the transient progresses is provided in Table 6.

Here the core channel power distribution remains similar to that obtained in the second study, with the highest flux close to the center of the core. Based on the plots, the magnitude of the power change has decreased with the addition of Gd_2O_3. This behaviour is further emphasized by the summary of results shown in Table 6.

Table 6: Natural uranium with Gd_2O_3 absolute results summary. Core Power (sum of all channel powers) in MW, Maximum Channel Power in kW, and Maximum Bundle Power in kW are provided from RFSP-IST for each time step in the LLOCA transient simulation.

Natural Uranium and Gd_2O_3				
Parameter	Initial Steady-State	Transient t=0.1s	Transient t=0.2s	Transient t=0.3s
Core Power (MW)	2061.4	2075.1	2139.2	2278.0
MCP (kW)	7708.3	7791.2	8029.4	8527.8
MBP (kW)	810.1	822.3	854.8	911.2

From a comparison of Table 6 with Table 4, it may be noted that the initial maxima channel and bundle power are higher in the Gd_2O_3 study than in the natural uranium study, while maintaining the same total core power due to flux normalization. This

is expected to be a result of the RFSP-IST simulations assuming the same time-average exit irradiations for both the natural uranium and burnable neutron absorber fuels. For the time steps in Case 2 and Case 3, it may be noted that the core, bundle, and channel powers in the third study with Gd_2O_3 remain slightly higher than the natural uranium case, but by the final time step the absolute powers are lower.

This behaviour is demonstrated again in the difference analyses as shown plotted in Figure 17.

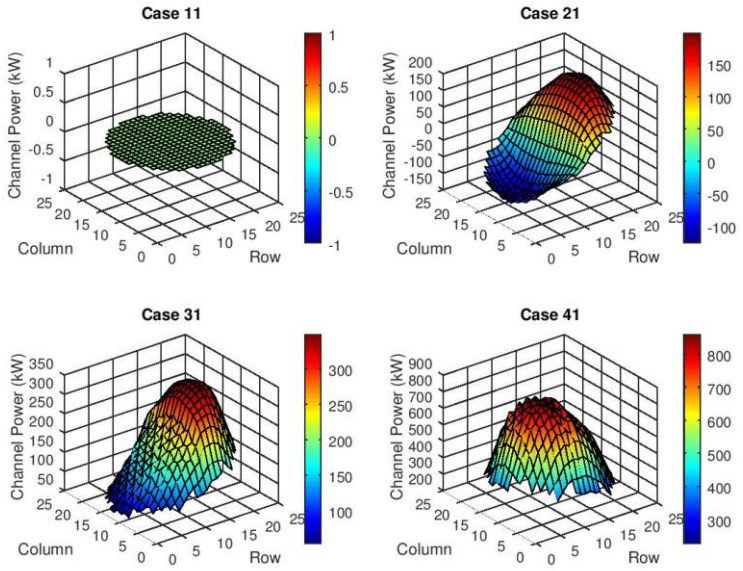

Figure 17: LLOCA transient natural uranium with Gd_2O_3 case difference results from RFSP-IST. Case 11 corresponds to the time at 0s, Case 21 at 0.1s, Case 31 at 0.2s, and Case 41 at 0.3s. Changes in channel power are shown are in units of kW and channel location in the core is depicted by the row and column along the x and y axis respectively. A summary of key parameters for each of the time steps as the transient progresses is provided in Table 7.

A comparison of Figure 17 with Figure 15 reveals that the magnitude of the power changes is dampened significantly by the presence of Gd_2O_3.

The significance of these magnitude changes is highlighted in the summary shown in Table 7.

Table 7: Natural uranium with Gd_2O_3 difference results summary. Change in Core Power (sum of all channel powers) in MW, Change in Maximum Channel Power in kW, and Change in Maximum Bundle Power in kW, relative to the initial steady-state power distribution, are provided from RFSP-IST for each time step in the LLOCA transient simulation.

Natural Uranium and Gd_2O_3			
Parameter	Transient t=0.1s	Transient t=0.2s	Transient t=0.3s
Δ Core Power (MW)	13.7	77.8	216.6
Δ MCP (kW)	82.9	321.1	216.6
Δ MBP (kW)	12.2	44.7	101.1

When comparing Table 7 against Table 5, one may note that the initial power increase is greater for the Gd_2O_3 case than the natural uranium case for total reactor power, channel power and bundle power. For the difference between Case 3 and Case 1 the dampening caused by the Gd_2O_3 addition begins to become more significant, as only the maximum channel power difference remains larger. In the difference between Case 4 and Case 1, each of the total reactor power, channel power, and bundle power changes are less for the case with Gd_2O_3 than for that with natural uranium fuel. These results confirm a marked improvement in margin from the addition of Gd_2O_3.

4.2 Phase Two Results

Phase Two of this study involved the addition of 180 mg Gd_2O_3 and 1000 mg B_2O_3 for comparison against a natural uranium fuel case. The Gd_2O_3 concentration is in-line with the recommendation by Chan *et al* and the B_2O_3 concentration is intended to replace the recommended 300 mg Eu_2O_3 as the long-lived neutron absorber which is in-line with the approximate equivalent neutron absorption cross section.

Simulations of interest include the natural uranium reference case, a case with the recommended burnable neutron absorber concentrations added evenly throughout each rod in the thirty-seven-element fuel, and a case with the recommended concentrations of burnable neutron absorbers added only to the center rod of the thirty-seven-element fuel. Within each simulation case three large loss of coolant accident runs were performed: fresh fuel with no saturating fission products, equilibrium saturating fission products in the fuel, and concentrations of nuclides equal to what one would expect following a long shutdown. Given the importance of accident analysis, and in the current refurbishment and potential new build environment, the simulations of a fresh core and a startup core following a long shutdown are of special interest.

The three nuclide concentration assumptions including fresh, equilibrium, and startup following a long shutdown are included as options in the RFSP-IST SCMHI card under the BURNT option. The NORM selection performs the transient calculations from the initial steady-state power distribution with no assumptions made related to the nuclide concentrations. Since the SIMULATE module up to the

point of the transient is for a fresh core, the simulation results for the NORM selection are to be treated as fresh with zero full power days burnup in core. The EQUIL selection sets all short-lived nuclides to pseudo-equilibrium values and serves as a reasonable approximation for an equilibrium simulation comparison. Lastly, the LONGS selection sets the concentrations of fission products that are decaying such as I-135, Xe-135, and Rh-105 to zero while simultaneously adding the concentration of Np-239 to Pu-239 as would be the case for an operational reactor that had undergone a shutdown of significant duration.

There is a total of nine transient simulations documented in this phase as described above and documented in Table 1. The approach of analyzing the raw and delta (comparison against initial steady-state power distribution) parameters, as summary tables, are described as follows:

Table 8 and Table 9 are for fresh natural uranium fuel, Table 10 and Table 11 are for fresh fuel with evenly distributed burnable neutron absorbers, Table 12 and Table 13 are for fresh fuel with center pin burnable neutron absorbers, Table 14 and Table 15 are for equilibrium natural uranium fuel, Table 16 and Table 17 are for equilibrium fuel with evenly distributed burnable neutron absorbers, Table 18 and Table 19 are for equilibrium fuel with center pin burnable neutron absorbers, Table 20 and Table 21 are for natural uranium fuel during a startup following a long shutdown, Table 22 and Table 23 are for fuel with evenly distributed burnable neutron absorbers during a startup following a long shutdown, and Table 24 and Table 25 are for fuel with center pin burnable neutron absorbers during a startup following a long shutdown.

The cross-sectional core maps of channel powers in kW are also shown for each of the three tenth of a second time steps through the transient simulation relative to the initial steady-state power distribution. In a similar manner, Figure 18 through Figure 20 are for fresh natural uranium fuel, Figure 21 through Figure 23 are for fresh fuel with evenly distributed burnable neutron absorbers, Figure 24 through Figure 26 are for fresh fuel with center pin burnable neutron absorbers, Figure 27 through Figure 29 are for equilibrium natural uranium fuel, Figure 30 through Figure 32 are for equilibrium fuel with evenly distributed burnable neutron absorbers, Figure 33 through Figure 35 are for equilibrium fuel with center pin burnable neutron absorbers, Figure 36 through Figure 38 are for natural uranium fuel during a startup following a long shutdown, Figure 39 through Figure 41 are for fuel with evenly distributed burnable neutron absorbers during a startup following a long shutdown, and Figure 42 through Figure 44 are for fuel with center pin burnable neutron absorbers during a startup following a long shutdown.

The primary parameter outlined for comparison is the maximum change in channel power. This parameter is calculated for each channel at each time step as a maximum in the entire core of the difference between the channel power at time t = x s less the channel power at time t = 0 s (in other words, the difference between channel powers at each time step in the transient simulation). This parameter is directly correlated to the maximum regional change in channel powers occurring in the core. In turn, high changes in channel power result in high changes in channel temperatures and increases the probability of fuel sheath failure and melting. As such, minimizing the

maximum regional change in channel powers minimizes the probability of fuel failure.

4.2.1 Fresh Natural Uranium Fuel

The first simulation performed was for natural uranium fuel with no burnup. This simulation serves as the base case for comparison against the two following simulations with burnable neutron absorbers added to the fuel. The fresh case is similar to what one would expect in a CANDU core that has yet to be operated, as would be the case for a new build or unit that has undergone a refurbishment and restored with completely new fuel. Table 8 provides a summary of significant parameters including total core power, maximum channel power, maximum bundle power, mean channel power, and minimum channel power for each time step in the transient simulation. For this case, no depleted uranium fuel was simulated.

Table 8: Raw RFSP-IST CERBERUS data for fresh natural uranium fuel. Core Power (sum of all channel powers) in MW, Maximum Channel Power in kW, Maximum Bundle Power in kW, Mean Channel Power in kW, and Minimum Channel Power in kW are provided from RFSP-IST for each time step in the LLOCA transient simulation.

Fresh Natural Uranium Fuel				
Parameter	Initial Steady-State	Transient t=0.1s	Transient t=0.2s	Transient t=0.3s
Core Power (MW)	2061.4	2069.9	2130.5	2276.7
Maximum Channel Power (kW)	7311.4	7382.0	7545.2	8261.5
Maximum Bundle Power (kW)	764.4	772.8	814.7	899.4
Mean Channel Power (kW)	5424.7	5447.2	5606.5	5991.3
Minimum Channel Power (kW)	2101.8	2090.1	2155.1	2238.5

Table 9 utilizes the data outlined in Table 8 to provide a summary of the change in core power, maximum channel power, mean channel power, and minimum channel power for each time step in the transient simulation relative to the initial steady-state power distribution at time t = 0 s. Due to the changes in initial power distribution for each case, the delta table is to be used for comparison between cases.

Table 9: Change in powers relative to initial power distribution for fresh natural uranium fuel. Change in Core Power (sum of all channel powers) in MW, Maximum Change in Channel Power in kW, Change in Mean Channel Power in kW, and Minimum Change in Channel Power in kW, relative to the initial steady-state power distribution, are provided from RFSP-IST for each time step in the LLOCA transient simulation.

Fresh Natural Uranium Fuel			
Parameter	Transient t=0.1s	Transient t=0.2s	Transient t=0.3s
Δ Core Power (MW)	8.5	69.1	215.3
Maximum Δ Channel Power (kW)	82.7	326.5	1104.0
Δ Mean Channel Power (kW)	22.5	181.8	566.6
Minimum Δ Channel Power (kW)	-44.0	53.3	136.7

For the purpose of visualizing the transient oscillation with respect to channel powers for each case a cross-sectional core map of channel powers are provided in Figure 18, Figure 19, and Figure 20. Similar to the study conducted in Phase One, the initial shift in power due to the negative CANDU fuel temperature reactivity coefficient is toward the right side of the unit at the 0.1s time step then shifts back to the break side of the reactor as the void reactivity coefficient takes over at 0.2s and 0.3s. It may be noted that the magnitude of the change in each parameter is different for each of the nine simulations performed in this phase of the study. These magnitude changes must be analyzed to determine if the addition of burnable neutron absorbers can mitigate the effects of coolant voiding in CANDU reactors during a hypothetical large loss of coolant accident. The following figures associated with this simulation also emphasize the significance of the checkerboard pattern in adjacent channels resulting from where the coolant loss is greatest in the core.

	1	2	3	4	5	6	7	8	9	10	11	12	13	14	15	16	17	18	19	20	21	22	
A									16	11	22	26	27	28									A
B						9	4	16	9	23	17	34	37	39	39	35	30						B
C					7		13	6	23	14	33	41	46	50	50	47	41	35					C
D				5	-3	9	0	19	9	28	22	47	56	60	61	58	52	45	37				D
E			1	-8	4	-6	13	2	22	15	35	52	61	67	69	67	62	55	46	36			E
F			-11	-2	-12	3	-5	15	7	29	24	53	63	69	74	73	69	63	55	45			F
G		-13	-13	-18	-9	-11	7	-2	20	14	39	55	64	72	77	79	76	70	63	52	39		G
H		-15	-23	-18	-19	-1	-11	10	2	27	24	56	66	73	79	82	81	76	69	58	45		H
J	-14	-25	-24	-29	-13	-19	-2	-8	12	10	38	55	65	73	78	82	82	79	74	63	49	36	J
K	-19	-25	-33	-21	-28	-10	-18	1	-4	21	21	53	64	72	78	82	82	79	76	66	53	39	K
L	-18	-31	-31	-38	-19	-28	-8	-16	6	4	32	50	62	71	77	82	83	81	77	68	55	41	L
M	-22	-29	-40	-36	-38	-26	-27	-13	-11	14	14	47	60	69	76	81	83	81	77	67	54	40	M
N	-20	-33	-36	-44	-35	-37	-24	-24	-1	-2	24	45	57	67	74	79	80	78	74	64	51	37	N
O	-21	-29	-40	-39	-44	-34	-34	-19	-17	9	10	43	55	65	72	75	76	73	69	59	47	34	O
P		-28	-33	-43	-37	-40	-29	-28	-12	-6	20	40	52	62	69	72	70	66	61	53	42		P
Q		-21	-32	-35	-40	-33	-35	-22	-20	4	5	37	49	58	64	66	63	58	54	46	36		Q
R			-24	-34	-32	-37	-28	-29	-15	-10	15	34	45	53	58	59	56	50	45	38			R
S			-21	-25	-32	-29	-33	-24	-23	-1	1	31	41	48	52	52	48	42	37	30			S
T				-21	-23	-30	-26	-28	-17	-14	7	23	33	40	43	42	39	34	28				T
U					-18	-19	-23	-19	-19	-9	-5	18	26	31	34	33	29	25					U
V						-14	-13	-16	-11	-10	-1	13	19	23	24	23	19						V
W									-8	-4	-2	9	13	15									W
	1	2	3	4	5	6	7	8	9	10	11	12	13	14	15	16	17	18	19	20	21	22	

Figure 18: Variation of channel power (kW) over the first 0.1 s of the transient for fresh natural uranium fuel. Results obtained from RFSP-IST. A summary of key parameters for each of the time steps as the transient progresses is provided in Table 9.

	1	2	3	4	5	6	7	8	9	10	11	12	13	14	15	16	17	18	19	20	21	22	
A									120	105	120	106	97	88									A
B						117	122	158	144	168	140	145	135	123	109	91	72						B
C					134	141	186	179	213	183	201	179	169	157	140	122	100	79					C
D				140	152	204	201	246	219	252	200	205	196	183	167	148	126	102	79				D
E			132	152	208	209	262	240	283	232	257	221	211	198	183	166	145	122	98	73			E
F			144	203	208	270	249	300	253	287	228	230	216	203	192	176	158	137	116	90			F
G		127	187	202	256	249	307	270	309	254	284	241	222	208	197	183	166	148	129	105	77		G
H		166	187	249	241	302	274	324	272	307	246	247	227	211	200	186	171	156	141	117	90		H
J	131	160	228	234	290	267	321	280	320	262	292	246	227	212	199	186	173	160	148	127	99	69	J
K	125	193	213	282	256	312	279	327	274	307	242	242	225	210	198	186	173	161	153	133	106	75	K
L	145	176	246	248	304	274	326	279	318	257	282	236	222	209	197	186	176	165	156	137	110	78	L
M	127	196	215	282	261	313	277	318	267	295	232	232	219	206	196	186	177	166	156	136	109	78	M
N	134	164	233	237	292	265	312	269	305	247	271	230	216	204	194	184	175	164	153	132	105	73	N
O	107	170	190	253	241	296	260	303	254	285	227	230	214	200	191	181	173	160	146	124	97	67	O
P		132	193	199	251	237	288	251	285	234	263	225	209	196	187	176	163	148	134	112	86		P
Q		121	143	191	193	248	227	274	230	262	211	215	200	187	179	166	151	134	119	97	73		Q
R			130	144	184	187	240	214	251	206	234	202	189	178	168	154	137	119	103	81			R
S			90	128	137	179	180	227	195	228	181	188	180	169	157	142	122	103	85	64			S
T				87	122	131	169	164	201	167	191	167	161	151	138	123	104	84	65				T
U					80	111	117	147	137	156	132	140	135	125	113	98	80	62					U
V						66	91	94	115	103	116	109	103	94	83	69	53						V
W									66	79	70	74	69	61									W
	1	2	3	4	5	6	7	8	9	10	11	12	13	14	15	16	17	18	19	20	21	22	

Figure 19: Variation of channel power (kW) over the first 0.2 s of the transient for fresh natural uranium fuel. Results obtained from RFSP-IST. A summary of key parameters for each of the time steps as the transient progresses is provided in Table 9.

	1	2	3	4	5	6	7	8	9	10	11	12	13	14	15	16	17	18	19	20	21	22	
A									373	335	354	301	267	234									A
B						381	412	501	473	513	436	410	369	324	277	225	174						B
C					444	487	605	598	666	589	597	504	459	409	355	298	239	185					C
D				473	534	674	686	785	720	763	623	579	530	476	419	359	297	236	180				D
E			460	548	702	730	854	808	877	749	759	627	574	517	461	402	340	279	220	162			E
F			533	707	745	891	857	950	835	866	712	656	593	534	485	428	370	311	256	197			F
G		482	682	747	892	875	994	911	956	816	832	691	615	551	501	447	389	333	284	226	166		G
H		615	712	898	878	1006	949	1031	900	928	773	713	633	564	513	459	404	351	307	251	190		H
J	492	624	845	880	1000	953	1054	955	1004	854	866	717	638	569	513	460	410	362	323	270	208	145	J
K	492	732	823	1000	946	1057	982	1056	923	946	776	710	636	569	514	461	412	367	334	284	223	157	K
L	557	697	924	949	1062	1000	1086	974	1015	854	848	696	630	567	514	465	420	378	342	292	231	164	L
M	510	756	850	1040	989	1104	1003	1070	923	934	757	689	625	564	513	465	423	381	344	292	230	163	M
N	522	665	895	930	1065	1000	1089	965	1002	843	839	689	622	560	509	462	420	377	337	283	220	154	N
O	437	668	770	964	942	1071	971	1042	900	919	758	696	620	554	503	454	413	367	323	268	205	141	O
P		545	753	803	945	911	1025	921	966	814	828	686	608	543	494	443	391	341	298	244	185		P
Q		484	590	750	770	913	868	961	833	859	715	660	585	522	475	421	364	311	267	214	158		Q
R			520	593	715	740	874	807	868	735	749	621	557	498	449	394	334	279	232	181			R
S			375	512	561	689	708	820	730	767	626	580	528	474	421	363	301	243	195	145			S
T				365	482	532	645	637	715	612	622	517	473	424	372	316	258	203	153				T
U					329	433	467	550	523	551	465	435	397	353	306	254	201	152					U
V						267	351	371	421	386	397	343	308	269	228	182	137						V
W									254	281	250	236	208	178									W
	1	2	3	4	5	6	7	8	9	10	11	12	13	14	15	16	17	18	19	20	21	22	

Figure 20: Variation of channel power (kW) over the first 0.3 s of the transient for fresh natural uranium fuel. Results obtained from RFSP-IST. A summary of key parameters for each of the time steps as the transient progresses is provided in Table 9.

4.2.2 Fresh Fuel with Evenly Distributed BNAs

The second simulation performed was for fuel with 180 mg Gd_2O_3 and 1000 mg B_2O_3 evenly distributed in each element of the thirty-seven-element fuel with no burnup. This simulation serves the first case for comparison against the natural uranium simulation with burnable neutron absorbers added to the fuel. Table 10 provides a summary of significant parameters including total core power, maximum channel power, maximum bundle power, mean channel power, and minimum channel power for each time step in the transient simulation.

Table 10: Raw RFSP-IST CERBERUS data for fresh fuel with evenly distributed BNAs. Core Power (sum of all channel powers) in MW, Maximum Channel Power in kW, Maximum Bundle Power in kW, Mean Channel Power in kW, and Minimum Channel Power in kW are provided from RFSP-IST for each time step in the LLOCA transient simulation.

Fresh Fuel with Evenly Distributed BNAs				
Parameter	Initial Steady-State	Transient t=0.1s	Transient t=0.2s	Transient t=0.3s
Core Power (MW)	2061.4	2075.9	2146.3	2299.7
Maximum Channel Power (kW)	7792.4	7875.0	8137.9	8693.9
Maximum Bundle Power (kW)	824.6	836.8	867.7	934.2
Mean Channel Power (kW)	5424.7	5462.9	5648.2	6051.9
Minimum Channel Power (kW)	2405.9	2383.4	2485.4	2635.9

Table 11 utilizes the data outlined in Table 10 to provide a summary of the change in core power, maximum channel power, mean channel power, and minimum channel power for each time step in the transient simulation relative to the initial steady-state power distribution at time t = 0 s. Due to the changes in initial power distribution for each case, these delta tables should be used for comparison between cases.

Table 11: Change in powers relative to initial power distribution for fresh fuel with evenly distributed BNAs. Change in Core Power (sum of all channel powers) in MW, Maximum Change in Channel Power in kW, Change in Mean Channel Power in kW, and Minimum Change in Channel Power in kW, relative to the initial steady-state power distribution, are provided from RFSP-IST for each time step in the LLOCA transient simulation.

Fresh Fuel with Evenly Distributed BNAs			
Parameter	Transient t=0.1s	Transient t=0.2s	Transient t=0.3s
Δ Core Power (MW)	14.5	84.9	238.3
Maximum Δ Channel Power (kW)	176.6	346.4	995.9
Δ Mean Channel Power (kW)	38.1	223.5	627.2
Minimum Δ Channel Power (kW)	-98.3	72.6	230.0

Cross-sectional core maps of channel powers are provided in Figure 21, Figure 22, and Figure 23. Comparing the results from the natural uranium case in Table 8 and Table 9 with the evenly distributed burnable neutron absorber case one may note that the change in total core power is greater in the case when burnable neutron absorbers are added. However, it is also demonstrated that the maximum change in channel power is lower when burnable neutron absorbers are added. Thus, the increase in total core power is attributed to the larger magnitude of change in minimum channel power. This is still an improvement for the hypothetical large loss of coolant accident because the regionalized maximum change in power is dampened as is shown from the lower maximum change in channel power. As such, it is expected that actuation of the shutdown system will be able to better mitigate the power transient resulting during the case with burnable neutron absorbers than for natural uranium. In addition, the margin to fuel failure is improved because the sheath temperature increase is expected to be proportional to the change in channel powers throughout the transient.

	1	2	3	4	5	6	7	8	9	10	11	12	13	14	15	16	17	18	19	20	21	22	
A									9	17	29	49	58	69									A
B						-11	-8	-2	6	18	32	59	71	80	85	81	77						B
C					-19	-18	-14	-7	4	18	38	71	87	98	103	100	93	89					C
D				-27	-27	-26	-22	-12	-1	14	39	79	99	114	121	121	114	104	96				D
E			-34	-36	-37	-36	-29	-20	-8	14	36	84	106	124	135	137	133	122	108	96			E
F			-44	-47	-48	-48	-38	-29	-11	8	38	85	109	130	144	149	149	140	126	111			F
G		-47	-58	-59	-66	-56	-49	-34	-18	8	34	85	112	135	151	159	162	155	141	121	105		G
H		-59	-64	-75	-69	-67	-54	-43	-21	1	35	86	114	138	156	165	171	166	153	134	113		H
J	-53	-60	-76	-77	-80	-71	-64	-45	-30	1	29	85	115	140	157	167	175	172	161	143	117	96	J
K	-52	-70	-78	-85	-82	-81	-66	-55	-30	-7	30	84	114	140	158	168	177	175	166	149	123	96	K
L	-59	-70	-88	-88	-88	-81	-74	-56	-38	-7	24	83	112	139	157	168	173	172	168	151	125	99	L
M	-56	-75	-85	-98	-90	-93	-76	-68	-38	-9	24	80	110	137	155	167	172	171	167	150	124	98	M
N	-58	-70	-90	-93	-98	-88	-86	-63	-40	-12	22	77	107	133	152	164	169	168	163	146	120	93	N
O	-54	-71	-82	-97	-92	-96	-80	-72	-43	-14	19	72	103	129	148	159	166	163	156	138	113	91	O
P		-65	-81	-86	-96	-89	-86	-65	-51	-15	18	69	98	124	143	153	160	157	145	127	108		P
Q		-62	-69	-81	-83	-89	-75	-69	-42	-15	15	64	93	117	134	143	148	143	131	113	99		Q
R			-63	-69	-77	-75	-75	-58	-46	-15	15	61	87	109	124	130	133	126	114	101			R
S			-51	-59	-64	-68	-61	-58	-37	-14	13	57	81	101	113	117	116	108	95	84			S
T				-48	-52	-54	-54	-45	-38	-13	12	51	72	88	97	99	95	87	80				T
U					-40	-42	-40	-38	-26	-13	9	42	60	72	79	78	74	70					U
V						-29	-30	-27	-21	-8	5	32	46	55	61	58	55						V
W									-14	-6	6	24	33	42									W
	1	2	3	4	5	6	7	8	9	10	11	12	13	14	15	16	17	18	19	20	21	22	

Figure 21: Variation of channel power (kW) over the first 0.1 s of the transient for fresh fuel with evenly distributed BNAs. Results obtained from RFSP-IST. A summary of key parameters for each of the time steps as the transient progresses is provided in Table 11.

	1	2	3	4	5	6	7	8	9	10	11	12	13	14	15	16	17	18	19	20	21	22	
A									144	145	148	163	160	167									A
B						120	138	155	168	173	184	198	197	194	188	166	151						B
C					127	143	162	187	199	214	221	243	240	236	224	204	180	165					C
D				127	146	168	196	214	235	235	258	278	276	273	262	243	218	190	171				D
E			118	141	165	196	216	243	246	269	268	304	301	299	291	274	251	222	191	165			E
F			136	156	189	206	239	247	272	270	296	319	315	315	312	297	280	252	220	190			F
G		122	134	174	193	234	240	272	271	294	291	327	327	329	327	315	303	278	244	206	176		G
H		119	155	174	217	232	261	267	293	289	313	336	338	339	338	328	319	295	263	226	189		H
J	97	129	152	194	211	249	250	282	281	306	303	341	343	344	342	332	327	306	276	239	193	157	J
K	104	124	167	187	225	234	263	267	296	292	319	345	344	346	344	335	329	310	285	249	202	157	K
L	97	133	156	197	207	241	248	279	278	304	305	346	343	346	344	335	323	306	288	253	206	162	L
M	103	122	164	178	214	218	255	254	287	289	313	339	338	342	341	333	321	304	287	251	205	160	M
N	89	124	145	185	190	228	229	264	270	290	296	333	332	335	334	327	316	299	280	244	197	153	N
O	93	107	146	161	196	202	236	236	268	272	291	317	322	326	326	319	310	291	269	232	187	150	O
P		110	122	158	172	209	208	243	238	268	271	305	310	314	315	308	301	281	251	215	180		P
Q		94	116	134	167	175	208	210	240	244	264	288	293	297	298	289	280	257	227	193	166		Q
R			98	120	139	169	173	207	206	235	241	273	275	278	276	266	253	229	199	174			R
S			86	96	123	140	166	172	203	209	231	255	257	258	253	239	224	198	168	146			S
T				86	95	119	134	160	163	190	197	226	227	228	220	205	185	161	144				T
U					82	90	111	125	145	151	169	189	190	189	181	165	145	132					U
V						73	82	103	108	122	127	147	148	147	142	125	111						V
W									89	88	99	110	110	114									W
	1	2	3	4	5	6	7	8	9	10	11	12	13	14	15	16	17	18	19	20	21	22	

Figure 22: Variation of channel power (kW) over the first 0.2 s of the transient for fresh fuel with evenly distributed BNAs. Results obtained from RFSP-IST. A summary of key parameters for each of the time steps as the transient progresses is provided in Table 11.

	1	2	3	4	5	6	7	8	9	10	11	12	13	14	15	16	17	18	19	20	21	22	
A									447	427	414	413	384	381									A
B						419	464	508	523	515	514	503	471	439	409	349	306						B
C					464	505	557	615	630	640	621	615	572	532	483	423	361	324					C
D				484	540	605	678	715	746	717	727	706	657	614	563	501	435	369	324				D
E			473	548	625	712	762	813	800	812	770	773	717	673	623	563	498	428	359	306			E
F			553	625	724	776	845	853	876	833	842	815	752	708	665	608	552	482	410	348			F
G		520	583	705	779	873	878	928	895	899	843	841	785	739	698	643	596	529	452	375	316		G
H		542	659	745	857	897	945	940	957	905	898	867	812	764	722	668	625	560	487	409	338		H
J	457	570	680	806	865	951	936	983	948	951	888	884	826	777	730	677	639	579	509	432	345	278	J
K	472	578	728	810	907	934	976	965	987	930	930	896	833	784	736	683	644	586	523	448	359	277	K
L	468	606	721	843	873	948	953	996	958	958	906	902	831	783	736	684	633	578	529	455	366	284	L
M	478	585	736	810	892	911	974	954	979	926	924	890	823	777	731	680	630	576	527	453	364	281	M
N	440	579	693	816	844	926	923	970	939	931	885	876	810	764	720	670	621	567	516	441	352	270	N
O	443	531	674	758	848	872	930	911	935	886	869	839	790	746	703	655	610	554	497	421	335	266	O
P		524	602	721	787	873	861	911	866	873	818	811	763	720	682	634	595	536	465	392	324		P
Q		468	549	634	736	774	831	824	848	806	795	769	724	683	647	597	555	494	423	353	300		Q
R			482	559	636	720	730	788	759	772	734	731	681	642	603	552	506	443	374	321			R
S			411	460	552	615	675	688	727	699	704	685	637	599	555	501	450	386	319	272			S
T				400	438	513	561	616	611	632	607	609	566	531	486	432	375	317	276				T
U					365	394	455	491	524	516	522	512	476	444	402	350	298	262					U
V						308	339	395	398	410	398	400	375	348	320	270	230						V
W									319	300	308	303	281	274									W
	1	2	3	4	5	6	7	8	9	10	11	12	13	14	15	16	17	18	19	20	21	22	

Figure 23: Variation of channel power (kW) over the first 0.3 s of the transient for fresh fuel with evenly distributed BNAs. Results obtained from RFSP-IST. A summary of key parameters for each of the time steps as the transient progresses is provided in Table 11.

4.2.3 Fresh Fuel with Center Pin BNAs

The third simulation performed was for fuel with 180 mg Gd_2O_3 and 1000 mg B_2O_3 distributed only in the center element of the thirty-seven-element fuel with no burnup. This simulation serves the second case for comparison against the natural uranium simulation with burnable neutron absorbers added to the fuel. Table 12 provides a summary of significant parameters including total core power, maximum channel power, maximum bundle power, mean channel power, and minimum channel power for each time step in the transient simulation.

Table 12: Raw RFSP-IST CERBERUS data for fresh fuel with center pin BNAs. Core Power (sum of all channel powers) in MW, Maximum Channel Power in kW, Maximum Bundle Power in kW, Mean Channel Power in kW, and Minimum Channel Power in kW are provided from RFSP-IST for each time step in the LLOCA transient simulation.

Fresh Fuel with Center Pin BNAs				
Parameter	Initial Steady-State	Transient t=0.1s	Transient t=0.2s	Transient t=0.3s
Core Power (MW)	2061.4	2075.0	2138.6	2276.3
Maximum Channel Power (kW)	7732.8	7815.6	8052.8	8549.2
Maximum Bundle Power (kW)	813.4	825.7	857.9	914.1
Mean Channel Power (kW)	5424.7	5460.4	5627.9	5990.4
Minimum Channel Power (kW)	2426.4	2395.7	2486.4	2651.3

Table 13 utilizes the data outlined in Table 12 to provide a summary of the change in core power, maximum channel power, mean channel power, and minimum channel power for each time step in the transient simulation relative to the initial steady-state power distribution at time t = 0 s. Due to the changes in initial power distribution for each case, these delta tables should be used for comparison between cases.

Table 13: Change in powers relative to initial power distribution for fresh fuel with center pin BNAs. Change in Core Power (sum of all channel powers) in MW, Maximum Change in Channel Power in kW, Change in Mean Channel Power in kW, and Minimum Change in Channel Power in kW, relative to the initial steady-state power distribution, are provided from RFSP-IST for each time step in the LLOCA transient simulation.

Fresh Fuel with Center Pin BNAs			
Parameter	Transient t=0.1s	Transient t=0.2s	Transient t=0.3s
Δ Core Power (MW)	13.6	77.2	214.9
Maximum Δ Channel Power (kW)	199.4	348.8	852.6
Δ Mean Channel Power (kW)	35.7	203.1	565.6
Minimum Δ Channel Power (kW)	-128.4	52.0	224.9

Cross-sectional core maps of channel powers are provided in Figure 24, Figure 25, and Figure 26. Comparing the results from the natural uranium case in Table 8 and Table 9 with the center pin burnable neutron absorbers one may note that the change in total core power is lower in the case when burnable neutron absorbers are added to only the center element. It is also demonstrated that the maximum change in channel power is lower when burnable neutron absorbers are added. This is an improvement for the hypothetical large loss of coolant accident because both the regionalized maximum change in power is dampened along with the total core power change. The improvement demonstrated by addition of burnable neutron absorbers to only the center pin is shown to be greater than the improvement from addition of burnable neutron absorbers evenly within each element of the fuel, as seen in Table 10 and Table 11. This result is attributed to spectral changes that occur in the fuel during the accident when burnable neutron absorbers are added only to the center element compared with absorbers added to each element in the fuel bundle.

	1	2	3	4	5	6	7	8	9	10	11	12	13	14	15	16	17	18	19	20	21	22	
A									2	12	27	51	62	76									A
B						-22	-18	-12	-3	12	29	61	77	88	95	91	88						B
C					-32	-31	-27	-21	-7	9	34	73	93	108	114	113	106	102					C
D				-42	-43	-43	-39	-29	-15	4	34	81	106	125	135	136	130	118	110				D
E			-49	-54	-56	-56	-49	-39	-24	2	29	85	114	136	150	154	150	139	124	110			E
F			-63	-68	-71	-71	-61	-50	-28	-5	31	87	117	142	160	167	168	159	144	128			F
G		-66	-79	-83	-92	-82	-74	-56	-38	-6	26	86	119	147	168	178	184	177	161	139	121		G
H		-80	-87	-101	-97	-95	-80	-67	-41	-14	26	86	121	151	173	185	193	189	175	154	131		H
J	-71	-81	-102	-105	-109	-100	-91	-70	-50	-15	20	85	122	152	174	187	198	196	184	164	135	111	J
K	-69	-92	-104	-114	-112	-110	-94	-80	-51	-23	21	84	121	153	175	189	199	198	190	171	141	111	K
L	-77	-92	-115	-118	-118	-110	-102	-81	-60	-22	14	83	120	152	174	189	196	196	192	174	144	114	L
M	-74	-98	-112	-128	-120	-123	-104	-94	-60	-25	15	80	117	149	173	187	195	194	191	172	143	113	M
N	-75	-92	-116	-122	-128	-118	-115	-88	-61	-27	14	77	114	146	169	184	191	191	186	167	138	108	N
O	-71	-92	-107	-125	-121	-126	-108	-97	-63	-28	11	72	110	142	164	179	187	186	179	159	130	106	O
P		-85	-105	-112	-125	-117	-113	-88	-71	-30	10	69	105	136	159	172	182	179	166	146	125		P
Q		-80	-89	-104	-109	-115	-99	-92	-60	-28	8	65	99	128	150	161	168	163	150	130	114		Q
R			-82	-89	-99	-98	-97	-78	-64	-28	8	62	93	120	138	147	151	144	130	117			R
S			-66	-76	-83	-88	-81	-77	-52	-25	6	58	88	111	126	132	132	123	109	97			S
T				-62	-67	-70	-70	-61	-52	-23	6	52	77	97	109	112	108	99	92				T
U					-52	-55	-53	-50	-37	-21	4	43	64	80	88	88	84	80					U
V						-39	-40	-36	-29	-15	2	33	49	61	68	66	63						V
W									-20	-11	3	25	36	47									W
	1	2	3	4	5	6	7	8	9	10	11	12	13	14	15	16	17	18	19	20	21	22	

Figure 24: Variation of channel power (kW) over the first 0.1 s of the transient for fresh fuel with center pin BNAs. Results obtained from RFSP-IST. A summary of key parameters for each of the time steps as the transient progresses is provided in Table 13.

	1	2	3	4	5	6	7	8	9	10	11	12	13	14	15	16	17	18	19	20	21	22	
A									123	129	135	156	158	169									A
B						95	112	128	143	151	167	189	194	194	192	173	159						B
C					97	112	129	153	167	186	199	230	235	236	229	211	189	176					C
D				94	111	128	155	173	196	201	232	263	269	273	268	252	229	202	184				D
E			84	103	122	149	168	195	201	230	237	286	292	299	297	284	264	236	205	179			E
F			96	111	139	152	184	194	223	228	263	298	305	314	317	308	294	268	236	206			F
G		84	89	122	135	173	180	214	218	249	256	306	316	327	332	326	319	295	261	223	192		G
H		76	105	116	155	166	198	206	237	242	276	313	326	337	344	339	335	314	283	244	206		H
J	61	85	97	132	144	180	183	219	223	257	264	317	330	341	347	344	343	325	297	259	211	173	J
K	67	76	110	123	157	164	196	203	237	241	280	320	331	343	349	346	345	329	306	269	220	173	K
L	59	85	97	132	139	172	179	213	218	253	264	320	329	342	348	346	339	325	309	273	224	177	L
M	65	73	105	111	145	148	186	188	228	239	273	314	325	338	345	344	337	323	308	272	223	175	M
N	52	78	88	120	122	159	160	200	212	241	257	308	319	332	339	338	331	317	300	264	215	168	N
O	58	63	92	99	131	134	170	173	212	224	254	293	310	323	331	330	325	309	288	251	204	165	O
P		68	72	102	110	144	144	182	183	222	235	282	298	311	320	318	316	298	269	233	197		P
Q		56	72	83	111	115	149	152	189	201	230	267	282	294	302	299	294	273	243	209	181		Q
R			59	77	90	117	120	156	158	195	210	254	265	276	281	274	266	243	214	188			R
S			55	60	82	94	120	126	161	173	203	237	248	257	257	247	234	210	180	158			S
T				56	62	83	95	121	126	158	172	211	220	226	224	212	194	171	155				T
U					56	61	81	93	116	125	149	176	184	188	184	170	152	140					U
V						52	59	79	85	102	111	137	144	146	145	129	116						V
W									72	74	88	104	107	114									W
	1	2	3	4	5	6	7	8	9	10	11	12	13	14	15	16	17	18	19	20	21	22	

Figure 25: Variation of channel power (kW) over the first 0.2 s of the transient for fresh fuel with center pin BNAs. Results obtained from RFSP-IST. A summary of key parameters for each of the time steps as the transient progresses is provided in Table 13.

	1	2	3	4	5	6	7	8	9	10	11	12	13	14	15	16	17	18	19	20	21	22	
A									400	386	378	384	362	365									A
B						367	409	449	466	462	467	466	443	418	394	340	301						B
C					404	440	486	540	556	571	560	568	536	506	465	411	355	321					C
D				418	467	523	589	624	656	634	655	650	614	582	541	487	427	366	324				D
E			406	470	536	614	658	707	698	719	687	709	668	637	598	546	488	424	358	308			E
F			473	532	619	663	728	735	765	731	753	744	699	668	637	589	540	477	409	351			F
G		444	493	600	660	746	750	801	775	790	748	766	727	696	667	623	584	523	451	378	321		G
H		457	558	627	728	760	808	805	830	790	799	788	751	718	689	647	612	554	486	412	343		H
J	385	482	570	681	728	807	795	844	816	832	785	802	763	730	696	655	625	572	508	435	349	283	J
K	399	484	613	679	766	787	831	822	853	808	824	812	768	735	701	659	629	579	522	451	363	282	K
L	392	510	601	709	732	801	806	851	822	836	799	816	766	735	701	660	618	571	528	458	370	289	L
M	403	488	617	675	750	763	826	809	843	804	817	806	759	728	696	656	615	568	526	455	368	287	M
N	368	486	577	685	704	781	777	828	805	812	780	793	746	716	685	646	606	559	514	443	356	275	N
O	375	443	566	632	713	730	788	772	805	769	769	759	728	699	669	632	596	547	495	423	339	271	O
P		442	502	606	658	737	724	777	741	761	722	734	703	675	650	612	582	529	464	394	328		P
Q		394	462	531	620	649	706	699	731	701	704	697	668	641	616	577	543	487	422	355	304		Q
R			405	471	535	610	616	675	651	675	649	663	629	602	575	533	494	437	373	322			R
S			348	388	467	520	576	586	629	610	626	623	590	563	530	484	439	380	318	274			S
T				340	371	437	478	530	526	555	539	555	525	500	464	418	367	313	275				T
U					312	336	391	423	457	453	467	467	443	418	384	338	291	259					U
V						265	292	343	347	363	355	366	349	328	306	261	225						V
W									282	266	278	278	262	259									W
	1	2	3	4	5	6	7	8	9	10	11	12	13	14	15	16	17	18	19	20	21	22	

Figure 26: Variation of channel power (kW) over the first 0.3 s of the transient for fresh fuel with center pin BNAs. Results obtained from RFSP-IST. A summary of key parameters for each of the time steps as the transient progresses is provided in Table 13.

4.2.4 Equilibrium Natural Uranium Fuel

The fourth simulation performed was for natural uranium fuel with equilibrium nuclide concentrations including the negative reactivity contribution from the high absorption cross section saturating fission product Xe-135. This simulation serves the base equilibrium case for comparison against the cases with burnable neutron absorbers added to the fuel and most closely represents what one would expect starting from a normally operating reactor in steady state. Table 14 provides a summary of significant parameters including total core power, maximum channel power, maximum bundle power, mean channel power, and minimum channel power for each time step in the transient simulation.

Table 14: Raw RFSP-IST CERBERUS data for equilibrium natural uranium fuel Core Power (sum of all channel powers) in MW, Maximum Channel Power in kW, Maximum Bundle Power in kW, Mean Channel Power in kW, and Minimum Channel Power in kW are provided from RFSP-IST for each time step in the LLOCA transient simulation.

Equilibrium Natural Uranium Fuel				
Parameter	Initial Steady-State	Transient t=0.1s	Transient t=0.2s	Transient t=0.3s
Core Power (MW)	2061.4	2073.2	2138.9	2294.4
Maximum Channel Power (kW)	7378.1	7432.8	7704.9	8478.4
Maximum Bundle Power (kW)	768.3	776.3	828.9	924.8
Mean Channel Power (kW)	5424.7	5455.9	5628.6	6038.0
Minimum Channel Power (kW)	2060.7	2064.0	2110.5	2199.0

Table 15 utilizes the data outlined in Table 14 to provide a summary of the change in core power, maximum channel power, mean channel power, and minimum channel power for each time step in the transient simulation relative to the initial steady-state power distribution at time t = 0 s. Due to the changes in initial power distribution for each case, these delta tables should be used for comparison between cases.

Table 15: Change in powers relative to initial power distribution for equilibrium natural uranium fuel. Change in Core Power (sum of all channel powers) in MW, Maximum Change in Channel Power in kW, Change in Mean Channel Power in kW, and Minimum Change in Channel Power in kW, relative to the initial steady-state power distribution, are provided from RFSP-IST for each time step in the LLOCA transient simulation.

Equilibrium Natural Uranium Fuel			
Parameter	Transient t=0.1s	Transient t=0.2s	Transient t=0.3s
Δ Core Power (MW)	11.8	77.5	233.1
Maximum Δ Channel Power (kW)	60.2	404.9	1243.4
Δ Mean Channel Power (kW)	31.3	203.9	613.3
Minimum Δ Channel Power (kW)	-4.2	49.8	136.0

Cross-sectional core maps of channel powers are provided in Figure 27, Figure 28, and Figure 29. Comparing the results of the equilibrium natural uranium fuel against the fresh natural uranium fuel in Table 8 and Table 9 it may be noted that larger changes are seen for both total core power and maximum change in channel power for the equilibrium fuel case. This characteristic is attributed to the fact that for an equilibrium core the saturating fission product Xe-135 is built into the fuel, adding negative reactivity due to its high neutron absorption cross section. In addition, burning the fuel to equilibrium nuclide concentrations increases the content of fissile Pu-239 in the fuel and reduces the margin to prompt criticality due to reducing the delayed neutron fraction in the fuel. As such, a higher change in power is noted for the equilibrium fuel case. It should be noted that the large axial power discrepancy is also present for this natural uranium simulation.

	1	2	3	4	5	6	7	8	9	10	11	12	13	14	15	16	17	18	19	20	21	22	
A									23	18	26	27	27	26									A
B						20	16	28	21	34	26	37	37	36	34	29	24						B
C					21	17	32	24	40	29	44	45	47	46	44	40	34	27					C
D				20	16	32	24	43	30	46	35	50	53	53	52	49	43	36	28				D
E			17	13	29	22	42	29	46	34	49	52	56	57	57	55	50	43	36	27			E
F			11	25	19	35	26	44	31	47	35	53	55	57	59	58	55	49	43	34			F
G		7	16	14	26	22	39	28	44	32	50	53	55	58	60	59	57	53	49	40	30		G
H		12	9	20	17	35	24	41	29	46	34	53	55	58	60	60	59	56	53	46	35		H
J	8	6	16	12	28	19	35	24	41	29	48	51	54	57	59	60	59	58	56	49	39	27	J
K	3	11	7	24	13	30	18	36	24	41	30	49	53	56	58	59	59	58	58	52	42	29	K
L	5	3	12	8	24	13	30	18	35	24	43	47	51	55	57	59	60	60	59	54	44	30	L
M	1	9	3	14	8	19	12	24	18	36	25	45	50	54	57	59	60	60	59	53	44	30	M
N	4	0	8	3	14	7	18	12	30	19	38	43	48	53	56	58	60	59	58	52	42	29	N
O		5	0	9	3	14	7	19	13	31	22	42	47	51	55	57	59	58	56	49	39	27	O
P		-1	5	-1	9	3	14	8	20	16	35	41	46	50	54	56	56	54	51	44	34		P
Q		1	-3	2	-1	9	3	15	9	28	19	39	44	48	52	53	52	49	45	38	28		Q
R			0	-4	2	-1	9	4	16	12	31	37	42	46	49	49	47	43	38	31			R
S			-3	-2	-4	2	-1	10	6	24	16	35	41	44	46	45	41	36	31	24			S
T				-4	-2	-4	2	0	11	8	25	32	37	40	40	39	34	29	23				T
U					-4	-1	-3	3	2	10	11	26	31	33	32	30	26	21					U
V						-2	0	-2	4	4	11	20	23	23	22	20	16						V
W									1	5	5	14	15	15									W
	1	2	3	4	5	6	7	8	9	10	11	12	13	14	15	16	17	18	19	20	21	22	

Figure 27: Variation of channel power (kW) over the first 0.1 s of the transient for equilibrium natural uranium fuel. Results obtained from RFSP-IST. A summary of key parameters for each of the time steps as the transient progresses is provided in Table 15.

	1	2	3	4	5	6	7	8	9	10	11	12	13	14	15	16	17	18	19	20	21	22	
A									135	118	129	111	99	87									A
B						136	144	182	167	189	156	153	138	121	104	85	66						B
C					158	170	220	212	246	211	222	188	173	154	134	113	91	71					C
D				167	186	244	244	291	259	288	226	217	199	179	159	137	114	91	69				D
E			161	189	252	259	316	291	332	272	289	235	215	194	174	153	130	107	85	62			E
F			181	251	261	330	309	360	305	332	260	246	222	200	182	162	141	120	99	76			F
G		161	237	257	320	312	374	332	367	299	321	259	230	206	188	168	147	127	110	88	64		G
H		210	241	317	307	373	343	393	330	358	283	267	236	210	191	171	152	133	118	98	74		H
J	166	209	294	303	363	339	396	347	384	312	334	267	237	211	190	171	153	137	124	105	81	56	J
K	162	251	279	359	332	391	353	400	336	362	281	264	235	210	190	171	154	139	128	110	87	61	K
L	186	231	320	326	386	353	405	351	385	310	325	258	232	209	189	172	157	143	131	113	90	64	L
M	166	257	285	366	342	400	355	397	331	353	272	254	229	206	188	171	158	144	132	113	90	64	M
N	173	218	306	314	378	347	396	341	374	300	316	252	227	204	186	170	157	143	129	110	86	60	N
O	141	223	253	332	320	381	337	380	317	343	267	253	225	201	183	167	155	140	124	104	80	55	O
P		176	252	266	327	310	366	320	352	285	307	248	220	197	180	163	146	130	115	95	72		P
Q		156	190	249	256	318	295	344	288	315	248	237	211	189	173	155	137	118	103	83	61		Q
R			167	191	237	245	305	274	310	252	274	222	200	180	164	145	125	106	89	70			R
S			118	164	180	228	234	285	246	275	213	206	189	171	153	134	112	92	74	55			S
T				114	155	170	213	209	248	204	222	183	169	153	136	117	96	76	58				T
U					102	138	149	181	170	185	155	153	141	127	111	93	75	57					U
V						83	112	117	137	124	132	119	109	96	82	66	50						V
W									80	91	80	81	73	62									W
	1	2	3	4	5	6	7	8	9	10	11	12	13	14	15	16	17	18	19	20	21	22	

Figure 28: Variation of channel power (kW) over the first 0.2 s of the transient for equilibrium natural uranium fuel. Results obtained from RFSP-IST. A summary of key parameters for each of the time steps as the transient progresses is provided in Table 15.

	1	2	3	4	5	6	7	8	9	10	11	12	13	14	15	16	17	18	19	20	21	22	
A									397	358	374	316	279	241									A
B						410	446	538	511	549	467	434	387	335	284	228	175						B
C					481	531	656	651	720	637	639	535	483	426	365	303	241	184					C
D				514	585	736	753	856	788	829	675	616	558	496	432	367	300	235	176				D
E			501	602	769	807	939	892	962	821	823	669	604	538	474	409	343	278	216	157			E
F			587	777	826	987	953	1053	925	950	777	702	626	556	498	435	372	310	252	192			F
G		532	753	830	989	976	1107	1017	1060	902	909	741	650	573	515	452	389	329	279	220	159		G
H		679	792	999	980	1121	1064	1151	1004	1025	848	766	668	587	526	463	401	345	301	245	184		H
J	542	695	942	986	1117	1069	1180	1072	1119	948	949	770	675	593	526	464	407	355	316	263	201	138	J
K	545	815	924	1121	1065	1186	1105	1183	1034	1047	852	763	673	593	527	465	409	361	327	276	215	149	K
L	616	779	1034	1070	1194	1128	1220	1097	1134	950	932	750	667	592	528	469	418	373	335	284	222	155	L
M	566	843	957	1171	1118	1243	1133	1202	1036	1037	834	742	662	589	527	470	422	377	338	284	222	154	M
N	577	744	1003	1051	1200	1130	1225	1087	1121	938	922	743	660	585	523	467	420	374	332	277	214	147	N
O	486	744	865	1084	1066	1206	1097	1170	1009	1020	834	750	658	579	517	461	416	367	320	263	200	136	O
P		607	840	904	1061	1029	1152	1037	1079	905	910	740	646	568	509	451	395	342	296	240	180		P
Q		536	659	838	866	1023	978	1076	931	950	786	711	621	547	490	430	370	313	266	211	154		Q
R			575	662	796	829	976	904	965	814	819	667	591	522	465	403	340	281	232	179			R
S			415	566	625	765	791	910	811	844	686	623	561	498	437	373	306	245	194	142			S
T				403	532	591	712	706	788	674	678	555	503	446	387	326	263	204	152				T
U					362	475	515	603	575	601	507	467	423	372	318	262	205	154					U
V						292	382	405	457	419	428	366	326	281	235	186	138						V
W									275	302	268	251	219	186									W
	1	2	3	4	5	6	7	8	9	10	11	12	13	14	15	16	17	18	19	20	21	22	

Figure 29: Variation of channel power (kW) over the first 0.3 s of the transient for equilibrium natural uranium fuel. Results obtained from RFSP-IST. A summary of key parameters for each of the time steps as the transient progresses is provided in Table 15.

4.2.5 Equilibrium Fuel with Evenly Distributed BNAs

The fifth simulation performed was for fuel with 180 mg Gd_2O_3 and 1000 mg B_2O_3 evenly distributed in each element of the thirty-seven-element fuel with equilibrium nuclide concentrations assumed. This simulation serves the first case for comparison against the equilibrium natural uranium simulation with burnable neutron absorbers added to the fuel. Table 16 provides a summary of significant parameters including total core power, maximum channel power, maximum bundle power, mean channel power, and minimum channel power for each time step in the transient simulation.

Table 16: Raw RFSP-IST CERBERUS data for equilibrium fuel with evenly distributed BNAs. Core Power (sum of all channel powers) in MW, Maximum Channel Power in kW, Maximum Bundle Power in kW, Mean Channel Power in kW, and Minimum Channel Power in kW are provided from RFSP-IST for each time step in the LLOCA transient simulation.

Equilibrium Fuel with Evenly Distributed BNAs				
Parameter	Initial Steady-State	Transient t=0.1s	Transient t=0.2s	Transient t=0.3s
Core Power (MW)	2061.4	2077.4	2152.6	2318.1
Maximum Channel Power (kW)	7795.5	7887.8	8169.2	8770.3
Maximum Bundle Power (kW)	823.7	837.8	873.2	941.3
Mean Channel Power (kW)	5424.7	5467.0	5664.6	6100.2
Minimum Channel Power (kW)	2392.9	2365.8	2471.6	2647.8

Table 17 utilizes the data outlined in Table 16 to provide a summary of the change in core power, maximum channel power, mean channel power, and minimum channel power for each time step in the transient simulation relative to the initial steady-state power distribution at time t = 0 s. Due to the changes in initial power distribution for each case, these delta tables should be used for comparison between cases.

Table 17: Change in powers relative to initial power distribution for equilibrium fuel with evenly distributed BNAs. Change in Core Power (sum of all channel powers) in MW, Maximum Change in Channel Power in kW, Change in Mean Channel Power in kW, and Minimum Change in Channel Power in kW, relative to the initial steady-state power distribution, are provided from RFSP-IST for each time step in the LLOCA transient simulation.

Equilibrium Fuel with Evenly Distributed BNAs			
Parameter	Transient t=0.1s	Transient t=0.2s	Transient t=0.3s
Δ Core Power (MW)	16.1	91.2	256.7
Maximum Δ Channel Power (kW)	206.1	387.4	1046.1
Δ Mean Channel Power (kW)	42.3	239.9	675.4
Minimum Δ Channel Power (kW)	-119.3	69.8	254.9

Cross-sectional core maps of channel powers are provided in Figure 30, Figure 31, and Figure 32. Like the fresh fuel case, when comparing the results from the equilibrium natural uranium case in Table 14 and Table 15 with evenly distributed burnable neutron absorbers in Table 16 and Table 17 one may note that the change in total core power is greater in the case when burnable neutron absorbers are added. However, the maximum change in channel power is again lower when burnable neutron absorbers are added. Thus, this is again an improvement for the hypothetical large loss of coolant accident because the regionalized maximum change in power is dampened as shown from the lower maximum change in channel power. Larger magnitude power changes are noted for both change in maximum channel power and total core power, in line with expectation given the reduced delayed neutron fraction due to accumulation of Pu-239 in the fuel, along with build-up of neutron absorbing Xe-135. It should also be noted that the difference in adjacent channel powers is lower for the case with evenly distributed burnable neutron absorbers compared visually with the natural uranium case, implying an improvement to axial flux balance.

	1	2	3	4	5	6	7	8	9	10	11	12	13	14	15	16	17	18	19	20	21	22	
A									8	18	32	56	67	80									A
B						-16	-12	-5	4	19	36	66	82	93	100	95	91						B
C					-26	-25	-20	-13	1	18	42	80	99	114	120	117	109	105					C
D				-36	-36	-35	-30	-19	-5	13	43	89	113	132	141	141	134	122	113				D
E			-43	-47	-48	-47	-40	-29	-14	12	39	95	122	144	157	160	156	144	128	113			E
F			-57	-60	-62	-62	-51	-40	-18	6	41	96	125	150	168	174	174	164	148	131			F
G		-60	-72	-75	-82	-72	-63	-45	-26	5	36	96	128	156	176	185	190	182	166	143	124		G
H		-74	-80	-92	-87	-84	-69	-55	-30	-2	37	96	130	159	181	192	200	195	180	158	134		H
J	-65	-75	-94	-96	-99	-90	-80	-59	-39	-4	31	95	131	161	182	195	205	202	189	168	138	113	J
K	-64	-86	-96	-105	-102	-100	-83	-69	-40	-12	31	94	130	161	183	196	206	204	195	175	144	113	K
L	-72	-86	-107	-109	-108	-100	-92	-70	-49	-12	25	92	128	160	182	196	202	201	197	178	147	117	L
M	-69	-92	-104	-119	-111	-113	-94	-83	-49	-15	25	89	126	157	180	194	201	200	196	176	146	115	M
N	-70	-86	-109	-114	-119	-108	-105	-78	-51	-18	23	86	122	153	176	190	197	196	191	171	141	110	N
O	-66	-87	-100	-117	-113	-116	-98	-87	-54	-19	20	80	117	149	171	185	193	191	183	162	133	108	O
P		-80	-98	-105	-116	-108	-104	-80	-62	-21	19	77	112	142	165	178	187	183	170	150	127		P
Q		-75	-84	-98	-101	-107	-91	-83	-52	-20	16	72	106	134	155	166	173	167	153	133	116		Q
R			-77	-83	-92	-91	-90	-71	-56	-20	15	68	99	125	143	151	155	148	133	119			R
S			-62	-71	-77	-82	-75	-70	-45	-18	13	64	93	116	130	135	135	126	111	99			S
T				-58	-63	-65	-65	-55	-45	-17	12	57	82	101	112	115	111	101	94				T
U					-49	-51	-49	-46	-32	-16	9	47	68	83	91	91	86	82					U
V						-36	-37	-33	-26	-11	5	36	52	64	70	68	65						V
W									-18	-8	6	27	38	49									W
	1	2	3	4	5	6	7	8	9	10	11	12	13	14	15	16	17	18	19	20	21	22	

Figure 30: Variation of channel power (kW) over the first 0.1 s of the transient for equilibrium fuel with evenly distributed BNAs. Results obtained from RFSP-IST. A summary of key parameters for each of the time steps as the transient progresses is provided in Table 17.

	1	2	3	4	5	6	7	8	9	10	11	12	13	14	15	16	17	18	19	20	21	22	
A									153	155	161	179	179	189									A
B						123	142	162	176	184	198	218	219	217	213	190	173						B
C					129	145	166	193	209	227	239	266	266	265	253	232	206	191					C
D				126	146	169	199	221	245	249	277	304	306	306	297	276	250	219	198				D
E			116	139	164	196	220	249	256	283	288	331	333	335	329	312	288	255	220	192			E
F			132	153	187	206	241	253	281	284	316	347	348	352	352	338	320	290	254	220			F
G		117	129	169	189	232	242	276	280	308	312	356	361	367	369	359	347	319	281	239	205		G
H		113	148	168	212	229	261	271	301	303	333	365	372	378	382	373	365	340	304	261	220		H
J	91	122	143	186	204	244	249	285	289	320	323	370	377	384	385	378	374	352	319	277	225	183	J
K	97	115	158	179	217	230	261	270	303	304	339	373	379	386	387	380	376	356	328	288	234	183	K
L	89	124	146	187	199	235	245	280	284	316	324	374	377	385	387	380	369	351	332	292	238	188	L
M	95	112	153	167	204	211	251	254	292	300	332	367	372	380	383	377	367	348	330	290	237	186	M
N	81	115	134	174	180	220	224	264	275	301	315	359	364	373	376	371	360	342	322	282	229	178	N
O	86	98	135	151	187	194	231	235	272	282	307	341	353	362	366	361	353	334	309	268	217	174	O
P		101	113	148	163	201	202	241	241	277	287	328	339	348	354	348	343	321	288	248	209		P
Q		87	107	125	158	167	202	208	242	253	278	310	321	329	334	326	318	294	261	222	193		Q
R			91	112	131	162	168	205	208	242	255	294	300	307	309	299	288	262	228	201			R
S			80	89	116	134	162	171	205	216	243	274	280	286	283	270	253	226	193	169			S
T				80	90	114	131	159	165	195	208	243	248	252	246	231	209	184	165				T
U					78	86	108	124	146	156	178	203	207	209	201	185	164	150					U
V						70	80	102	109	125	134	157	162	162	159	141	126						V
W									90	91	104	118	120	127									W
	1	2	3	4	5	6	7	8	9	10	11	12	13	14	15	16	17	18	19	20	21	22	

Figure 31: Variation of channel power (kW) over the first 0.2 s of the transient for equilibrium fuel with evenly distributed BNAs Results obtained from RFSP-IST. A summary of key parameters for each of the time steps as the transient progresses is provided in Table 17.

	1	2	3	4	5	6	7	8	9	10	11	12	13	14	15	16	17	18	19	20	21	22	
A									485	463	453	453	425	425									A
B						449	497	547	563	558	559	550	519	487	456	391	345						B
C					495	537	595	657	677	689	675	673	630	590	538	473	406	366					C
D				514	572	643	720	764	798	773	787	771	723	681	627	561	489	417	368				D
E			501	577	660	753	809	864	856	871	834	843	787	745	694	630	560	483	407	349			E
F			581	658	761	820	893	906	932	893	908	886	825	782	740	681	620	545	465	397			F
G		545	611	739	819	918	927	982	953	960	909	913	860	816	776	720	670	597	512	427	361		G
H		567	688	780	898	943	995	995	1015	967	965	941	888	843	803	748	703	633	551	465	386		H
J	477	593	710	841	906	996	985	1036	1005	1012	955	957	903	857	811	757	718	653	576	491	392	318	J
K	490	601	757	845	946	978	1023	1017	1044	991	997	970	909	863	817	762	722	660	592	509	408	316	K
L	486	628	749	876	910	989	999	1046	1013	1018	973	975	907	862	816	763	710	651	598	516	415	324	L
M	494	606	762	841	927	950	1017	1002	1032	984	988	961	897	854	810	758	705	647	596	513	412	320	M
N	456	598	718	846	877	963	965	1017	990	987	948	945	881	839	796	746	695	637	582	499	399	307	N
O	459	550	698	787	880	908	969	955	983	939	927	904	859	818	777	728	682	623	560	476	380	302	O
P		543	624	747	818	907	898	952	911	923	874	873	828	789	753	704	665	601	525	443	368		P
Q		487	569	657	763	805	865	863	890	853	846	827	785	747	713	663	619	553	476	399	341		Q
R			501	579	660	747	760	823	797	815	783	785	737	701	664	611	563	496	420	362			R
S			426	477	572	639	702	719	762	739	749	735	690	654	610	554	500	431	358	308			S
T				415	455	533	584	643	642	667	647	653	613	579	534	477	417	354	310				T
U					379	409	473	514	550	545	555	548	515	483	441	386	330	293					U
V						320	354	412	418	432	423	428	405	378	351	297	255						V
W									336	317	327	324	304	298									W
	1	2	3	4	5	6	7	8	9	10	11	12	13	14	15	16	17	18	19	20	21	22	

Figure 32: Variation of channel power (kW) over the first 0.3 s of the transient for equilibrium fuel with evenly distributed BNAs. Results obtained from RFSP-IST. A summary of key parameters for each of the time steps as the transient progresses is provided in Table 17.

4.2.6 Equilibrium Fuel with Center Pin BNAs

The sixth simulation performed was for fuel with 180 mg Gd_2O_3 and 1000 mg B_2O_3 distributed only in the center element of the thirty-seven-element fuel with equilibrium nuclide concentrations assumed. This simulation serves the second case for comparison against the equilibrium natural uranium simulation with burnable neutron absorbers added to the fuel. Table 18 provides a summary of significant parameters including total core power, maximum channel power, maximum bundle power, mean channel power, and minimum channel power for each time step in the transient simulation.

Table 18: Raw RFSP-IST CERBERUS data for equilibrium fuel with center pin BNAs. Core Power (sum of all channel powers) in MW, Maximum Channel Power in kW, Maximum Bundle Power in kW, Mean Channel Power in kW, and Minimum Channel Power in kW are provided from RFSP-IST for each time step in the LLOCA transient simulation.

Equilibrium Fuel with Center Pin BNAs				
Parameter	Initial Steady-State	Transient t=0.1s	Transient t=0.2s	Transient t=0.3s
Core Power (MW)	2061.4	2075.8	2143.2	2290.6
Maximum Channel Power (kW)	7796.4	7881.3	8134.5	8671.2
Maximum Bundle Power (kW)	826.5	839.2	868.8	931.9
Mean Channel Power (kW)	5424.7	5462.7	5640.0	6028.0
Minimum Channel Power (kW)	2398.6	2372.6	2467.8	2629.8

Table 19 utilizes the data outlined in Table 18 to provide a summary of the change in core power, maximum channel power, mean channel power, and minimum channel power for each time step in the transient simulation relative to the initial steady-state power distribution at time t = 0 s. Due to the changes in initial power distribution for each case, these delta tables should be used for comparison between cases.

Table 19: Change in powers relative to initial power distribution for equilibrium fuel with center pin BNAs. Change in Core Power (sum of all channel powers) in MW, Maximum Change in Channel Power in kW, Change in Mean Channel Power in kW, and Minimum Change in Channel Power in kW, relative to the initial steady-state power distribution, are provided from RFSP-IST for each time step in the LLOCA transient simulation.

Equilibrium Fuel with Center Pin BNAs			
Parameter	Transient t=0.1s	Transient t=0.2s	Transient t=0.3s
Δ Core Power (MW)	14.4	81.8	229.2
Maximum Δ Channel Power (kW)	192.2	354.8	928.9
Δ Mean Channel Power (kW)	38.0	215.2	603.3
Minimum Δ Channel Power (kW)	-114.7	60.8	231.2

Cross-sectional core maps of channel powers are provided in Figure 33, Figure 34, and Figure 35. Comparing the results from the equilibrium natural uranium case in Table 14 and Table 15 with the center pin containing burnable neutron absorber case in Table 18 and Table 19 it is noted that the change in total core power is lower when burnable neutron absorbers are added. A second improvement is noted as the regionalized maximum change in power is dampened. When comparing the equilibrium center pin burnable neutron absorber case against the fresh core center pin case in Table 12 and Table 13 it is again emphasized that larger power changes occur in the equilibrium case. This is due to a combination of the build-up of Xe-135 and Pu-239, along with the reduction in effectiveness of the burnable neutron absorbers due to the time they have spent in core to establish equilibrium conditions. It should also be noted that the difference in adjacent channel powers is lower for the case with evenly distributed burnable neutron absorbers compared with the natural uranium case, implying an improvement to axial flux balance.

	1	2	3	4	5	6	7	8	9	10	11	12	13	14	15	16	17	18	19	20	21	22	
A									5	15	28	51	61	74									A
B						-17	-14	-7	2	15	31	61	76	86	92	88	85						B
C					-27	-25	-21	-14	-2	14	37	73	92	105	111	109	102	98					C
D				-36	-36	-35	-31	-21	-8	9	38	81	104	122	131	131	125	113	105				D
E			-43	-46	-48	-47	-40	-30	-16	9	34	87	112	133	146	149	145	134	119	105			E
F			-55	-59	-61	-61	-51	-41	-19	2	36	88	116	139	156	162	162	153	138	122			F
G		-58	-70	-73	-80	-70	-63	-45	-28	2	31	88	118	144	163	172	177	170	154	133	115		G
H		-71	-77	-89	-85	-82	-68	-55	-31	-5	32	88	121	148	169	179	186	181	168	147	125		H
J	-63	-72	-91	-92	-96	-87	-78	-58	-40	-6	26	87	121	149	170	181	191	188	176	156	128	105	J
K	-62	-83	-93	-101	-99	-97	-81	-68	-41	-14	27	86	120	150	170	183	192	191	182	163	134	106	K
L	-69	-82	-103	-105	-104	-97	-89	-69	-49	-14	21	85	119	149	170	182	189	188	184	166	137	109	L
M	-66	-88	-100	-115	-107	-109	-91	-81	-49	-16	21	82	116	146	168	181	187	187	183	165	136	108	M
N	-68	-83	-105	-109	-115	-104	-101	-76	-50	-19	19	79	113	143	164	177	184	183	178	160	131	103	N
O	-63	-83	-96	-112	-108	-112	-95	-85	-53	-20	16	74	109	138	159	172	180	178	171	151	124	100	O
P		-76	-94	-101	-112	-104	-100	-77	-61	-22	15	70	104	133	154	166	175	171	159	140	119		P
Q		-72	-80	-93	-97	-103	-88	-80	-51	-21	13	66	98	125	145	155	161	156	143	124	109		Q
R			-74	-80	-89	-87	-86	-68	-55	-21	12	63	92	116	133	141	145	138	124	111			R
S			-59	-68	-74	-79	-72	-68	-44	-19	11	59	86	108	121	126	126	118	104	93			S
T				-55	-60	-62	-62	-53	-44	-18	10	52	76	94	105	107	103	95	88				T
U					-46	-49	-47	-44	-32	-17	7	43	63	77	85	85	80	76					U
V						-34	-36	-32	-25	-11	4	33	48	59	65	63	60						V
W									-17	-8	5	25	35	45									W
	1	2	3	4	5	6	7	8	9	10	11	12	13	14	15	16	17	18	19	20	21	22	

Figure 33: Variation of channel power (kW) over the first 0.1 s of the transient for equilibrium fuel with center pin BNAs Results obtained from RFSP-IST. A summary of key parameters for each of the time steps as the transient progresses is provided in Table 19.

	1	2	3	4	5	6	7	8	9	10	11	12	13	14	15	16	17	18	19	20	21	22	
A									134	137	143	161	161	171									A
B						106	124	141	155	162	177	196	199	198	194	173	159						B
C					111	126	144	169	183	201	212	240	241	241	231	212	188	175					C
D				108	126	146	174	192	216	219	247	274	277	278	271	253	229	201	182				D
E			99	119	141	170	190	218	224	251	255	299	302	305	301	286	264	235	203	177			E
F			113	130	161	177	210	220	248	251	283	313	316	321	321	310	294	266	233	203			F
G		101	109	145	161	201	209	242	245	273	277	321	328	335	337	329	319	294	259	220	188		G
H		95	126	142	183	197	228	236	265	268	298	330	338	345	349	342	335	313	280	241	203		H
J	76	103	120	159	174	212	215	250	253	284	287	334	343	351	352	347	344	324	294	255	207	169	J
K	83	96	134	151	187	197	228	234	267	269	303	337	344	352	355	349	346	328	303	266	216	169	K
L	74	105	122	160	170	203	212	245	249	280	289	338	343	351	354	349	339	323	306	270	220	173	L
M	81	93	130	140	175	180	218	220	258	266	297	332	338	347	351	346	337	321	304	268	219	172	M
N	67	97	112	148	153	190	192	231	241	267	280	325	331	341	344	340	332	315	297	260	211	164	N
O	73	82	115	126	160	165	201	203	240	249	275	309	321	331	335	332	325	308	285	247	200	161	O
P		86	94	126	137	173	173	211	210	246	256	297	309	318	324	320	316	296	266	229	193		P
Q		72	91	105	135	142	175	179	213	223	249	281	292	301	306	300	293	271	240	205	178		Q
R			76	95	111	140	144	179	181	215	227	266	273	281	284	275	265	241	211	185			R
S			68	75	99	114	140	147	180	191	218	248	255	261	259	248	233	208	178	156			S
T				69	76	99	112	139	143	173	185	220	226	230	225	212	193	169	153				T
U					67	73	94	107	129	137	160	184	189	191	185	170	151	139					U
V						61	69	89	95	111	119	143	147	148	145	129	116						V
W									80	80	94	107	109	116									W
	1	2	3	4	5	6	7	8	9	10	11	12	13	14	15	16	17	18	19	20	21	22	

Figure 34: Variation of channel power (kW) over the first 0.2 s of the transient for equilibrium fuel with center pin BNAs. Results obtained from RFSP-IST. A summary of key parameters for each of the time steps as the transient progresses is provided in Table 19.

	1	2	3	4	5	6	7	8	9	10	11	12	13	14	15	16	17	18	19	20	21	22	
A									427	411	401	405	380	381									A
B						395	438	481	498	493	496	491	465	437	410	353	312						B
C					435	473	523	581	597	611	598	601	564	530	485	427	367	331					C
D				451	503	565	635	673	706	683	700	690	648	612	565	506	442	377	333				D
E			439	508	580	664	712	764	756	774	740	754	707	670	626	569	506	437	368	316			E
F			512	577	671	721	789	799	827	791	809	794	741	704	668	615	561	493	421	360			F
G		480	536	651	720	811	818	870	843	854	808	817	772	735	700	650	607	541	465	387	328		G
H		497	606	684	793	831	880	879	901	858	862	843	798	759	725	676	636	574	500	422	350		H
J	418	522	623	741	797	881	870	919	891	902	850	858	812	772	732	685	651	593	524	446	357	289	J
K	432	527	667	743	836	862	907	900	928	880	891	870	818	778	738	690	655	599	538	463	371	288	K
L	426	553	657	773	802	875	883	929	898	907	866	875	816	777	737	691	643	591	544	469	378	295	L
M	436	532	672	740	819	838	902	887	918	875	883	863	808	770	732	686	640	588	541	467	376	292	M
N	400	528	631	747	773	853	852	903	879	880	845	849	793	757	719	675	630	578	529	454	363	280	N
O	406	483	615	692	778	801	859	845	875	835	829	812	774	738	703	659	619	565	509	433	345	275	O
P		479	548	660	720	803	793	846	808	823	779	783	746	712	681	638	603	546	477	403	334		P
Q		428	502	579	675	710	767	763	792	759	757	742	707	675	645	600	562	503	433	363	310		Q
R			441	512	582	662	672	731	707	727	698	705	664	633	600	554	511	450	382	329			R
S			377	421	507	565	623	636	678	657	670	661	621	590	552	502	453	391	325	280			S
T				368	402	472	517	571	568	595	576	587	552	522	483	432	378	321	282				T
U					337	362	420	455	489	485	496	493	464	436	399	350	300	266					U
V						285	314	367	371	386	377	385	364	342	317	269	231						V
W									300	283	293	292	274	269									W
	1	2	3	4	5	6	7	8	9	10	11	12	13	14	15	16	17	18	19	20	21	22	

Figure 35: Variation of channel power (kW) over the first 0.3 s of the transient for equilibrium fuel with center pin BNAs. Results obtained from RFSP-IST. A summary of key parameters for each of the time steps as the transient progresses is provided in Table 19.

4.2.7 Startup Following Long Shutdown Natural Uranium Fuel

The seventh simulation performed was for natural uranium fuel with startup following a long shutdown nuclide concentrations including the absence of the negative reactivity contribution from the saturating fission product Xe-135, addition of a positive reactivity contribution from the buildup of fissile Pu-239 and Pu-241, and addition of negative reactivity contribution from the buildup of Sm-149 and Sm-151. This simulation serves the base case for comparison against the cases with burnable neutron absorbers added to the fuel. Table 20 provides a summary of significant parameters including total core power, maximum channel power, maximum bundle power, mean channel power, and minimum channel power for each time step in the transient simulation.

Table 20: Raw RFSP-IST CERBERUS data for startup natural uranium fuel following a long shutdown. Core Power (sum of all channel powers) in MW, Maximum Channel Power in kW, Maximum Bundle Power in kW, Mean Channel Power in kW, and Minimum Channel Power in kW are provided from RFSP-IST for each time step in the LLOCA transient simulation.

Startup Following Long Shutdown Natural Uranium Fuel				
Parameter	Initial Steady-State	Transient t=0.1s	Transient t=0.2s	Transient t=0.3s
Core Power (MW)	2061.4	2072.6	2136.9	2289.3
Maximum Channel Power (kW)	7222.8	7279.2	7523.0	8283.7
Maximum Bundle Power (kW)	749.4	756.4	807.2	897.4
Mean Channel Power (kW)	5424.7	5454.3	5623.5	6024.6
Minimum Channel Power (kW)	2150.7	2151.4	2203.6	2294.6

Table 21 utilizes the data outlined in Table 20 to provide a summary of the change in core power, maximum channel power, mean channel power, and minimum channel power for each time step in the transient simulation relative to the initial steady-state power distribution at time t = 0 s. Due to the changes in initial power distribution for each case, these delta tables should be used for comparison between cases.

Table 21: Change in powers relative to initial power distribution for startup natural uranium fuel following a long shutdown. Change in Core Power (sum of all channel powers) in MW, Maximum Change in Channel Power in kW, Change in Mean Channel Power in kW, and Minimum Change in Channel Power in kW, relative to the initial steady-state power distribution, are provided from RFSP-IST for each time step in the LLOCA transient simulation.

Startup Following Long Shutdown Natural Uranium Fuel			
Parameter	Transient t=0.1s	Transient t=0.2s	Transient t=0.3s
Δ Core Power (MW)	11.2	75.5	227.9
Maximum Δ Channel Power (kW)	65.6	382.7	1195.1
Δ Mean Channel Power (kW)	29.7	198.8	599.8
Minimum Δ Channel Power (kW)	-9.8	52.9	139.7

Cross-sectional core maps of channel powers are provided in Figure 36, Figure 37, and Figure 38. Comparing the results of the long shutdown fuel in Table 20 and Table 21 against the fresh natural uranium fuel in Table 8 and Table 9 it may be noted that larger changes are seen for both total core power and maximum change in channel power for the long shutdown fuel case. This characteristic is attributed to the fact that for core following a long shutdown an overall positive reactivity contribution is yielded from the combined effects of the lack of saturating fission product Xe-135, the build-up of fissile Pu-239 and Pu-241, and the less significant neutron absorbing effects from the build-up of Sm-149 and Sm-151. As for the equilibrium fuel case in Table 14 and Table 15, the fuel is burned prior to the long shutdown, increasing the nuclide concentrations of fissile Pu-239 in the fuel and reducing the margin to prompt criticality due to a reduction of the delayed neutron fraction in the fuel. Therefore, a larger change in power is noted for the long shutdown fuel case than for the fresh fuel case and also for the equilibrium case.

	1	2	3	4	5	6	7	8	9	10	11	12	13	14	15	16	17	18	19	20	21	22	
A									23	17	26	28	28	27									A
B						18	14	26	20	33	25	38	39	38	36	32	27						B
C					18	14	28	21	36	27	42	45	48	49	47	44	38	31					C
D				17	12	27	20	37	26	41	32	50	54	56	56	53	48	41	33				D
E			14	9	24	16	34	23	39	29	44	52	57	59	60	59	55	49	41	31			E
F			6	19	12	27	19	35	25	41	32	51	56	59	62	62	60	55	49	39			F
G		3	9	7	17	14	30	20	36	27	44	52	56	60	63	64	62	59	54	45	34		G
H		5	2	12	9	24	15	31	21	38	30	51	55	59	63	64	64	62	59	51	39		H
J	2	-1	7	3	17	9	24	15	31	23	41	49	54	59	62	64	64	63	62	55	44	31	J
K	-2	3	-1	13	3	18	9	25	16	33	26	47	53	57	61	63	64	64	64	58	47	33	K
L		-4	3	-2	12	2	18	9	25	18	36	45	51	56	60	63	65	65	65	59	49	35	L
M	-4	0	-6	2	-3	6	2	13	10	28	21	43	50	55	60	63	65	66	66	59	49	34	M
N	-2	-7	-1	-7	1	-4	7	3	21	13	32	42	48	55	59	63	65	65	64	58	47	32	N
O	-5	-3	-8	-1	-7	2	-3	8	5	24	18	41	47	53	58	62	64	64	62	55	43	30	O
P		-8	-4	-9	-1	-7	3	-1	11	10	30	40	46	52	57	60	61	60	57	49	38		P
Q		-4	-9	-6	-9	-1	-6	5	2	21	16	38	45	50	55	57	57	54	51	43	32		Q
R			-5	-10	-5	-9	0	-4	8	7	26	37	43	49	53	54	52	48	44	36			R
S			-7	-6	-9	-5	-7	2	0	18	13	35	42	47	50	50	47	42	36	28			S
T				-7	-5	-9	-3	-5	6	5	22	32	38	43	44	43	40	34	27				T
U					-6	-4	-7	-1	-1	8	9	27	33	36	36	34	30	25					U
V						-5	-2	-4	2	2	10	21	25	27	26	23	20						V
W									-1	4	4	14	16	17									W
	1	2	3	4	5	6	7	8	9	10	11	12	13	14	15	16	17	18	19	20	21	22	

Figure 36: Variation of channel power (kW) over the first 0.1 s of the transient for startup natural uranium fuel following a long shutdown. Results obtained from RFSP-IST. A summary of key parameters for each of the time steps as the transient progresses is provided in Table 21.

	1	2	3	4	5	6	7	8	9	10	11	12	13	14	15	16	17	18	19	20	21	22	
A									135	117	130	112	101	89									A
B						135	142	180	165	187	154	153	139	124	107	88	69						B
C					156	167	216	207	240	206	219	188	173	156	137	117	95	74					C
D				164	181	238	236	281	252	282	221	214	198	180	161	140	118	95	73				D
E			158	183	246	249	303	281	322	263	282	231	212	193	175	155	134	112	89	66			E
F			175	244	251	318	294	346	291	320	249	240	218	198	182	164	145	124	104	80			F
G		156	228	247	306	298	357	314	351	284	308	251	225	203	187	169	150	131	115	93	68		G
H		203	232	303	294	357	324	374	312	341	268	258	229	206	190	172	154	137	123	103	79		H
J	160	200	282	289	348	322	375	327	365	295	318	257	230	207	189	172	156	141	129	111	87	61	J
K	156	241	267	344	313	370	331	378	316	343	266	254	228	206	188	171	156	143	134	116	93	66	K
L	180	222	305	309	366	331	383	329	364	291	309	248	225	204	187	172	159	147	137	119	96	69	L
M	160	246	271	348	321	377	332	373	311	334	256	244	222	202	186	172	160	148	137	119	96	68	M
N	167	209	292	298	357	325	373	320	353	282	299	242	220	201	185	171	159	147	135	116	92	65	N
O	135	215	242	315	303	360	316	358	298	324	253	244	219	198	183	169	158	144	130	110	86	59	O
P		168	242	252	309	294	346	301	333	269	293	240	215	194	180	165	150	135	120	101	77		P
Q		151	182	239	243	303	279	326	272	301	237	230	207	187	173	157	140	123	109	88	65		Q
R			162	183	228	233	291	260	296	241	264	217	197	179	165	148	129	111	94	75			R
S			113	160	173	220	223	274	236	266	207	203	188	172	156	137	117	97	79	59			S
T				110	151	164	207	201	241	198	218	182	169	155	139	121	101	81	62				T
U					100	136	144	177	166	182	152	153	143	130	115	97	79	60					U
V						82	111	115	136	123	133	120	111	99	85	69	53						V
W									80	92	81	82	75	65									W
	1	2	3	4	5	6	7	8	9	10	11	12	13	14	15	16	17	18	19	20	21	22	

Figure 37: Variation of channel power (kW) over the first 0.2 s of the transient for startup natural uranium fuel following a long shutdown. Results obtained from RFSP-IST. A summary of key parameters for each of the time steps as the transient progresses is provided in Table 21.

	1	2	3	4	5	6	7	8	9	10	11	12	13	14	15	16	17	18	19	20	21	22	
A									397	358	376	318	281	243									A
B						411	444	536	507	546	464	432	386	336	286	231	178						B
C					480	528	650	642	709	627	630	529	478	423	365	305	244	188					C
D				513	580	727	740	838	769	810	658	604	547	488	428	366	302	239	181				D
E			500	597	760	791	916	867	934	796	799	651	589	527	467	405	343	281	220	161			E
F			582	768	809	962	924	1018	892	916	748	679	607	542	487	429	370	311	255	195			F
G		527	744	814	965	945	1068	977	1018	864	873	713	628	556	501	443	384	329	281	223	163		G
H		672	779	976	951	1084	1022	1104	960	980	810	735	643	568	511	452	395	343	302	248	187		H
J	539	686	924	960	1083	1029	1133	1023	1069	903	906	738	648	572	510	452	400	352	316	266	205	142	J
K	541	804	904	1090	1028	1141	1057	1130	984	999	811	730	646	572	511	453	402	357	326	278	219	153	K
L	612	768	1011	1038	1153	1083	1168	1045	1082	904	888	718	640	570	511	457	410	369	334	286	226	160	L
M	562	831	934	1137	1078	1195	1083	1148	987	990	795	712	636	568	510	458	415	373	337	286	226	159	M
N	574	734	982	1020	1160	1086	1176	1039	1071	895	882	713	635	565	508	457	413	371	332	280	218	151	N
O	483	736	848	1055	1033	1163	1053	1123	965	977	799	722	635	561	504	452	410	365	320	266	204	140	O
P		602	828	885	1033	997	1112	997	1038	869	876	715	626	553	498	444	392	342	299	244	184		P
Q		534	653	826	848	998	948	1042	899	920	759	690	605	535	482	425	368	315	270	216	158		Q
R			574	656	787	813	954	880	939	791	799	653	579	514	460	402	341	285	237	184			R
S			416	567	621	758	778	894	795	828	672	613	554	494	436	374	310	251	200	147			S
T				405	534	589	709	699	780	666	672	552	501	447	389	330	269	211	158				T
U					365	479	517	604	574	601	507	469	425	376	323	268	212	159					U
V						296	388	408	462	423	433	371	332	288	242	192	144						V
W									279	308	273	257	225	192									W
	1	2	3	4	5	6	7	8	9	10	11	12	13	14	15	16	17	18	19	20	21	22	

Figure 38: Variation of channel power (kW) over the first 0.3 s of the transient for startup natural uranium fuel following a long shutdown. Results obtained from RFSP-IST. A summary of key parameters for each of the time steps as the transient progresses is provided in Table 21.

4.2.8 Startup Following Long Shutdown Fuel with Evenly Distributed BNAs

The eighth simulation performed was for fuel with 180 mg Gd_2O_3 and 1000 mg B_2O_3 evenly distributed in each element of the thirty-seven-element fuel with long shutdown nuclide concentrations assumed. This simulation serves the first case with assumed long shutdown nuclide concentrations for comparison against the natural uranium simulation with burnable neutron absorbers added to the fuel. Table 22 provides a summary of significant parameters including total core power, maximum channel power, maximum bundle power, mean channel power, and minimum channel power for each time step in the transient simulation.

Table 22: Raw RFSP-IST CERBERUS data for startup fuel with evenly distributed BNAS following a long shutdown. Core Power (sum of all channel powers) in MW, Maximum Channel Power in kW, Maximum Bundle Power in kW, Mean Channel Power in kW, and Minimum Channel Power in kW are provided from RFSP-IST for each time step in the LLOCA transient simulation.

Startup Following Long Shutdown Fuel with Evenly Distributed BNAs				
Parameter	Initial Steady-State	Transient t=0.1s	Transient t=0.2s	Transient t=0.3s
Core Power (MW)	2061.4	2077.1	2151.0	2313.1
Maximum Channel Power (kW)	7754.1	7845.2	8120.4	8705.7
Maximum Bundle Power (kW)	816.5	830.6	867.4	933.6
Mean Channel Power (kW)	5424.7	5466.1	5660.5	6087.0
Minimum Channel Power (kW)	2408.6	2380.2	2484.9	2661.4

Table 23 utilizes the data outlined in Table 22 to provide a summary of the change in core power, maximum channel power, mean channel power, and minimum channel power for each time step in the transient simulation relative to the initial steady-state power distribution at time t = 0 s. Due to the changes in initial power distribution for each case, these delta tables should be used for comparison between cases.

Table 23: Change in powers relative to initial power distribution for startup fuel with evenly distributed BNAs following a long shutdown. Change in Core Power (sum of all channel powers) in MW, Maximum Change in Channel Power in kW, Change in Mean Channel Power in kW, and Minimum Change in Channel Power in kW, relative to the initial steady-state power distribution, are provided from RFSP-IST for each time step in the LLOCA transient simulation.

Startup Following Long Shutdown Fuel with Evenly Distributed BNAs			
Parameter	Transient t=0.1s	Transient t=0.2s	Transient t=0.3s
Δ Core Power (MW)	15.7	89.6	251.7
Maximum Δ Channel Power (kW)	207.0	383.1	1019.0
Δ Mean Channel Power (kW)	41.4	235.7	662.3
Minimum Δ Channel Power (kW)	-122.8	67.6	252.8

Cross-sectional core maps of channel powers are provided in Figure 39, Figure 40, and Figure 41. Comparing the results from the long shutdown natural uranium case in Table 21 with evenly distributed burnable neutron absorbers indicates an improvement for the hypothetical large loss of coolant accident because the regionalized maximum change in power is dampened as demonstrated by the comparison of each maximum change in channel power. The changes in maximum channel power and total core power are greater for the long shutdown case shown in this section than for the equilibrium core conditions in Table 17, as well as for the fresh core conditions in Table 11. This result is in line with expectation for the following reasons: the absence of neutron absorbing Xe-135, the build-up of fissile Pu-239 with a delayed neutron fraction lower than for U-235, and the depletion of the burnable neutron absorbers added to the CANLUB lining. A combination of these effects reduces the effectiveness of the burnable neutron absorbers resulting in the largest power increase of the three sets of simulations.

	1	2	3	4	5	6	7	8	9	10	11	12	13	14	15	16	17	18	19	20	21	22	
A									7	17	31	55	67	80									A
B						-17	-14	-7	3	18	35	66	82	93	100	95	92						B
C					-28	-26	-22	-14	-1	16	41	80	99	114	120	118	110	106					C
D				-38	-38	-37	-32	-21	-7	11	41	88	113	132	142	142	135	123	114				D
E			-45	-49	-50	-50	-42	-31	-16	10	37	94	121	144	157	161	157	145	129	114			E
F			-59	-62	-65	-64	-53	-42	-20	4	40	95	125	150	168	175	175	165	149	132			F
G		-62	-75	-77	-85	-75	-66	-48	-29	3	35	95	127	155	176	186	191	183	167	144	125		G
H		-76	-82	-95	-90	-88	-72	-58	-32	-5	35	94	130	159	181	193	201	196	181	159	135		H
J	-67	-77	-97	-99	-102	-93	-83	-62	-42	-6	29	94	130	161	182	195	206	203	191	169	139	114	J
K	-66	-88	-99	-108	-105	-103	-86	-72	-43	-15	29	92	129	161	183	196	207	205	197	176	146	115	K
L	-74	-89	-110	-112	-112	-104	-95	-73	-52	-14	23	91	127	159	182	196	203	203	199	179	149	118	L
M	-71	-95	-107	-123	-114	-116	-98	-87	-52	-17	23	88	125	157	180	194	202	201	198	178	147	117	M
N	-73	-89	-112	-117	-123	-112	-108	-81	-54	-20	21	85	121	153	176	191	198	197	193	173	142	111	N
O	-68	-89	-103	-120	-116	-120	-102	-91	-57	-21	18	79	117	149	171	186	194	192	185	164	134	109	O
P		-82	-101	-108	-120	-111	-107	-82	-64	-23	17	76	112	143	166	179	188	185	172	151	129		P
Q		-77	-86	-101	-104	-111	-94	-86	-55	-22	14	71	106	134	156	167	174	168	154	134	118		Q
R			-79	-86	-95	-94	-93	-73	-58	-22	14	67	99	125	144	152	156	149	134	120			R
S			-64	-73	-80	-84	-77	-73	-48	-20	12	63	93	116	131	136	137	127	113	100			S
T				-60	-65	-67	-67	-57	-47	-19	11	56	82	102	113	116	112	103	95				T
U					-50	-52	-51	-47	-34	-18	8	47	68	84	92	92	87	83					U
V						-37	-38	-34	-27	-12	5	36	52	64	71	68	65						V
W									-18	-9	5	27	38	49									W
	1	2	3	4	5	6	7	8	9	10	11	12	13	14	15	16	17	18	19	20	21	22	

Figure 39: Variation of channel power (kW) over the first 0.1 s of the transient for startup fuel with evenly distributed BNAs following a long shutdown Results obtained from RFSP-IST. A summary of key parameters for each of the time steps as the transient progresses is provided in Table 23.

	1	2	3	4	5	6	7	8	9	10	11	12	13	14	15	16	17	18	19	20	21	22	
A									150	152	159	177	177	187									A
B						119	139	158	173	181	195	215	217	216	212	189	173						B
C					125	141	162	188	204	222	234	263	264	263	252	231	205	190					C
D				122	142	165	194	215	239	243	272	300	302	303	294	275	249	218	198				D
E			112	134	159	190	213	242	249	277	282	326	329	332	326	310	286	255	220	192			E
F			127	148	181	199	233	245	274	277	309	341	343	348	349	336	319	289	253	220			F
G		113	124	163	182	224	233	268	272	300	304	349	356	363	365	356	345	318	281	239	205		G
H		108	142	161	204	220	252	262	292	295	325	358	366	374	378	370	363	338	304	261	220		H
J	87	117	137	179	196	235	239	275	279	311	315	363	371	379	381	375	371	350	318	277	225	184	J
K	93	110	151	171	209	220	252	260	293	295	331	366	373	381	383	377	373	354	328	288	234	184	K
L	85	119	139	179	191	226	235	270	274	307	316	366	370	380	382	377	367	349	331	292	239	188	L
M	91	107	146	159	196	202	241	244	282	292	323	359	366	375	379	374	364	347	330	290	237	186	M
N	77	109	128	166	172	211	215	254	266	292	307	352	358	368	372	368	358	341	322	282	229	178	N
O	82	93	129	144	179	185	222	226	263	274	300	335	348	358	363	359	352	333	309	268	217	175	O
P		97	107	142	155	193	194	233	233	269	280	323	334	345	351	346	342	321	288	249	209		P
Q		82	102	119	151	160	195	200	235	246	271	305	317	326	331	325	317	294	261	223	193		Q
R			86	107	125	156	161	199	201	236	249	289	297	305	307	298	287	262	229	201			R
S			76	85	111	129	156	165	199	211	239	270	278	284	282	269	253	226	193	169			S
T				77	86	110	126	154	160	191	204	240	246	250	245	230	209	184	166				T
U					75	83	105	120	143	153	175	201	206	208	201	185	164	151					U
V						68	77	99	106	123	131	156	161	161	158	141	126						V
W									88	89	103	117	120	126									W
	1	2	3	4	5	6	7	8	9	10	11	12	13	14	15	16	17	18	19	20	21	22	

Figure 40: Variation of channel power (kW) over the first 0.2 s of the transient for startup fuel with evenly distributed BNAs following a long shutdown Results obtained from RFSP-IST. A summary of key parameters for each of the time steps as the transient progresses is provided in Table 23.

	1	2	3	4	5	6	7	8	9	10	11	12	13	14	15	16	17	18	19	20	21	22	
A									476	455	445	446	418	419									A
B						441	487	536	553	548	549	541	511	480	450	386	341						B
C					486	526	583	644	664	676	662	661	619	581	531	467	401	362					C
D				504	560	630	705	748	781	756	771	757	710	669	618	553	483	412	364				D
E			491	566	647	737	791	845	836	852	815	826	772	732	683	621	552	477	402	345			E
F			569	644	745	801	872	884	911	872	887	867	808	767	727	670	611	538	459	392			F
G		534	598	723	800	897	904	958	928	936	887	892	841	800	762	708	660	589	506	422	358		G
H		555	673	762	877	920	970	969	989	942	942	919	869	825	787	734	691	624	545	460	382		H
J	467	581	694	822	884	972	959	1010	979	986	931	935	883	839	795	743	707	644	569	486	389	315	J
K	480	589	741	825	924	953	997	990	1016	965	972	947	889	845	801	749	710	651	585	503	404	313	K
L	476	615	732	856	888	965	973	1019	986	992	947	952	886	844	800	749	698	642	591	511	412	321	L
M	485	594	746	822	905	925	992	975	1005	959	963	939	877	836	794	744	694	638	588	508	409	318	M
N	447	587	703	828	856	940	940	991	964	962	924	923	862	822	781	733	684	628	575	494	395	305	N
O	450	539	683	769	860	885	946	930	959	916	905	884	841	802	763	716	672	615	554	472	376	300	O
P		532	611	731	799	886	876	930	889	902	853	854	811	774	740	694	656	594	519	439	365		P
Q		477	557	644	747	786	846	842	870	833	828	810	771	734	702	653	611	547	472	395	338		Q
R			491	568	646	732	743	806	780	798	767	770	725	690	654	603	557	490	417	359			R
S			418	468	561	626	689	704	748	725	735	723	679	644	602	548	494	427	355	305			S
T				407	446	523	573	631	629	655	635	643	604	571	527	472	413	351	308				T
U					372	402	465	505	541	536	546	541	508	477	436	382	327	290					U
V						315	348	406	411	426	417	423	400	374	347	295	253						V
W									331	313	323	321	300	295									W
	1	2	3	4	5	6	7	8	9	10	11	12	13	14	15	16	17	18	19	20	21	22	

Figure 41: Variation of channel power (kW) over the first 0.3 s of the transient for startup fuel with evenly distributed BNAs following a long shutdown. Results obtained from RFSP-IST. A summary of key parameters for each of the time steps as the transient progresses is provided in Table 23.

4.2.9 Startup Following Long Shutdown Fuel with Center Pin BNAs

The ninth simulation performed was for fuel with 180 mg Gd_2O_3 and 1000 mg B_2O_3 distributed only in the center element of the thirty-seven-element fuel with long shutdown nuclide concentrations assumed. This simulation serves the second case with assumed long shutdown nuclide concentrations for comparison against the natural uranium simulation with burnable neutron absorbers added to the fuel. Table 24 provides a summary of significant parameters including total core power, maximum channel power, maximum bundle power, mean channel power, and minimum channel power for each time step in the transient simulation.

Table 24: Raw RFSP-IST CERBERUS data for startup fuel with center pin BNAs following a long shutdown. Core Power (sum of all channel powers) in MW, Maximum Channel Power in kW, Maximum Bundle Power in kW, Mean Channel Power in kW, and Minimum Channel Power in kW are provided from RFSP-IST for each time step in the LLOCA transient simulation.

Startup Following Long Shutdown Fuel with Center Pin BNAs				
Parameter	Initial Steady-State	Transient t=0.1s	Transient t=0.2s	Transient t=0.3s
Core Power (MW)	2061.4	2075.5	2141.6	2285.8
Maximum Channel Power (kW)	7751.6	7835.2	8082.3	8603.8
Maximum Bundle Power (kW)	817.6	830.2	861.8	920.8
Mean Channel Power (kW)	5424.7	5461.8	5635.7	6015.2
Minimum Channel Power (kW)	2419.5	2392.0	2486.3	2649.1

Table 25 utilizes the data outlined in Table 24 to provide a summary of the change in core power, maximum channel power, mean channel power, and minimum channel power for each time step in the transient simulation relative to the initial steady-state power distribution at time t = 0 s. Due to the changes in initial power distribution for each case, these delta tables should be used for comparison between cases.

Table 25: Change in powers relative to initial power distribution for startup fuel with center pin BNAs following a long shutdown. Change in Core Power (sum of all channel powers) in MW, Maximum Change in Channel Power in kW, Change in Mean Channel Power in kW, and Minimum Change in Channel Power in kW, relative to the initial steady-state power distribution, are provided from RFSP-IST for each time step in the LLOCA transient simulation.

Startup Following Long Shutdown Fuel with Center Pin BNAs			
Parameter	Transient t=0.1s	Transient t=0.2s	Transient t=0.3s
Δ Core Power (MW)	14.1	80.2	224.4
Maximum Δ Channel Power (kW)	193.0	350.5	902.3
Δ Mean Channel Power (kW)	37.0	211.0	590.4
Minimum Δ Channel Power (kW)	-118.3	58.6	229.6

Cross-sectional core maps of channel powers are provided in Figure 42, Figure 43, and Figure 44. Similar to the fresh and equilibrium fuel cases in Table 20, Table 21 and Table 22, Table 23 respectively, results from the long shutdown case with burnable neutron absorbers added to the center pin of the fuel bundle indicate that an improvement is seen with respect to the maximum change in channel power. In addition, the maximum change in core power is dampened when compared against the natural uranium case. Similar effects may be noted with respect to flux flattening in both the radial and axial directions across the core from the visual aid provided in the Figure 42, Figure 43, and Figure 44.

	1	2	3	4	5	6	7	8	9	10	11	12	13	14	15	16	17	18	19	20	21	22	
A									4	14	27	50	61	74									A
B						-18	-15	-9	0	14	30	60	75	86	93	88	85						B
C					-28	-27	-23	-16	-3	13	36	73	92	105	111	109	102	98					C
D				-38	-38	-37	-33	-23	-10	8	36	81	104	122	131	132	125	114	106				D
E			-44	-48	-50	-49	-43	-32	-19	7	32	86	112	133	146	149	146	135	120	106			E
F			-57	-61	-64	-64	-53	-43	-22	0	34	87	115	139	156	162	163	154	139	123			F
G		-60	-73	-75	-83	-73	-65	-48	-31	-1	30	87	118	144	163	173	178	171	155	134	116		G
H		-74	-80	-93	-88	-86	-71	-58	-33	-8	30	87	120	148	169	180	187	182	169	148	126		H
J	-65	-75	-94	-96	-99	-91	-82	-61	-43	-9	24	86	120	149	170	182	192	189	178	158	130	107	J
K	-64	-85	-96	-105	-102	-100	-84	-71	-44	-17	25	85	120	149	170	183	193	192	184	165	136	107	K
L	-71	-85	-106	-108	-108	-100	-92	-72	-52	-16	19	84	118	148	170	183	190	189	186	167	139	110	L
M	-68	-91	-103	-118	-110	-112	-95	-84	-52	-19	19	81	116	146	168	181	188	188	185	166	138	109	M
N	-70	-85	-108	-113	-118	-108	-105	-79	-53	-21	18	78	112	143	164	178	185	184	180	161	133	104	N
O	-65	-86	-99	-116	-112	-115	-98	-88	-56	-22	15	73	108	138	160	173	181	180	172	153	126	102	O
P		-79	-97	-104	-115	-107	-103	-80	-63	-24	14	69	104	133	154	167	176	173	160	141	120		P
Q		-74	-83	-96	-100	-107	-91	-83	-54	-23	11	65	98	125	145	156	162	157	144	126	110		Q
R			-76	-82	-92	-90	-89	-71	-57	-23	11	62	92	117	134	142	146	139	126	112			R
S			-61	-70	-76	-81	-74	-71	-47	-21	9	58	86	108	122	127	128	119	105	94			S
T				-57	-62	-64	-65	-55	-47	-19	9	52	76	95	105	108	104	96	89				T
U					-48	-51	-49	-46	-33	-18	6	43	63	78	85	86	81	77					U
V						-36	-37	-33	-26	-12	3	33	49	60	66	64	61						V
W									-18	-9	4	25	35	46									W
	1	2	3	4	5	6	7	8	9	10	11	12	13	14	15	16	17	18	19	20	21	22	

Figure 42: Variation of channel power (kW) over the first 0.1 s of the transient for startup fuel with center pin BNAs following a long shutdown. Results obtained from RFSP-IST. A summary of key parameters for each of the time steps as the transient progresses is provided in Table 25.

	1	2	3	4	5	6	7	8	9	10	11	12	13	14	15	16	17	18	19	20	21	22	
A									130	135	140	159	160	170									A
B						103	121	137	151	159	173	193	196	196	193	173	158						B
C					107	122	139	164	178	196	207	236	239	238	229	211	188	175					C
D				104	122	141	168	186	209	213	242	269	274	275	269	251	228	200	182				D
E			95	115	135	164	183	210	217	244	249	293	297	302	298	284	263	234	202	177			E
F			108	125	155	169	202	212	240	243	276	307	311	317	318	308	292	265	233	203			F
G		96	103	139	154	193	200	233	237	265	269	315	323	330	334	326	317	293	259	220	189		G
H		90	120	134	175	188	218	227	256	259	290	323	332	340	345	339	333	311	280	241	203		H
J	72	98	114	151	165	202	205	240	243	275	279	327	337	345	348	343	341	322	293	255	208	170	J
K	78	91	127	143	178	187	218	224	257	259	295	330	338	347	351	346	343	326	302	266	217	170	K
L	70	100	115	152	161	194	202	235	239	271	280	331	336	346	350	346	337	322	305	270	221	174	L
M	77	88	123	132	167	171	208	210	248	256	288	325	332	342	347	343	335	320	304	268	219	172	M
N	63	92	105	140	144	181	183	221	232	258	272	318	325	336	340	338	330	314	297	260	212	165	N
O	69	76	108	119	152	156	192	194	231	241	268	303	316	327	332	329	324	307	285	248	201	162	O
P		81	88	119	129	165	165	202	202	238	249	292	304	315	321	318	315	296	266	230	194		P
Q		68	86	99	128	134	168	171	206	216	242	276	288	298	304	298	292	271	241	206	179		Q
R			71	90	105	133	137	172	174	208	221	261	270	278	282	274	264	241	211	186			R
S			64	71	95	109	135	141	175	185	213	245	253	259	258	247	233	208	178	156			S
T				66	72	94	108	134	138	169	181	217	224	229	224	212	193	170	153				T
U					64	70	91	103	125	134	157	181	187	190	184	170	152	139					U
V						59	66	87	93	109	117	141	146	147	145	129	116						V
W									78	79	92	107	109	115									W
	1	2	3	4	5	6	7	8	9	10	11	12	13	14	15	16	17	18	19	20	21	22	

Figure 43: Variation of channel power (kW) over the first 0.2 s of the transient for startup fuel with center pin BNAs following a long shutdown. Results obtained from RFSP-IST. A summary of key parameters for each of the time steps as the transient progresses is provided in Table 25.

	1	2	3	4	5	6	7	8	9	10	11	12	13	14	15	16	17	18	19	20	21	22	
A									418	403	393	398	374	375									A
B						386	429	471	488	483	486	482	457	430	404	348	307						B
C					425	463	511	568	584	598	585	589	554	521	477	420	362	327					C
D				441	492	552	621	657	689	666	684	675	635	600	555	498	436	372	329				D
E			430	497	567	648	694	745	736	754	721	737	691	657	614	559	499	432	364	313			E
F			500	564	655	702	769	777	806	770	789	775	724	689	655	604	552	486	416	356			F
G		470	523	635	701	790	795	847	819	831	786	797	754	719	686	639	597	533	459	383	325		G
H		485	591	667	772	808	856	854	876	833	838	822	779	742	710	663	625	565	494	418	347		H
J	409	511	607	723	775	857	844	893	864	876	826	836	792	755	717	671	640	583	517	441	354	286	J
K	423	515	651	723	814	838	881	873	901	855	866	848	798	760	722	677	643	590	531	457	368	285	K
L	417	541	641	753	780	851	857	902	872	882	841	852	796	760	722	677	632	582	537	464	375	293	L
M	427	520	656	720	798	814	877	860	892	850	859	841	788	753	717	673	629	579	535	462	372	290	M
N	392	516	615	728	752	830	828	878	853	856	821	828	775	741	705	663	620	570	523	449	360	278	N
O	397	472	601	674	758	778	836	821	851	812	808	792	756	723	689	648	609	558	503	429	343	273	O
P		469	535	644	702	783	772	823	786	802	759	766	730	698	669	628	594	539	472	399	332		P
Q		419	491	565	659	691	748	743	772	740	739	727	693	662	634	591	554	497	429	360	308		Q
R			431	501	569	647	655	714	690	710	682	691	652	622	591	546	505	445	379	327			R
S			369	412	496	552	609	621	663	643	656	648	611	581	544	496	449	388	323	278			S
T				361	394	463	506	560	556	583	565	577	544	515	477	428	375	319	280				T
U					330	355	413	446	480	476	488	485	458	431	394	346	297	264					U
V						280	308	361	365	380	372	380	360	338	314	267	230						V
W									295	279	290	288	271	267									W
	1	2	3	4	5	6	7	8	9	10	11	12	13	14	15	16	17	18	19	20	21	22	

Figure 44: Variation of channel power (kW) over the first 0.3 s of the transient for startup fuel with center pin BNAs following a long shutdown. Results obtained from RFSP-IST. A summary of key parameters for each of the time steps as the transient progresses is provided in Table 25.

4.2.10 Phase Two Summary

The results outlined in Table 8 through Table 25 and Figure 18 through Figure 44 are summarized in Table 26 in order to facilitate a comparison between the delta cases with burnable neutron absorbers added to the fuel against the delta natural uranium case. For each parameter, the delta for the individual burnable neutron absorber simulation is compared against the same delta for the corresponding natural uranium simulation as described in Equation 23:

$$\Delta p_{comp} = \Delta p_{bna} - \Delta p_{nu} \quad 23$$

where Δp_{comp} is the parameter calculated for inclusion in Table 26, Δp_{bna} is the change in the burnable neutron absorber parameter for the simulation of interest, and Δp_{nu} is the natural uranium parameter for the simulation of interest.

As such, a positive value for Δp_{comp} indicates that an increase in that parameter has occurred for the given burnable neutron absorber case relative to the natural uranium case, whereas a negative would indicate that a decrease has occurred. When considering this, the change in maximum channel power and the change in total core power would optimally yield negative values indicating a dampening in the power pulse during the hypothetical large loss of coolant accident.

The most important parameter for the purposes of this study is the maximum change in channel power. The safety analysis is based primarily on maintaining fuel geometry and limiting fuel failure, which is dependent on the sheath temperature and the power ramp occurring in that bundle. By demonstrating an improvement in regionalized channel powers, and ultimately the maximum change in channel power, one may conclude that these margins are improved.

The results presented in Table 26 demonstrate that the maximum change in channel power is improved for all the burnable neutron absorber simulations. The results also indicate that the magnitude of the improvement is greater for the addition of burnable neutron absorbers in the center pin than for the absorbers evenly distributed in each element case. The range of maximum to minimum channel power changes vary over the six burnable neutron absorber simulations that are compared against the three natural uranium simulations and are discussed further in Section 5.

Table 26: Summary of significant parameters relative to the natural uranium fuel case as described in Equation 23.

Summary										
		Fresh			Equilibrium			Long Shutdown		
Case	Parameter	Transient t=0.1s	Transient t=0.2s	Transient t=0.3s	Transient t=0.1s	Transient t=0.2s	Transient t=0.3s	Transient t=0.1s	Transient t=0.2s	Transient =0.3s
Evenly Distributed BNAs	Δ Maximum Channel Power (kW)	93.9	19.9	-108.1	145.9	-17.5	-197.3	141.4	0.4	-176.1
	Δ Minimum Channel Power (kW)	-54.3	19.3	93.3	-115.1	20.0	118.9	-113.0	14.7	113.1
	Δ Core Power (MW)	6.0	15.8	23.0	4.2	13.7	23.6	4.5	14.0	23.7
Center Pin BNAs	Δ Maximum Channel Power (kW)	116.7	22.3	-251.4	132.0	-50.1	-314.5	127.4	-32.2	-292.8
	Δ Minimum Channel Power (kW)	-84.4	-1.3	88.2	-110.5	11.0	95.2	-108.5	5.7	89.9
	Δ Core Power (MW)	5.0	8.1	-0.3	2.6	4.3	-3.8	2.8	4.6	-3.6

5 Discussion

5.1 Phase One

5.1.1 Phase One Overview

The Phase One study demonstrated that the initial flux and power shift away from the break region following the hypothetical large loss of coolant accident is expected as a result of the negative fuel temperature reactivity coefficient. Subsequently, as the large reactivity coefficient due to voiding overcomes the fuel temperature negative reactivity feedback, the power distribution shifts back to the break quadrant. These results may be linked to the primary research objective of this study, which is to demonstrate that the addition of burnable neutron absorbers mitigates the effect of coolant voiding on CANDU 37-element fuel. The addition of Gd_2O_3 demonstrates a marked improvement in the magnitude of the power pulse following the modeled hypothetical large loss of coolant accident.

5.1.2 Simulation Results

The initial flux shape of the Gd_2O_3 simulation had higher peak channel powers in the center of the core. It is expected that the change in the initial flux shape is a result of both natural uranium and Gd_2O_3 simulations using the same time-average exit irradiations. The higher peak channel powers lead to a greater power response to the changing fuel temperature and coolant voiding during the transient steps. As such, it is important to analyze the change in the power distribution relative to the initial flux shape for each case rather than the absolute channel powers.

The initial power shift from 0-0.1 s leads to a power reduction in the break region and to an increase in power on the opposite side of the core. This results from flux normalization. The larger initial decrease in the break region and increase on the opposite side of the core for the Gd_2O_3 case implies a more negative fuel temperature reactivity coefficient than for natural uranium. As the large void coefficient overcomes the fuel temperature negative reactivity feedback from 0.2-0.3s the higher power distribution shifts back towards the break quadrant.

Comparing Table 7 with Table 5, it is noted that both the core and maximum channel power changes are less for the simulation with Gd_2O_3 added to the fuel. The magnitude of the initial power shift calculated at 0.1 s, and subsequently back to the break region of the core, was also shown to be dampened with the addition of Gd_2O_3. In other words, the transient side-to-side oscillation is said to be slower for the case with burnable neutron absorbers. Due to the relationship between power changes and temperature increases in the fuel, it is noted that these results indicate an improvement in the margin to fuel failure during a hypothetical large loss of coolant accident.

Comparing Figure 17 with Figure 15 it may be noted that the magnitude of the variation in adjacent channel powers is lower in the case when Gd_2O_3 is added to the fuel. This is demonstrated by the peaks associated with Figure 15 when compared with the flatter nature of the transient in Figure 17. The lower variation in adjacent channel powers again emphasizes that the regional power increases experienced with Gd_2O_3 present in the fuel is dampened. This factor indicates that the actuation of one or both of the shutdown systems in response to the unit trip following the accident would be more effective.

5.1.3 Phase One Summary

Important results can be summarized in the three following points:

- The core and maximum channel power changes are dampened by Gd_2O_3, meaning they are lower than for natural uranium.
- The transient side-to-side oscillation is slower for the Gd_2O_3 case than for natural uranium.
- The axial core balance is better maintained in the Gd_2O_3 case.

5.2 Phase Two

5.2.1 Phase Two Overview

The results outlined in Table 26 give a thorough overview of the parameters that will be discussed in this section. Overall, the results are in line with theory and the expected outcome for the nine simulations that were performed. The primary parameter of interest is the maximum channel power as individual overpower and margin to critical channel power are important for the maintenance of fuel integrity within each channel in the core. Total core power change is also discussed in this section. Linking these results from this phase of the study back to the primary research objective, to demonstrate that the addition of burnable neutron absorbers mitigates the effect of coolant voiding on CANDU 37-element fuel, it should most importantly be noted that the addition of burnable neutron absorbers Gd_2O_3 and B_2O_3 led to an improvement by lowering the power pulse following the modeled hypothetical large loss of coolant accident.

The key finding from the second phase study is that the addition of burnable neutron absorbers Gd_2O_3 and B_2O_3 reduces the maximum channel power change at the end of the transient simulation for all nuclide concentrations simulated. An additional

result, similar to the results obtained in Phase One, is that the flux shape is generally flatter when burnable neutron absorbers are added when compared with the natural uranium case as shown in the core maps in Figure 18 through Figure 44. When compared with even distribution throughout the bundle, the addition of burnable neutron absorbers to only the center element led to larger channel power reductions and reductions in total core power for each set of nuclide concentrations.

The main assumption made throughout each study was that the thermalhydraulic parameters including the moderator temperature and density, coolant temperature, and fuel temperature were constant through each transient simulation. Overall, the thermalhydraulic parameters at each node are expected to be largely the same resulting from the hypothetical large loss of coolant accident occurring in the same region for each large break simulation. Since the break modeled was large in magnitude, the impact of a large break is expected to be the most significant. Smaller effects due to reactivity coefficients for the moderator, coolant, and fuel would not be reflected as a result of this assumption. As such, this study is used to demonstrate that an improvement can be gained from the addition of burnable neutron absorbers, but accepts that the precise magnitude change for each case would need to be obtained using a full core thermalhydraulics model fully coupled with the IST physics codes throughout.

5.2.2 Feasibility Assessment

To demonstrate the feasibility of the results outlined in Table 26, the results for total core power change in the evenly distributed burnable neutron absorber case were assessed. The largest change in total core power occurs in the long shutdown case, the second largest occurs for the equilibrium case, and the lowest change occurs in the fresh fuel case. With respect to maximum change in channel power, the largest improvement was obtained for the equilibrium case, the second largest was the long shutdown case, and the third largest was the fresh fuel case. These results are in line with what one would expect as described in the following three paragraphs.

During a long shutdown it is assumed that the fuel in core was burned prior to shut down, meaning that the entire concentration of burnable neutron absorbers in the fuel is not effective. In addition, the high neutron absorption cross section nuclide Xe-135 concentration goes to zero, provided that the duration of the shutdown is greater than thirty-six hours, as is the case in this simulation. This results from the flux term leading to the production of Xe-135 being eliminated and the remaining Xe-135 being left to decay away. Fissile Pu-239 reaches an equilibrium during the shutdown due to the flux dependent flux term disappearing and drastically reducing the loss term from absorption leading to fission. Depending on the duration of the outage, it is also possible to build in fissile Pu-241 in a similar manner. Neutron absorbing Sm-149 also builds to an equilibrium load during the shutdown, but not enough to offset the positive reactivity contribution from Pu-239 and Pu-241. As such, the excess reactivity from these nuclide concentrations at the time of this accident simulation in addition to the reduced concentrations of burnable neutron absorbers due to burn prior to the outage, result in the largest magnitude full core power increase.

The equilibrium case is the second greatest in terms of full core power increase. Similar to the long shutdown case, the burnable neutron absorbers added to the fuel have been depleted and are therefore not fully effective for neutron absorption at the time of the accident simulation. In addition, the equilibrium case assumes neutron absorbing Xe-135 is at full saturation load, adding negative reactivity and no reactivity contribution from Pu-239 for an equilibrium core.

Lastly, the fresh core simulation has fully effective burnable neutron absorbers, and no reactivity contribution from neutron absorbing Xe-135, Sm-149, Sm-151, and Rh-105 or fissile Pu-239. The relatively large negative reactivity contribution from the fully effective burnable neutron absorbers when compared with the other nuclide concentrations leads to the largest dampening effect and subsequently the lowest total core power change for this series of simulations, in line with theory and expectation.

5.2.3 Evenly Distributed BNAs

It is interesting to note that, while the maximum change in channel power is improved for the evenly distributed BNA case for each set of nuclide concentrations, the minimum change in channel power increases. This effect compensates in a negative manner for the improvement in maximum channel power change to the point that the total core change in power is higher for the BNA case when compared against the natural uranium case. Despite the larger increase in core power, this result implies that the flux shape is much flatter in these simulations. That is, the spread between the maximum and minimum channel power changes is smaller. As such, these simulations still indicate an improvement due to the overpower reduction of the highest power channel and region in the core.

These results are further justified by knowing that the safety analysis is based on maintaining fuel geometry during the accident; that is, preventing sheath failure and melting. It is understood that the sheath temperature and the power are correlated. As such, a demonstration that the regional power changes that occur on a channel power level are lower implies a reduction in localized temperatures as well. Despite the larger total core power change, it is expected that shutdown system actuation will better mitigate the power pulse due to lower regionalized power peaks. This stems from the result that the highest regionalized peak power in the burnable neutron absorber simulation was lower than the highest peak in the natural uranium case as shown through the maximum change in channel power parameter.

5.2.4 Center Pin BNAs

The simulations with center pin burnable neutron absorbers show that the equilibrium nuclide concentration had the largest reduction in channel power change, the long shutdown nuclide concentrations had the second largest reduction, and the fresh fuel has the lowest reduction relative to the natural uranium case. These results are similar in nature to the results yielded with evenly distributed burnable neutron absorbers but with a larger magnitude change. With respect to maximum change in channel power, the largest impact was seen for the equilibrium case, the second highest for the long shutdown case, and the third largest for the fresh fuel case. These

results are in line with what one would expect as described in the following two paragraphs.

Burnable neutron absorber addition to only the center element of the fuel is expected to cause less flux dampening during normal operation than the evenly distributed case simply due to the lower total concentration of burnable neutron absorbers. In addition, spectrum changes and a larger imbalance between the neutron production and loss rates in the voided regions of the bundle during the transient simulation lead to a greater reduction in power when BNAs are added only to the center pin. As such, during the hypothetical loss of coolant accident scenario, targeting the center element only is expected to yield a greater result than evenly distributing the burnable neutrons absorbers throughout each element. This is due to both the larger expected magnitude change as well as spectrum and void changes surrounding each impacted bundle.

The physics implications of adding burnable neutron absorbers to only the center pin of the thirty-seven-element fuel bundle are a larger magnitude reduction in channel powers and core powers that ultimately stems from the six-factor formula. When a neutron is born from fission, it is highly energetic, and it has a low probability of inducing fission in fissile U-235. At the high energy range, some neutrons are lost due to leakage and some induce fission in fissionable U-238. As the neutrons leave the fuel and enter the moderator region, they are thermalized, and some are lost due to resonance absorption during slowing down. Once neutrons reach thermal energy levels some are lost due again to leakage, others are lost due to absorption in non-fissile materials, and some are absorbed in fissile U-235 inducing further fissions.

The positive void reactivity in CANDU reactors is due primarily to two factors. The first is an increase in the fast-fission factor due to the loss of moderating primary heat transport system coolant surrounding the fuel. The second is due to a decrease in resonance absorption. When burnable neutron absorbers are added uniformly to each of the thirty-seven elements in the fuel bundle the impact of the change in each of the fast fission factor and resonance escape probability is mitigated evenly as expected. When burnable neutron absorbers are added only to the center pin of the fuel bundle, there is absorption occurring at the center pin unevenly with respect to the remainder of the fuel bundle. The uneven nature of this burnable neutron absorber distribution in the fuel bundle results in an overall decrease in the neutron reproduction factor for thermal neutrons during the accident simulation as a result of spectral changes that occur in the fuel. This means that, on average, less neutrons are produced per neutron absorbed in the fuel for this case when compared against both the natural uranium fuel case and the evenly distributed burnable neutron absorber case. This phenomenon results in a lower overall magnitude power change.

5.2.5 Potential Economic Benefit for Small In-Core Break

It is expected that the addition of burnable neutron absorbers to the fuel could provide economic benefits in addition to the safety margin improvement for the case of a startup core following a long shutdown. Power holds during the startup transient following a unit shutdown are analyzed and implemented with the intention of

building up Xe-135 concentration in the fuel. This is the reason behind the requirements of available negative reactivity for the shutdown systems in the reactor, stemming from a small in-core loss of coolant accident with a heavily over poisoned moderator, as is the case during a startup transient. In this scenario, the primary heat transport heavy water, which is not poisoned, passes through a break into the poisoned moderator heavy water causing a drastic increase in core reactivity due to dilution of the moderator. It is expected that power holds could be reduced or eliminated altogether as the burnable neutron absorbers added to the fuel bundle could fill that role in the absence of Xe-135.

5.2.6 Phase Two Summary

The important results from this phase of the study may be summarized in the following points:

- The addition of burnable neutron absorbers has a positive impact on maximum changes in channel powers for all nuclide concentrations simulated including fresh fuel, equilibrium fuel, and startup fuel following a long shutdown.
- The addition of burnable neutron absorbers to only the center element of the fuel bundle has a greater positive impact on the power changes than for evenly distributing the burnable neutron absorbers throughout all elements in the fuel bundle.
- The addition of burnable neutron absorbers to the fuel may improve economics as well as safety during the startup following a long shutdown due to a minimization of the time required for power holds to build-up poison loads in the fuel.

5.2.7 Sources of Uncertainty

There are several sources of uncertainty, and computational bias, in the series of computations performed throughout this study. These sources of uncertainty and error are important to discuss to provide justification that the results presented are credible and to demonstrate that each has been taken into consideration. Generally, industry standard deterministic codes are benchmarked against station data and stochastic models as outlined in Section 3.3.2. This section provides some of the reasoning and justification for errors and uncertainty in the results presented.

The first source of error that should be noted is in the microscopic cross sections accumulated by WIMS-AECL from the ENDF/B library themselves. A significant amount of research and effort have been placed on evaluation of the uncertainty in these cross sections, resulting in covariance files associated with each evaluated nuclear data library. It is understood that when collecting data related to microscopic cross sections for various nuclides there are both modelling, and measurement uncertainty associated with each experiment. The precise impact of the covariance files associated with the nuclides of interest has been deemed outside the scope of this study. The accumulation and propagation of uncertainty associated with each nuclide for each phase of this study would not prove to be a trivial endeavor.

The second source of error is the grouping (eighty-nine energy groups) used in the WIMS-AECL computations and the two energy groups subsequently used in the RFSP-IST computations. It should be noted that a focus of RFSP-IST is fuel management calculations. In addition, most neutrons in CANDU reactors are in the thermal region. These two factors make is reasonable to use only two energy groups for the purposes of these computations. The purpose of condensing the energy groups used in each set of computations is ultimately for time savings relative to accuracy of results (stochastic simulation run times are exponentially larger than deterministic). This time-cost to benefit analysis performed is justified by means of comparison against true station data along with stochastic models such as the MCNP Monte Carlo simulations as outlined in Section 3.3.2. As less energy groups are used it is expected that simulation precision is reduced, and it is a requirement that these deterministic codes be benchmarked against stochastic models to demonstrate feasibility for use. The results described in Section 3.3.2 are indicative of an inherent computational bias, separate from uncertainty stemming from the nuclear data itself.

The last source of uncertainty for discussion important to this study is the error associated with the improved quasistatic model used in the RFSP-IST CERBERUS module computations. Sensitivity and uncertainty analyses have been conducted using codes such as TSUNAMI to characterize how accurate coolant void reactivity computations are for time-dependent models such as the CERBERUS. These methods are again based on Monte Carlo computations and take into consideration the aforementioned nuclear data covariance files. As such, small changes in the defined nuclear data and properties associated with the model can be assessed to determine corresponding changes to core reactivity. From one such study associated with the specific set of codes used throughout this study it was determined that the bias in coolant void reactivity is 0.5 +/- 0.57 mk [66], which is well within the 2.0 +/- 1.1 mk uncertainty outlined in the RFSP-IST Theory Manual and documented in Section 3.3.2.

6 Conclusion

A model has been developed to create input files for two dimensional WIMS-AECL computed uniform parameter and simple cell model fuel tables for thirty-seven element fuel. The fuel tables are passed to the three-dimensional RFSP-IST full core SIMULATE module for computation of the steady-state core power distribution for a generic CANDU-6 core. This initial power distribution is passed to the RFSP-IST CERBERUS module for computation of the change in power distribution throughout a fast transient resulting from a hypothetical large loss of coolant accident using the improved quasi-static model.

The study conducted and outlined in this paper was split into two phases. The first phase consisted of model development and established an understanding of the transient progression and the impact from the addition of burnable neutron absorbers. This was accomplished through the modelling of natural uranium fuel and the comparison against a simulation with Gd_2O_3 distributed evenly throughout the thirty-seven elements in the fuel bundle for comparison. The second phase consisted of the addition of 180 mg Gd_2O_3 and 1000 mg B_2O_3 in line with the recommendation from Chan *et al.* The intent of this phase was to simulate the recommended concentrations of short-lived and long-lived burnable neutron absorbers to target the xenon-free and plutonium transients respectively during normal reactor operation. Nine simulations were performed including fresh fuel, equilibrium fuel, and startup fuel following a long shutdown of the reactor. For each set of assumed nuclide concentrations three simulations were performed for comparison including a natural uranium case, a case with burnable neutron absorbers evenly distributed through each element in the fuel bundle, and a case with burnable neutron absorbers added only to the center pin of the fuel bundle.

The results show a reduction in the core enthalpy change when burnable neutron absorbers are added, along with a reduction in the side-to-side power oscillation during the transient, and an improved axial flux balance. The reduction in the enthalpy change implies that the positive void reactivity experienced in CANDU reactors during loss of coolant accidents could be reduced through the addition of burnable neutron absorbers in the fuel. Also, it was determined that the addition of

burnable neutron absorbers has a positive impact on the maximum change in channel power throughout the transient simulations. This included simulation comparisons for burnable neutron absorber addition evenly throughout each of the thirty-seven elements in the fuel bundle and in only the center element of the fuel bundle for fresh, equilibrium, and startup following a long shutdown core nuclide conditions. Overall, the results of this study demonstrate that the addition of burnable neutron absorbers mitigates the effect of coolant voiding on CANDU 37-element fuel. The addition of Gd_2O_3 and B_2O_3 demonstrated a marked improvement in the magnitude of the power pulse following each modeled hypothetical large loss of coolant accident.

7 Recommendations

In line with previous studies conducted related to the addition of burnable neutron absorbers in CANDU fuel, it is recommended that burnable neutron absorber studies be pursued further as the safety and economic benefits of implementation have been evidenced. Given this recommendation, it is further advised that the use of burnable neutron absorbers in future CANDU designs be further investigated and actual CANDU fuel bundles with such burnable neutron absorbers be eventually manufactured and irradiated in a research type reactor for operational testing and analysis, to confirm the predictions from the computer simulations.

For the purpose of improving the analyses conducted in this study, it is recommended that a full core thermalhydraulics model be developed and implemented to improve the results by providing temperature and density feedback to the RFSP-IST CERBERUS module. This will allow more accurate results specific to the fuel and reactor being modeled. For the type of design change required by modifications to the fuel such as the addition of burnable neutron absorbers, a full safety analysis will need to be conducted requiring these models and results.

An optimization of the burnable neutron absorber concentrations for the purpose of mitigation of the void reactivity effects during a large loss of coolant accident is recommended. In addition, it is expected that some combination of burnable neutron absorbers and their distribution in the fuel bundle will be optimal for both economic and safety benefits and, as such, a study is recommended to determine these parameters. This study should consider the results outlined in the extended refuelling study, end flux peaking study, and large loss of coolant accident study performed. Considering that the center pin burnable neutron absorber addition leads to the largest improvement in power pulse mitigation during the hypothetical large loss of coolant accident, it is expected that the safety aspect of this argument will lean toward recommending this type of implementation. It is anticipated that the addition of burnable neutron absorbers to only the center pin, or the inner rings of the fuel bundle rather than the entire bundle will produce drastically different results during extended refuelling simulations, potentially reducing the already low burnup loss experienced.

Lastly, the potential to improve economics of startup transients by minimization of the power holds required from the addition of burnable neutron absorbers to the fuel should be investigated. The potential to save time between the operation of the reactor at low power critical to operation at full power steady state could prove to be of significant station interest.

References

[1] Dr. Lorne McConnell, "NPD: Canada's First Nuclear Power Station," 2002. [Online]. Available: http://www.cns-snc.ca/media/history/npd/2002_NPD_Lorne_McConnell.htm. [Accessed 11 March 2019].

[2] V. G. Snell, "Safety of CANDU Nuclear Power Stations," AECL-6329, 1978.

[3] CANDU Canteach, "22107.8 Operating Policies and Principles".

[4] Nuclear Energy Agency, "Nuclear Fuel Behavior in Loss-of-coolant Accident (LOCA) Conditions," 2009.

[5] Dirk J. Oh, Myeong Y. Ohn, Kang M. Lee, Ho C. Suk, "Safety Assessment for LOCA in CANDU Reactor Loaded with CANFLEX-NU Fuel Bundles," Korea Atomic Energy Research Institute, No Date.

[6] A.P. Muzumdar, D.A. Meneley, "Large LOCA Margins in CANDU Reactors - An Overview of the COG Report," in *Proceedings of CNS 30th Annual Conference*, Calgary, CA, 2009.

[7] B. Rouben, "Core-Physics Aspects of Safety Analysis," AECL, 1997.

[8] V. G. Snell, "The Essential CANDU, A Textbook on the CANDU Nuclear Power Plant Technology, Reactor Safety Design and Safety Analysis," University Network of Excellence in Nuclear Engineering (UNENE), ISBN 0-9730040.

[9] Atomic Energy of Canada Limited, CANDU Nuclear Power System, Mississauga, Ontario: Sheridan Park Research Community TDS1-105, January 1981.

[10] Dr. George Bereznai, Nuclear Power Plant Systems and Operation Reference Text, Oshawa, Ontario: University of Ontario Institute of Technology, 2005.

[11] Chan, P. K., Paquette, S., and Bonin, H. W., "Variation of Burnable Neutron Absorbers in Heavy Water-Moderated Fuel Lattice: A Potential to Improve CANDU Reactor Operating Margin," Nuclear Technology. 1.191.2015.

[12] J. J. Song, P. K. Chan, H. W. Bonin, and S. Paquette, "Fuelling Study of a CANDU Reactor Using Fuels Containing Burnable Neutron Absorbers," Nuclear Technology, 195(3), 310, 2016.

[13] D. Pierce, P. K. Chan, and H. Bonin, "Mitigation of End Flux Peaking in CANDU Fuel Bundles using Neutron Absorbers," Submitted to ASME Journal of Nuclear Engineering and Radiation Science. NERS-19-1003, 2019.

[14] National Training Centre, "DOE Fundamentals: Nuclear Physics and Reactor Theory," U.S. Department of Energy, 2015.

[15] Jonkmans, G., "WIMS-AECL Version 3.1 User's Manual, ISTP-05-5115.," CANDU Owner's Group Inc., 2006.

[16] Schwanke, P., "RFSP-IST Version REL_3.04: User's Manual, SQAD-06-5054, 153-117360-UM-002," CANDU Owner's Group Inc., 2006.

[17] Weston M. Stacey, Nuclear Reactor Physics, John Wiley & Sons Inc., 2001.

[18] Lamarsh, John. R, Baratta, Anthony J. , Introduction to Nuclear Engineering 3E, Prentice Hall: New Jersey, 2001.

[19] James J. Duderstadt, Louis J. Hamilton, Nuclear Reactor Analysis, Chapter 2 The Nuclear Physics of Chain Reactions, New York: John Wiley & Sons, Inc., 1976.

[20] S. E. Liverhant, "Elementary Introduction to Nuclear Reactor Physics," Wiley, New York, 1960.

[21] Kenneth S. Krane, Introductory Nuclear Physics, Wiley. ISBN 978-0-471-80553-3, 1987.

[22] Arthur Beiser, Concepts of Modern Physics, McGraw-Hill. ISBN 0-07-244848-2, 2003.

[23] Editor-in-Chief Wm. J. Garland, "The Essential CANDU, A Textbook on the CANDU Nuclear Power Plant Technology, Chapter 2," University Network of Excellence in Nuclear Engineering (UNENE), ISBN 0-9730040, 2014.

[24] Neeb, Karl Heinz, The Radiochemistry of Nuclear Power Plants with Light Water Reactors, Berlin-New York: Walter de Gruyter ISBN 3-11-013242-7., 1997.

[25] IAEA, Manual for Reactor Produced Isotopes, Vienna: IAEA-TECDOC-1340, 2003.

[26] B.J. Allen, Neutron Radiative Capture: Neutron Physics and Nuclear Data in Science and Technology, Elsevier Ltd. 978-0-08-029330-1, 1984.

[27] World Nuclear Association, "Nuclear Fuel Cycle Overview," 2017. [Online]. Available: http://www.world-nuclear.org/information-library/nuclear-fuel-cycle/introduction/nuclear-fuel-cycle-overview.aspx. [Accessed 11 March 2019].

[28] Rivkees, Scott A.; Sklar, Charles; Freemark, Michael, The Management of Graves' Disease in Children, with Special Emphasis on Radioiodine Treatment, Journal of Clinical Endocrinology & Metabolism 3767–76, 1998.

[29] Perkins, Donald H., Introduction to High Energy Physics, Cambridge University Press. ISBN 978-0-521-62196-0, 1999.

[30] U.S. Department of Energy, DOE Fundamentals Handbook, Nuclear Physics and Reactor Theory, DOE-HDBK-1019/1-93, 1993.

[31] Bennet, L. G. I., Lewis, B. J., Bonin, H. W. and Corcoran, E. C., PHYS 491: Physics of Nuclear Reactors, Royal Military College of Canada/ Queen's University, 2013.

[32] Encyclopedia of Materials: Science and Technology (Second Edition), Nuclear Reactors: Shielding Materials, San Diego, California USA: Elsevier Ltd., 2001.

[33] J.E. Crist, Nuclear Theory - Course 227: Neutron Multiplication Factor and Reactivity, CANDU Canteach.

[34] M. Tucker, A Comparison of Reactivity Parameters of CANDU Fuel Bundles over Fuel, Hamilton, Canada, 2017.

[35] E. Critoph, Reactor Physics Aspects of CANDU Reactors, Chalk River, Ontario: Atomic Energy of Canada Limited, Chalk River Nuclear Laboratories.

[36] Ryan G. McClarren, Computational Nuclear Engineering and Radiological Science Using Python 1st Edition, Academic Press 978-0-12-812253-2, 2018.

[37] J.E. Crist, Nuclear Theory - Course 227: Changes in Reactor Power with Time, CANDU Canteach.

[38] Canteach, Course 22106 Module 12: Reactivity Effects Due to Temperature Changes and Coolant Voiding, CANDU Canteach, 1997.

[39] Los Alamos National Lab, ENDF/B-V U-238 Principal cross sections, Retrieved June, 2019.

[40] Carron, N.J., An Introduction to the Passage of Energetic Particles Through Matter, 2007.

[41] Canteach, Course 22106: Module 12 Reactivity Effects Due to Temperature Changes and Coolant Voiding, CANDU.

[42] CANDU 6 Program Team, "CANDU 6 Technical Summary," 2005.

[43] P. Chan, Nuclear Fuels Engineering Course Notes, 2015.

[44] Editor-in-Chief Wm. J. Garland, "The Essential CANDU, A Textbook on the CANDU Nuclear Power Plant Technology, Chapter 17," University Netwrok of Excellence in Nuclear Engineering (UNENE), ISBN 0-9730040, 2014.

[45] B. Rouben, CANDU Fuel-Management Course, Atomic Energy of Canada Ltd. .

[46] Pacific Gas and Electric Company, Preliminary Safety Analysis Report, Diablo Canyon Pressurized Water Reactor Unit 2, Vol. 1.

[47] G. Bereznai, CANDU Overview Chapter 4: Heat Transport, CANDU Canteach.

[48] Jong Hyun Kim; Dong Sik Jin; Soon Heung Chang, "Development of safety analysis methodology for moderator system failure of CANDU-6 reactor by thermal-hydraulics/physics coupling," *Nuclear Engineering and Design*, vol. 263, 2013.

[49] CANDU Canteach, Course 233 - Reactor & Auxiliaries - Module 1 - Moderator Heavy Water rev3.

[50] Gong Hongqi, R.S. Hart, Moderator, Heat Transport and Steam Systems, Third Qinshan Nuclear Power Company, Atomic Energy of Canada Limited.

[51] T. Nitheanandan and M. Brown, "Backup and Ultimate Heat Sinks in CANDU Reactors for Prolonged SBO Accidents," *Nuclear Engineering and Technology,* vol. 45, 2013.

[52] Editor-in-Chief Wm. J. Garland, The Essential CANDU, A Textbook on the CANDU Nuclear Power Plant Technology, Chapter 8, University Network of Excellence in Nuclear Engineering (UNENE), ISBN 0-9730040, 2014..

[53] CNSC Technical Training Group, Science and Reactor Fundamentals: Reactor Physics, 2003.

[54] CM. Bailey, R.D. Fournier, F.A.R. Laratta, "Regional Overpower Protection in CANDU Power Reactors," International Meeting on Thermal Nuclear Reactor Safety, Chicago, Illinois, 1982.

[55] CANDU Canteach, The Moderator Liquid Poson System: Course 233 - Reactor & Auxiliaries - Module 4 - Moderator Poison Addition.

[56] Dr. Jean Koclas, Reactor Control and Simulation, Ecole Polytechnique, Chulalongkorn University.

[57] Editor-in-Chief Wm. J. Garland, The Essential CANDU, A Textbook on the CANDU Nuclear Power Plant Technology, Chapter 13, University Network of Excellence in Nuclear Engineering (UNENE), ISBN 0-9730040, 2014..

[58] Roger G. Steed, Nuclear Power: In Canada and Beyond: Chapter 11, Renfrew, Canada: General Store Publishing House: ISBN-13: 978-1-897113-51-6.

[59] P.K. Chan; S. Paquette; T.A. Cunning; C. French; H.W. Bonin; M. Pandey; M. Murchie, "Margin Improvement Initiatives: Realistic Approaches," in *PBNC2014-135*, Vancouver, British Columbia,, 2014.

[60] G. Marleau, A. Hebert, R. Roy, A User's Guide for DRAGON Version DRAGON_98011 Release 3.03, Montreal, Canada: Ecole Polytechnique de Montreal Technical Report, IGE-174, Revision 4, 1998.

[61] M. Chadwick, P. Oblozinsky, Nuclear Data: New ENDF/B-VII Library, National Nuclear Data Center, Brookhaven National Laboratory.

[62] D.V. Altiparmakov, WIMS-AECL Theory Manual, COG 00-077.

[63] B. Rouben, EP 4P03/6P03: Reactivity Coefficients, McMaster University.

[64] W. Shen, RFSP-IST Version REL_3-04: Theory Manual, COG SQAD-06-5058 153-117360-STM-002 .

[65] X-5 Monte Carlo Team, MCNP – A General Monte Carlo N-Patricle Transport Code, Version 5 Volume 1: Overview and Theory, Los Alamos National Laboratory. , April 24, 2003..

[66] F. P. Adams, *Accuracy of Characterization of Coolant Void Reactivity*, CANDU Owner's Group, 2015.

Appendices

Appendix A.1 Octave script for processing WIMS output files

```
% Function for processing of WIMS output files
% Input: Name of text file containing WIMS output
%
function wims_process(filename)
  clear global
  % Open and read output file
  fopen(filename);
  wimsout=fileread(filename);
  % Parse file for multiplication factor extraction
  kinf=str2num(wimsout(strfind(wimsout, 'MAIN TRANSPORT SOLUTION')+38:strfind(wimsout, 'MAIN TRANSPORT SOLUTION')+46))
  % Close file
  fclose(filename);
endfunction
```

Appendix A.2 Octave script for processing RFSP output files

```
% Function for processing of RFSP output filese
% Input: Name of text file containing RFSP output
% Output: 3D cmap flux plot, maximum channel and bundle powers
%
function [cmap,maxcp,maxbp,maxcpchan,maxbpchan]=rfsp_process(filename)
  clear global
  % Open and read output file
  fopen(filename);
  rfspout=fileread(filename);
  % Parse file for channel power extraction
  % A row
  A09=str2num(rfspout(strfind(rfspout, 'A - 09')+20:strfind(rfspout, 'A - 09')+26));
  A10=str2num(rfspout(strfind(rfspout, 'A - 10')+20:strfind(rfspout, 'A - 10')+26));
  A11=str2num(rfspout(strfind(rfspout, 'A - 11')+20:strfind(rfspout, 'A - 11')+26));
  A12=str2num(rfspout(strfind(rfspout, 'A - 12')+20:strfind(rfspout, 'A - 12')+26));
  A13=str2num(rfspout(strfind(rfspout, 'A - 13')+20:strfind(rfspout, 'A - 13')+26));
  A14=str2num(rfspout(strfind(rfspout, 'A - 14')+20:strfind(rfspout, 'A - 14')+26));
  % B row
                    …
% Create cmap array with channel powers
  cmap=zeros(22,22);
  cmap=[NA, NA, NA, NA, NA, NA, NA, NA, A09,A10,A11,A12,A13,A14,NA, NA, NA, NA, NA, NA, NA, NA;
        NA, NA, NA, NA, NA, B06,B07,B08,B09,B10,B11,B12,B13,B14,B15,B16,B17,NA, NA, NA, NA, NA;
        NA, NA, NA, NA, C05,C06,C07,C08,C09,C10,C11,C12,C13,C14,C15,C16,C17,C18,NA, NA, NA, NA;
        NA, NA, NA, D04,D05,D06,D07,D08,D09,D10,D11,D12,D13,D14,D15,D16,D17,D18,D19,NA, NA, NA;
        NA, NA, E03,E04,E05,E06,E07,E08,E09,E10,E11,E12,E13,E14,E15,E16,E17,E18,E19,E20,NA, NA;
        NA, NA, F03,F04,F05,F06,F07,F08,F09,F10,F11,F12,F13,F14,F15,F16,F17,F18,F19,F20,NA, NA;
        NA, G02,G03,G04,G05,G06,G07,G08,G09,G10,G11,G12,G13,G14,G15,G16,G17,G18,G19,G20,G21,NA;
        NA, H02,H03,H04,H05,H06,H07,H08,H09,H10,H11,H12,H13,H14,H15,H16,H17,H18,H19,H20,H21,NA;
        J01,J02,J03,J04,J05,J06,J07,J08,J09,J10,J11,J12,J13,J14,J15,J16,J17,J18,J19,J20,J21,J22;
        K01,K02,K03,K04,K05,K06,K07,K08,K09,K10,K11,K12,K13,K14,K15,K16,K17,K18,K19,K20,K21,K22;
        L01,L02,L03,L04,L05,L06,L07,L08,L09,L10,L11,L12,L13,L14,L15,L16,L17,L18,L19,L20,L21,L22;
        M01,M02,M03,M04,M05,M06,M07,M08,M09,M10,M11,M12,M13,M14,M15,M16,M17,M18,M19,M20,M21,M22;
        N01,N02,N03,N04,N05,N06,N07,N08,N09,N10,N11,N12,N13,N14,N15,N16,N17,N18,N19,N20,N21,N22;
```

```
        O01,O02,O03,O04,O05,O06,O07,O08,O09,O10,O11,O12,O13,O14,O15
,O16,O17,O18,O19,O20,O21,O22;
        NA, P02,P03,P04,P05,P06,P07,P08,P09,P10,P11,P12,P13,P14,P15
,P16,P17,P18,P19,P20,P21,NA;
        NA, Q02,Q03,Q04,Q05,Q06,Q07,Q08,Q09,Q10,Q11,Q12,Q13,Q14,Q15
,Q16,Q17,Q18,Q19,Q20,Q21,NA;
        NA, NA, R03,R04,R05,R06,R07,R08,R09,R10,R11,R12,R13,R14,R15
,R16,R17,R18,R19,R20,NA, NA;
        NA, NA, S03,S04,S05,S06,S07,S08,S09,S10,S11,S12,S13,S14,S15
,S16,S17,S18,S19,S20,NA, NA;
        NA, NA, NA, T04,T05,T06,T07,T08,T09,T10,T11,T12,T13,T14,T15
,T16,T17,T18,T19,NA, NA, NA;
        NA, NA, NA, NA, U05,U06,U07,U08,U09,U10,U11,U12,U13,U14,U15
,U16,U17,U18,NA, NA, NA, NA;
        NA, NA, NA, NA, NA, V06,V07,V08,V09,V10,V11,V12,V13,V14,V15
,V16,V17,NA, NA, NA, NA, NA;
        NA, NA, NA, NA, NA, NA, NA, NA, W09,W10,W11,W12,W13,W14,NA,
 NA, NA, NA, NA, NA, NA, NA;];
  % Surface plot cmap
  surf(cmap);
  shading interp;
  h = findobj (gca (), "type", "surface");
  set (h, "edgecolor", "k");
  zlabel("Channel Power (kW)");
  xlabel("Row");
  ylabel("Column");
  colormap("jet");
  colorbar;
  % Extract relevant power information
  totalpower=str2num(rfspout(strfind(rfspout, 'TOTAL REACTOR POWER'
)+31:strfind(rfspout, 'TOTAL REACTOR POWER')+38))
  maxcp=str2num(rfspout(strfind(rfspout, 'MAXIMUM CHANNEL POWER=')+
31:strfind(rfspout, 'MAXIMUM CHANNEL POWER=')+38))
  maxbp=str2num(rfspout(strfind(rfspout, 'MAXIMUM BUNDLE  POWER=')+
31:strfind(rfspout, 'MAXIMUM BUNDLE  POWER=')+38))
  maxcpchan=(rfspout(strfind(rfspout, 'MAXIMUM CHANNEL POWER=')+69:
strfind(rfspout, 'MAXIMUM CHANNEL POWER=')+73))
  maxbpchan=(rfspout(strfind(rfspout, 'MAXIMUM BUNDLE  POWER=')+69:
strfind(rfspout, 'MAXIMUM BUNDLE  POWER=')+73))
  % Close file
  fclose(filename);
endfunction
```

Appendix A.3 Octave script for post-processing RFSP output files

```
% Script to generate 3D plots calling rfsp_process function
%
% Subplot abs
Fig e(1)
subplot(2,2,1)
[case1]=rfsp_process('cerb_scmcase1.txt')
title('Case 1')
subplot(2,2,2)
[case2]=rfsp_process('cerb_scmcase3.txt')
title('Case 2')
subplot(2,2,3)
[case3]=rfsp_process('cerb_scmcase4.txt')
title('Case 3')
subplot(2,2,4)
[case4]=rfsp_process('cerb_scmcase5.txt')
title('Case 4')
print -djpg cerbplot
% Subplot diff
figure(2)
subplot(2,2,1)
  surf(case1-case1);
  shading interp;
  h = findobj (gca (), "type", "surface");
  set (h, "edgecolor", "k");
  zlabel("Channel Power (kW)");
  xlabel("Row");
  ylabel("Column");
  colormap("jet");
  colorbar;
  title("Case 11")
subplot(2,2,2)
  surf(case2-case1);
  shading interp;
  h = findobj (gca (), "type", "surface");
  set (h, "edgecolor", "k");
  zlabel("Channel Power (kW)");
  xlabel("Row");
  ylabel("Column");
  colormap("jet");
  colorbar;
  title("Case 21")
subplot(2,2,3)
  surf(case3-case1);
  shading interp;
  h = findobj (gca (), "type", "surface");
  set (h, "edgecolor", "k");
  zlabel("Channel Power (kW)");
  xlabel("Row");
  ylabel("Column");
  colormap("jet");
  colorbar;
  title("Case 31")
subplot(2,2,4)
  surf(case4-case1);
  shading interp;
```

```
  h = findobj (gca (), "type", "surface");
  set (h, "edgecolor", "k");
  zlabel("Channel Power (kW)");
  xlabel("Row");
  ylabel("Column");
  colormap("jet");
  colorbar;
  title("Case 41")
print -djpg cerbplot2
```

Appendix A.4 Octave script for post-processing RFSP output files

```
1.  [cmap,maxcp,maxbp,maxcpchan,maxbpchan]=rfsp_process('C:\AECL-CC-
    CD326-X\X\Results\BNA_CP_LONGS\cerb_scmcase1.output');
2.  status = xlswrite('C:\AECL-CC-CD326-
    X\X\Results\xl.xlsx', cmap, 'scmcase1', 'A1:AV22');
3.
4.  [cmap,maxcp,maxbp,maxcpchan,maxbpchan]=rfsp_process('C:\AECL-CC-
    CD326-X\X\Results\BNA_CP_LONGS\cerb_scmcase2.output');
5.  status = xlswrite('C:\AECL-CC-CD326-
    X\X\Results\xl.xlsx', cmap, 'scmcase2', 'A1:AV22');
6.
7.  [cmap,maxcp,maxbp,maxcpchan,maxbpchan]=rfsp_process('C:\AECL-CC-
    CD326-X\X\Results\BNA_CP_LONGS\cerb_scmcase3.output');
8.  status = xlswrite('C:\AECL-CC-CD326-
    X\X\Results\xl.xlsx', cmap, 'scmcase3', 'A1:AV22');
9.
10. [cmap,maxcp,maxbp,maxcpchan,maxbpchan]=rfsp_process('C:\AECL-CC-
    CD326-X\X\Results\BNA_CP_LONGS\cerb_scmcase4.output');
11. status = xlswrite('C:\AECL-CC-CD326-
    X\X\Results\xl.xlsx', cmap, 'scmcase4', 'A1:AV22');
12.
13. [cmap,maxcp,maxbp,maxcpchan,maxbpchan]=rfsp_process('C:\AECL-CC-
    CD326-X\X\Results\BNA_CP_LONGS\cerb_scmcase5.output');
14. status = xlswrite('C:\AECL-CC-CD326-
    X\X\Results\xl.xlsx', cmap, 'scmcase5', 'A1:AV22');
```

Appendix A.5 BATCH script for preparation of SCM fuel tables

```
cd C:\AECL-CC-CD623-X\X\gen_wims

gen_wims.2.0.1.2

perl proc16.2.0.1.2.pl ftablecase.pin
copy *.t16 C:\AECL-CC-CD623-X\X
cd C:\AECL-CC-CD623-X\X
perl proc16.2.0.1.2.pl process_fuel.pin
cd C:\AECL-CC-CD623-X\X\gen_wims
del *.t16

perl proc16.2.0.1.2.pl referencecase.pin
copy *.t16 C:\AECL-CC-CD623-X\X
cd C:\AECL-CC-CD623-X\X
perl proc16.2.0.1.2.pl process_tube.pin
cd C:\AECL-CC-CD623-X\X\gen_wims
del *.t16

perl proc16.2.0.1.2.pl mtablecase.pin
copy *.t16 C:\AECL-CC-CD623-X\X
cd C:\AECL-CC-CD623-X\X
perl proc16.2.0.1.2.pl process_moder.pin
cd C:\AECL-CC-CD623-X\X\gen_wims
del *.t16

perl proc16.2.0.1.2.pl mictablecase.pin
copy *.t16 C:\AECL-CC-CD623-X\X
cd C:\AECL-CC-CD623-X\X
perl proc16.2.0.1.2.pl process_micro.pin
cd C:\AECL-CC-CD623-X\X\gen_wims
del *.t16

cd C:\AECL-CC-CD623-X\X
perl proc16.2.0.1.2.pl wrfspcase.pin
del *.t16

cd C:\AECL-CC-CD623-X\X\gen_wims
```

Appendix A.6 BATCH script for CERBERUS runs

```
cd C:\AECL-CC-CD326-X\X
set Executable=C:\AECL-CC-CD326-X\Executable\rfsp-ist.REL_3-04-
04PC.exe

copy cerb_scmcase1.input rfsp_input
%Executable% > out
copy rfsp_output cerb_scmcase1.output
copy out cerb_scmcase1_std.out
del out
del store
del rfsp_output
del rfsp_input

copy cerb_scmcase2.input rfsp_input
%Executable% > out
copy rfsp_output cerb_scmcase2.output
copy out cerb_scmcase2_std.out
del out
del store
del rfsp_output
del rfsp_input

copy cerb_scmcase3.input rfsp_input
%Executable% > out
copy rfsp_output cerb_scmcase3.output
copy out cerb_scmcase3_std.out
del out
del store
del rfsp_output
del rfsp_input

copy cerb_scmcase4.input rfsp_input
%Executable% > out
copy rfsp_output cerb_scmcase4.output
copy out cerb_scmcase4_std.out
del out
del store
del rfsp_output
del rfsp_input

copy cerb_scmcase5.input rfsp_input
%Executable% > out
copy rfsp_output cerb_scmcase5.output
copy out cerb_scmcase5_std.out
del out
del store
del rfsp_output
del rfsp_input

del *.t15
del *DAF*
del *.90
```